1-26-2017 12:00 AM

Discovery of Novel Diagnostic Biomarkers on Prostate Tumor Microparticles for Discriminating Between Low and High Risk Prostate Cancer and Improving Prostate Cancer Screening

Sabine Brett
The University of Western Ontario

Supervisor
Dr. Hon Leong
The University of Western Ontario

Graduate Program in Microbiology and Immunology
A thesis submitted in partial fulfillment of the requirements for the degree in Master of Science

Abstract

There are few protein-based biomarkers to accurately distinguish between patients with low risk prostate cancer from those with high risk disease in a non-invasive manner. Prostate specific antigen (PSA) is used for clinical follow-up of prostate cancer; however, it is not effective as a screening tool. As a result, many men with non-life threatening disease having to undergo unnecessary and painful biopsies. Therefore, there is a dire need for minimally invasive platforms for monitoring patients with clinically significant prostate cancer. Prostate cell microparticles (PCMPs) released by prostate epithelial cells into plasma are a potential source of biomarkers specific for prostate cancer. I undertook a translational prostate cancer research project to detect biomarkers expressed in PCMPs isolated from patient plasmas representing low and high grade prostate cancer, with the goal to differentiate patients. These novel biomarkers will offer a non−invasive means to differentiate between these two disease states.

Keywords

Prostate Cancer, Gleason Score, Biomarkers, Microparticles, STEAP1, Prostate Specific Antigen, Prostate Specific Membrane Antigen, Nanoscale Flow Cytometry, Atomic Force Microscopy, Protein G, Immunoprecipitation.

Co-Authorship Statement

Chapter 1, sections 1.1 through 1.8 were adapted from the published review:

S. I. Brett, Y. Kim, C. N. Biggs, J. L. Chin, and H. S. Leong, Prostate Cancer and Prostatic Disease, 2015.

Acknowledgments

So many amazing people have made the past two years an enjoyable experience. I have learned so much from each and one of you, and I feel so blessed to finish my degree with so many new friends.

Firstly, I must thank my supervisor, Dr. Hon Leong, for taking me as his first graduate student. Without his constant support, expertise and advice, I could have never developed this project into the thesis it is today. I cannot thank him enough for giving me the opportunity to learn and grow as a scientist-in-training.

To my committee members, Dr. Joseph Mymryk and Dr. Gregory Dekaban, thank you for all the challenging questions, for your input throughout the course of my project.

A very special thank-you to all the past members of the Leong lab, especially Coleen Biggs for being my first mentor in the arts of microparticle purification. Also, to our post-docs Dr. Karla Chinnery-Williams, Dr. Thamara Dayarathna, and Dr. Patrick Telmer; thank you for letting me plug my brain into yours, and learn as much as I could from you. To our technicians, Dr. Johanna Garzon, Yaroslav Fedyshyn, thank you for all your hard work; your daily efforts are the reason our lab operates like a well-oiled machine.

I am also immensely grateful for all the volunteers and students in the Leong Lab; thank you for all the laughs and the good times. Good luck to all of you in your future endeavours. Lastly, I am extremely lucky to have made lifetime friends in the lab, like Dr. Sohrab Ali, Yohan Kim, and Rachel Kim; you became my family during our time together in the lab, and I will be always grateful to count on such incredible people in my life.

I would also like to thank Charles Guo and DongXing from Dr. Jun Yang's laboratory in the Department of Mechanical and Materials Engineering at Western University, for their collaboration and expertise in atomic force microscopy.

A special thanks to the staff of the Biological Mass Spectrometry Laboratory at the University of Western Ontario, namely to Paula Pittock for her help with conducting mass spectrometry and protein analysis. Also, to Miljan for his help with the C18 desalting sample

preparation. The finishing touches to this project were done thank to all your efforts to have the mass spec result back to me in a timely manner.

I want to express sincere gratitude to my parents, my brother, and my boyfriend for their encouragement, patience, support, and love. Thank you for believing in me and pushing me to persevere, even when I doubted myself; I love you all very much. Last but never least, I would like to extend my gratitude to my aunt Dr. Adina Brett-Morris; as the only two scientists in the family, you always are an incredible source of knowledge and advice.

Sincerely,

Sabine

Table of Contents

List of Tables

List of Figures

List of Appendices

List of Abbreviations

PSA	Prostate specific antigen
PCa	Prostate cancer
PSMA	Prostate specific membrane antigen
STEAP1/2	Sixth transmembrane epithelial antigen of the prostate 1/2
EV	Extracellular vesicles
MPs	Microparticles
APB	Apoptotic bodies
miRNAs	microRNAs
PCCFs	Prostate cancer cell fragments
CTC	Circulating tumor cells
GS	Gleason score
NFC	Nanoscale flow cytometry
AFM	Atomic force microscopy
MVBs	Multivesicular bodies
EM	Electron microscopy
BPH	Benign prostatic hyperplasia
PSCA	Prostate stem cell antigen
EM	Electron microscopy

SEM	Scanning electron microscopy
MS	Mass spectrometry

Chapter 1

1 « Introduction»

1.1 Extracellular Vesicles

Extracellular vesicles (EVs) are a family of heterogeneous, cell-derived fragments or vesicles, which can be generated by cell membrane shedding or storage vesicle exocytosis. EV generation typically occurs following biological processes such as cell activation and modes of cell death such as necrosis and apoptosis (1). Initially perceived as cellular by-products or 'dust' of insignificant biological importance, recent research has shed light on the role of EVs as mediators of intercellular communication, blood coagulation and disease progression. Major sources or contributors of EVs in the blood are platelets, leukocytes and endothelial cells (2). Secretory glands comprised of epithelial cells also are a major source of EVs (3), but their contribution to the EV pool in blood is unclear. Several types of EVs are described throughout the literature (Fig.1); they are categorized according to their size, contents and mechanism by which they are released (4). For example, exosomes (30–100 nm) are EVs of cytoplasmic origin, released or exocytosed into the extracellular environment upon fusion of multivesicular bodies (MVBs) with the plasma membrane (5). Microparticles (MPs; Fig.1, middle panel), also known as microvesicles, are larger than exosomes measuring 100–1000 nm, and are the primary result of membrane blebs released from the surface of cells (1). Lastly, apoptotic bodies (APBs; Fig. 1, left panel) are larger cell derived vesicles, measuring up to 4000 nm, and are eponymously generated during cellular apoptosis (6).

Given their origin and release from cells, EVs are commonly endowed with a portion of membrane proteins, and in some APBs, genetic remnants of the parent cell (4). It is now generally accepted that EVs, such as platelet MPs, play a significant role in modulating normal physiological processes, such as coagulation (7) via expression of multifunctional cellular signaling proteins such as tissue factor (8). However, despite observations of elevated EVs in cancer patient plasmas (9) and other diseases (10), it has still not been determined whether they originate from tumors, whether they could serve as a rich

reservoir of biomarkers for disease detection and the role they play, if any, in disease progression.

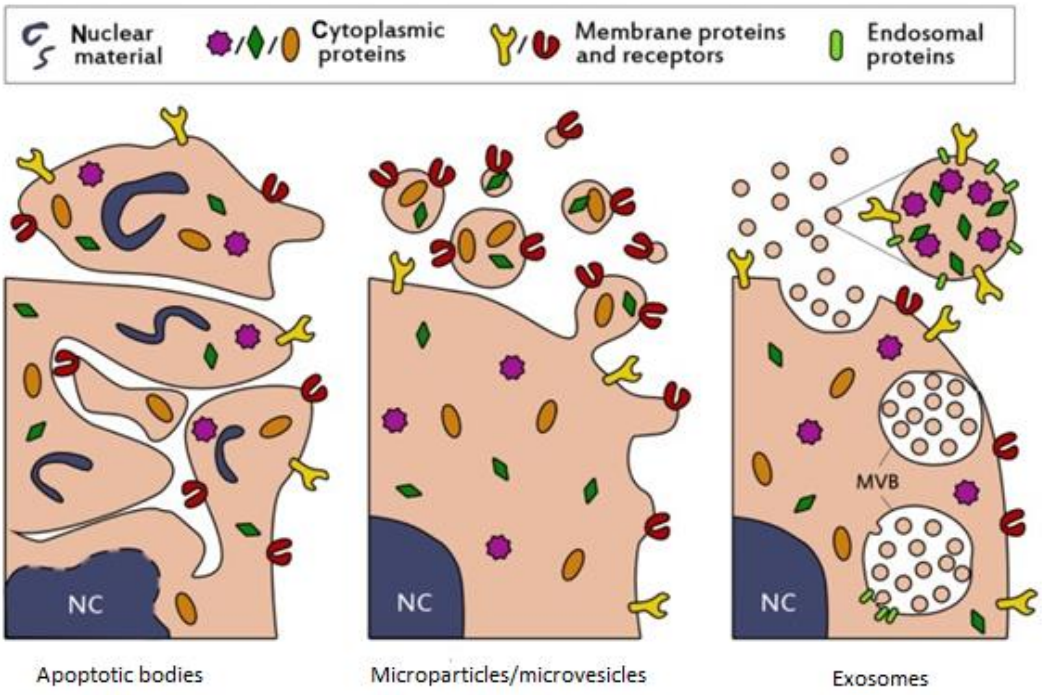

Figure 1. Schematic representation of the biogenesis of different extracellular vesicles.

The most common populations of extracellular vesicles found in biological fluids (saliva, plasma, semen, etc.) include apoptotic bodies (APBs, left panel), microparticles/microvesicles (middle panel), and exosomes (right panel). As an outcome of their biogenesis during cell apoptosis, APBs package a variety of cellular contents including DNA, RNA, and signaling molecules. During the process of cell membrane blebbing, membrane and cytosolic proteins are selectively packaged into microparticles/microvesicles (middle panel), resulting in the enrichment of specific proteins from the parent cell. Lastly, exosomes contain proteins that are primarily incorporated during formation of multivesicular bodies, such as tetraspanins CD9 and CD63. This figure was adapted from Kooijmans *et al.* (11).

1.2 Intercellular mode of communication

Heralded as an auxiliary means of signaling across vast cellular distances, the ability of EVs to transport oncogenic factors and regulatory RNA in a vesicle format has been a topic of intense debate that requires a rollback in perspective. First, classic examples of cell-to-cell communication are hormone-based paracrine signaling circuits. As a specific example, testosterone secreted by the testicles or adrenal glands into the circulation reaches the prostate to sustain gland viability. Testosterone, primarily in a soluble form, is an essential growth factor for prostate epithelium and only requires nanogram quantities to elicit a physiological impact. Upstream of this, an additional paracrine signaling circuit that relies on a brain–gland axis of communication represents another complex and sensitive means of cell-to-cell communication that occurs between the pituitary and testicles, in which luteinizing hormone is released into the circulation to induce testosterone production by Leydig cells.

In contrast to those classic examples, recent key studies have revealed processes by which EVs are able to interact with their target microenvironment, delivering various cargo types and facilitating cell-to-cell communication. As an example, leukocyte EVs are able to modulate endothelial cell activation by delivering pro-inflammatory agonists onto endothelial cells, resulting in the release of endothelium-derived cytokines and surface expression of ICAM-1, which is normally agonist-induced (12). Within an oncology context, glioblastoma cells have been shown to release EVs that express oncogenic factors such as EGFRvIII on their surface, impacting adjacent cells through vesicle–cell interactions (13). This represents the first description of ‘oncosomes’, wherein EVs that express transforming factors such as EGFRvIII are released from parental tumor cells via membrane blebs and merge with the plasma membranes of adjacent glioma cells lacking EGFRvIII receptor, resulting in the activation of transforming signaling pathways and alteration of EGFRvIII-regulated gene expression (13). Similarly, Peinado *et al.* (14) investigated the transfer of MET oncogene from tumor-derived exosomes to bone marrow progenitor cells, wherein exchange of MET oncogene induced the formation of a pro-angiogenic bone microenvironment and a pre-metastatic niche (14). Although both of these lauded studies suggest that EVs containing

oncogenic factors can accelerate oncogenesis or metastasis, the potency of these tumor-derived EVs falls far behind that of classic paracrine signaling mechanisms (pituitary-luteinizing hormone-leydig cells) because of the submilligram quantities needed to elicit a measurable effect *in vivo*. Hence, these observations may be overly optimistic given the field's lack of knowledge regarding the half-life of tumor-derived EVs and the propensity of the immune system to also release counteracting measures potentially in the form of exosomes.

Reports of nucleic acid transport via EVs have been the driving force for heightened awareness in EV research across many different disciplines. For example, Valadi *et al.*(15) recently demonstrated that RNA resident within exosomes derived from mouse mast cells was transferred to human mast cells, resulting in ectopic expression of mouse proteins in recipient cells (15). This advancement suggests that EVs are envoys between cells, able to deliver mRNA that can impact protein production in recipient cells of a measurable magnitude, akin to a hormone operating at the genetic level. Similarly, exosomes from colorectal cancer cells determined to be enriched with 15 mRNAs associated with M-phase processes of the cell cycle were delivered to healthy endothelial cells *in vitro*, subsequently stimulating the proliferation of recipient endothelial cells (16). Although the efficiency of this communication delivery system remains unclear, these findings suggest that EVs from malignant cells can facilitate the delivery of RNAs that encode factors responsible for cell proliferation. While it is unlikely that entire mRNA coding regions are transported via EVs, much smaller miRNA present within EVs are much more likely to be transferred (15). Studies of miRNA residing within EVs have dominated the field because of their regulatory nature and robustness against degradation. miRNAs are a family of small, non-coding RNAs (17–22 nucleotides in length) that regulate gene expression by degrading target mRNAs and nullifying translation of those target mRNAs (17). miRNAs can directly contribute to tumorigenesis through modulation of oncogenic or tumor suppressor pathways by targeting mRNAs of oncogenes or tumor suppressor genes to alter expression (18).

Given their impact and contributions to tumorigenesis, miRNA can also be used as biomarkers to identify patients with aggressive or life-threatening tumors in a non-invasive manner. As one example, Taylor and Gercel-Taylor (19) isolated exosomal miRNA from serum samples of patients with benign ovarian disease, patients with adenocarcinoma of the ovary and healthy volunteers to profile stage-specific miRNA-based biomarkers. The amount of total miRNA was significantly elevated in adenocarcinoma patients compared with patients with benign growth, and with minimal exosomal miRNA detected in healthy controls. The diversity or levels of most miRNAs was not significantly different between patients with early vs late-stage ovarian cancers, but expression profiles of exosomal and tumor cell-derived miRNAs were similar (19). In parallel, biomarker development for lung cancer has also resulted in a panel of miRNAs (20) validated as biomarkers for diagnosis and prognosis for this disease. As described previously in ovarian cancer patients, the total amount of exosomal miRNA was also elevated in patients with lung adenocarcinoma and low or undetectable in control samples. Most importantly, no significant differences were found when comparing miRNAs derived from circulating exosomes and miRNAs derived from lung tumors, indicating that exosomal miRNAs reflect the genomic identity of the tumor and can be used as a potential blood-based marker for lung adenocarcinoma. Hence, EVs derived from malignant cells may act as a system of miRNA transport to distant cells and used as a novel biomarker platform for cancer progression.

EVs generated by breast cancer cells have also been implicated in *de novo* miRNA processing and biogenesis due to the presence of Dicer, AGO2 and TRBP proteins within purified EVs (21). Overlooked in this same study is the contribution of EVs generated by other sources (endothelial, leukocyte and so on) that are present in the bloodstream with unknown miRNA content. If in fact miRNA biogenesis is exclusive to breast or breast cancer cells, this mechanism is unclear and conveniently specific to these sites and ultimately may not be applicable to prostate cells because these proteins are not present in prostasomes generated by the prostate (22). Studies like these continue to fall short in determining whether EV preparations are free of any plasma proteins, which could represent a source of the Dicer, AGO2 and TRBP detected. Currently, these studies

dominate currently published reports, lacking sufficient attention to the depletion of plasma proteins that continue to be present in purified samples. Although the use of atomic force microscopy is key to these evaluations (23), these reports still fail to examine the EV preparations at the nanoscale resolution to quantitate soluble protein contamination, marking these findings as suspect until further validations are performed.

1.3 Non-tumor derived EVs of physiological importance

1.3.1 Apoptotic bodies

Damaged, senescent and/or infected cells are often destined to undergo programmed cell death or apoptosis (Note to Sabine: some infections are lytic and cause necrosis, have to waffle a bit here or its an overstatement). This process is followed by degradation to maintain tissue homeostasis and a normal physiologic milieu (24). Although mechanisms of bleb formation are unclear during apoptosis, cells break apart and form membrane blebs called APBs, which can contain nucleic acids such as miRNA, mRNA or genomic DNA (25). Most importantly, APBs also display phosphatidylserine on their surface, an ‘eat-me’ signal for engulfment by phagocytes (for example, macrophages, dendritic cells) and some fibroblast cells in an immune silent manner (26,27). These APBs play key roles in adaptive immune responses in which self vs non-self antigens are processed for subsequent development of T- or B-cell-mediated immune responses, depending on the ongoing background of immune-based ‘danger signals’ in the body.

In cancer research, APBs have been shown to function as carriers for horizontal transfer of oncogenic DNA. In one such study, APBs transported oncogenic H-rasV12 and c-myc, to nearby normal mouse embryo fibroblast cells with a p53 knockout background (28), resulting in tumor-like growth and progression *in vitro*. Furthermore, phagocytosis of tumor APBs mediated by immature dendritic cells can induce immune tolerance by cross-presentation and activation of regulatory T cells (29), revealing a potential multifunctional role of APBs despite the lack of knowledge in this field.

1.3.2 Platelet MPs

The discovery of EVs occurred in parallel with the initial studies of blood coagulation, when researchers observed platelet-like activity in otherwise platelet-free serum samples (30). However, they were not formally described until the late 1960s, when Peter Wolf (31) used the term ‘platelet dust’ to describe small, membrane coated fragments he observed from activated platelets. Wolf considered these vesicles as by-products of platelet activation during storage, and concluded that coagulation activity in platelet-free samples was due to the action of ‘platelet dust’. The term ‘platelet dust’ was later replaced with ‘microparticles’ (32) and ‘exosomes’ (33), in which platelet MPs are membrane-derived and exosomes being the exocytosed storage granules (alphagranules, dense granules) of platelets. EVs, either MPs or exosomes, are secreted by platelets (34), endothelial cells (32) and leukocytes (33), and these types of cell fragments are relatively abundant in different bodily fluids (2). Through quantification of all circulating MPs *in vivo*, it is now understood that platelet EVs are the most abundant types of EVs, when compared with MPs from other circulating cells (10). Platelet EVs functionally contribute to coagulation and thrombosis because they are enriched in membrane receptors for key coagulation factors and prothrombotic proteins. For example, MPs derived from activated platelets express a high density of prothrombotic proteins on their surface, such as adhesive receptor P-selectins (8), plasminogen activator inhibitor-1 (PAI-1) and vitronectin (VN) (35), making thrombi resistant to fibrinolysis. In terms of cancer research, platelet EVs (MPs and/or exosomes) have been shown to promote tumor cell invasion *in vitro* by induction of MMP-2 synthesis in a prostate cell line (Clone-1) (36), but the impact of platelet MPs on several other prostate cell lines in vitro and in vivo is still unclear.

1.3.3 Endothelial MPs

Endothelial MPs are membrane-derived particles released upon apoptosis or necrosis, whereas endothelial EVs are likely exocytosed storage granules of endothelial cells, such as Weibel–Palade bodies, and are released upon activation by cytokine agents such as tumor necrosis factor-α (37). For example, in a study where human umbilical vein

endothelial cells were incubated with tumor necrosis factor-α and anti-tumor necrosis factor antibody, it was found that tumor necrosis factor-α elevated endothelial EV formations by a maximum of 2.5-fold within a 24-hour period (38). Recent studies have also demonstrated that neoplastic cells induce the release of endothelial EVs, revealing their potential as a novel biomarker for the detection of cancer and disease progression. For lung cancer, levels of circulating endothelial EVs were found to be significantly higher in lung cancer patients than in healthy control subjects suggesting that endothelial EVs may be involved in endothelial cell proliferation as occurs in angiogenesis (39), underscoring their pro-angiogenic effect in cancer progression. A subsequent study by this group examined the potential use of endothelial EVs for predicting 1- year mortality in patients with end-stage non-small cell lung cancer (34). In accordance with previous findings, the results of this study revealed that circulating levels of endothelial EVs were significantly higher in patients with 1-year mortality than in patients within the 1-year and above mortality category, demonstrating the potential of endothelial EVs as biomarkers for lung cancer prognosis (34). Yet again, these findings will require further research to validate endothelial EVs as a prognostic biomarker.

1.3.4 Leukocyte MPs

Leukocyte EVs are released by almost all immune cells when activated by inflammatory stimuli (40), further activating receptors on other leukocytes, resulting in the secretion of inflammatory and chemotactic cytokines. In detail, in *in vitro* co-cultures of leukocyte EVs with human umbilical vein endothelial cells, leukocyte EVs acted as inflammatory agonists on endothelial cells which resulted in the release of cytokines interleukin-6 and interleukin-8, and upregulation of leukocyte-endothelial cell adhesion molecules such as ICAM-1 (13). These findings suggest that circulating leukocyte EVs can activate a stress signaling pathway in endothelial cells, leading to an increase in pro-coagulant and pro-inflammatory activities.

Circulating leukocyte EVs have also been proposed as determinants for cardiovascular risk factors in asymptomatic subjects. Chironi et al. (37) examined the carotid, abdominal aorta and femoral arteries to measure levels of circulating MPs in a cohort of

asymptomatic subjects without previous cardiovascular diseases. Levels of leukocyte EVs were higher in subjects who carried atherosclerotic plaques in two or three sites compared with those without plaque at any sites. Therefore, the measurement of leukocyte EVs has demonstrated biomarker potential in cardiovascular disease in asymptomatic patients, thus offering encouraging signs of their application in other disease contexts but none as of yet with oncology although clearly applicable given the recent advances of immunotherapy for PCa treatment.

1.4 Limitation of previous methods of EV characterization and quantification

Several techniques have been described for the isolation and identification of EVs from different bodily fluid samples. Minimizing the amount of non-target EVs and other contaminants is a crucial step towards obtaining a homogenous mixture of EVs. Scientists have largely relied upon serial centrifugation and ultracentrifugation steps at increasing speeds and time intervals to isolate EVs from cells, proteins and large cellular debris (41). However, this method does not guarantee elimination of all non-target fragments from samples, resulting in enrichment, as opposed to purification of the desired EV population. This was presented by Mrvar-Brečko *et al.* (42), who reported that after several centrifugation steps, samples predominantly contained populations of unwanted cells mixed with EVs. This method is also time consuming, as it requires repeated centrifugation steps lasting hours. Immunoaffinity approaches that utilize paramagnetic beads conjugated with an antibody specific for antigens expressed on the surface of a target EV are rapid and more target-MP/exosome specific. Beads are mixed with the sample containing target cell fragments and passed through a column based magnet separation system (43). The vast majority of non-bead bound cells, non-target MPs and plasma proteins will pass through the column, whereas antigen-positive EVs bound to paramagnetic beads become indirectly immobilized to the column via magnets (44). For purification of prostate-derived EVs, magnetic beads can be conjugated with anti-CD9 or anti-prostate-specific membrane antigen antibody, and incubated with peripheral blood or platelet-poor plasma collected from PCa patients (44). This method is rapid and

customizable, in which the amount of ‘bait’ antibody used can be varied and the number of times the beads + EVs are washed can vary from two to eight times to fully eliminate plasma proteins and non-target EVs. Unfortunately, the major limitation of this method is the lack of bait antibodies available for target EVs and the cost of presently available ones.

Electron microscopy (EM) is a powerful method to visually characterize cell-derived vesicles, and scanning EM (SEM) is specifically used to visualize the morphology and relative size of platelet-derived EVs (31,42). In most cases, SEM can be used to visually differentiate EVs from erythrocytes and other circulating cells (42). SEM allows certain analyses that are not possible by other techniques such as determining whether objects are vesicular or proteinaceous by their ultrastructure; however, it does not quantify the concentration of vesicles isolated from a sample in a high-throughput manner. SEM also has significant drawbacks related to preparation of sample(s), with purified EVs inconsistently being immobilized onto the substrate (silica wafers or mica) for SEM imaging (32). Atomic force microscopy is another valuable tool that enables the determination of ultrastructure for all entities (EVs, plasma proteins) at an atomic resolution (23). Most recently, this technique was used to understand the ultrastructure of purified platelet MPs (23) and is the only instrument that offers information regarding protein contamination in purified EV fraction owing to its atomic level of resolution.

To enumerate EVs in any given sample, flow cytometry (FC)techniques would be best for quantitation of EV subpopulations given the multi-parametric nature of the technique. Hamilton and colleagues (45) first described the use of FC for detection of cell-derived vesicles released by human umbilical vein endothelial cells. The reliability of FC to characterize EVs has substantially improved despite previous ill-informed claims regarding the inability of optics to accurately acquire scatter of events smaller than 1 micron (μm). The emergence of nanoscale FC has made high-throughput, multi-parametric analysis of all events between 110 and 880 nm possible (46) regardless of the incident wavelength of light used. Using the nanoscale flow cytometer Apogee A50-Micro, polystyrene microspheres and silica-based beads can be size-resolved based on

100 nm increments (47), revealing the potential of this instrumentation to become first in class for analysis of MPs in complex biological mixtures (48).

1.5 A nanoscale based approach to EV purification and evaluation

In Figure 2, we present an idealized approach to purifying EVs, such as MPs, microvesicles and exosomes. The sequence of techniques proposed is important because they will allow the experimenter to evaluate their preparations at a nanoscale resolution while analyzing each EV as a single discrete event. First, either plasma, serum or urine can be used as the starting material and submitted to isolation or purification with the three main techniques. Technique selection for purification is dependent on the resources, instrumentation and amount of starting material available to the experimenter. We recommend immunoaffinity based approaches to generate ultra-pure preparations of antigen specific EVs, such as prostasomes or prostate cell fragments. Immunoaffinity-based approaches also enable the experimenter to 'wash' their sample repeatedly prior to elution, to maximally reduce the presence of non-target EVs and plasma or urine proteins. The first evaluation step should focus on the enrichment ratio of target EVs vs non-target EVs. In the case of PCCFs, nanoscale FC is recommended because all EV events in the sample will be evaluated and the percentage of events that bind the prostate biomarker can be used to infer enrichment. With exosomes, dynamic light scattering instruments must be used because nanoscale FC cannot analyze events smaller than 100 nm in diameter. Although this is the ideal instrument for that purpose, it does not inform the user of the target vs non-target EV ratio unless single fluorescence channel dynamic light scattering instruments are used. If these instruments are not available, then ELISA followed by sequential western immunoblotting is recommended. Finally, if an EV preparation is maximally enriched for target EVs, then the next step is to determine the extent of plasma protein 'contamination' in the sample. This is significant because of the potential for soluble RNA/DNA and miRNA–protein complexes to be present outside and alongside the EVs in the preparation. The definitive instrument to determine the contribution of EVs vs contaminating protein would be atomic force microscopy. Atomic

force microscopy eliminates all washing and processing of the sample and can be performed ‘dry’, wherein the solvent is dried off, leaving behind only EVs, ions and proteins. Owing to its atomic resolution, all events can be volumetrically analyzed, with events smaller than 100 nm in diameter quantitated and compared with much larger structures such as MPs. Alternatively, if there are suspicious ultra-structures present in the sample, SEM can be performed to determine whether the structure is vesicular in structure, or a protein aggregate. By following this scheme, an experimenter can readily purify EVs with the full knowledge of the contribution of non-target EVs and contaminant proteins and nucleic acids present in the purified sample.

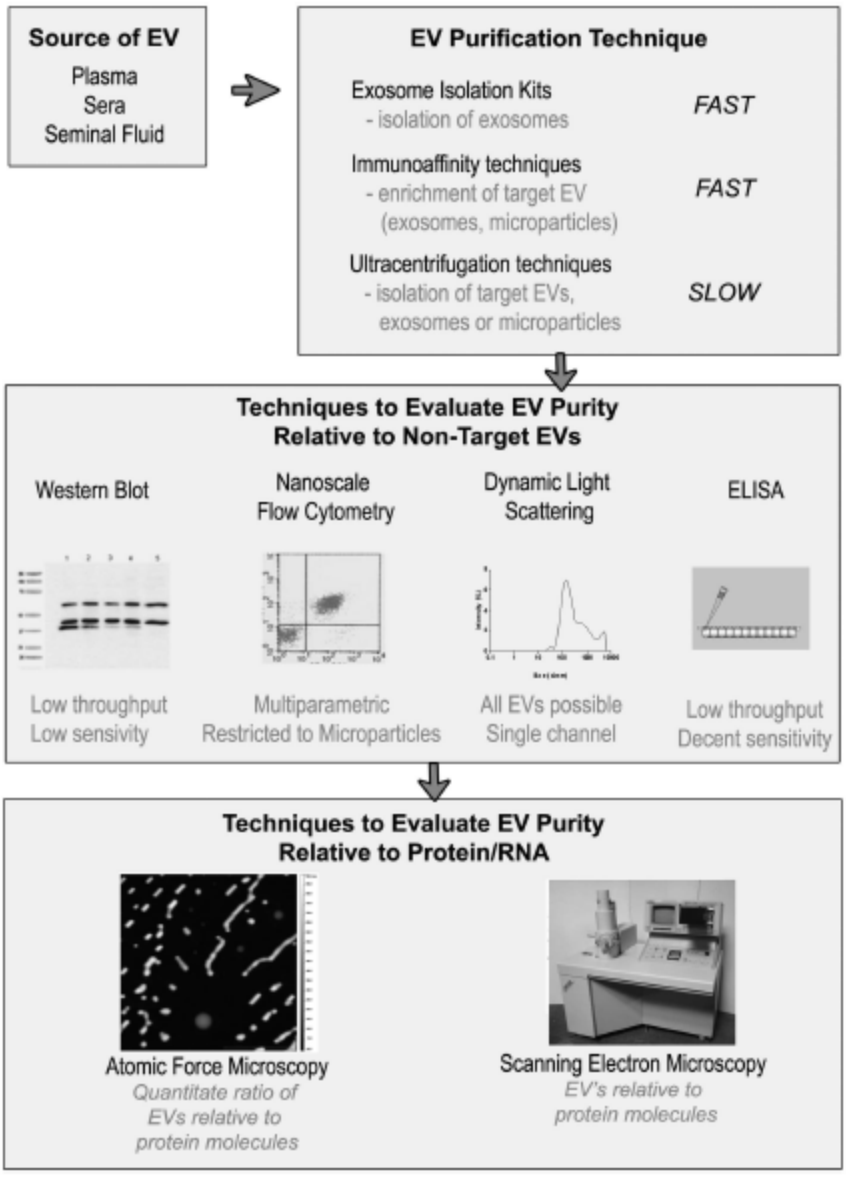

Figure 2. Summary of purification and evaluation strategy for extracellular vesicles (EVs) from biological samples.

This scheme can be used to isolate and evaluate EVs from plasma, sera or seminal fluid. Various techniques can be used to isolate EVs based on size, immunoreactivity to antibodies, or samples can be sent out for purification by third party vendors. Once purified, the experimenter may wish to consider the proportion of target EVs to non-target EVs using western blot, nanoscale flow cytometry, dynamic light scattering or ELISA. After determining the extent of non-target EVs in the sample, a second set of

techniques to determine the extent of contamination from non-EV proteins can be performed using either atomic force microscopy or scanning electron microscopy which can readily distinguish EVs from protein based on size.

1.6 Current state of prostate cancer diagnosis

Prostate cancer is the most commonly diagnosed visceral cancer among Canadian men. In 2016 it accounted for 21% of all newly diagnosed cancers, and for ~ 10 % of all cancer-related deaths among men in Canada (72). This translates to 65 Canadian men being diagnosed and another 11 dying from PCa every day. The prostate specific antigen (PSA) testing continues to be heavily relied upon as a monitoring and prognostication tool; however, it is produced and secreted by both normal prostate epithelium and PCa into the circulation (4). For this reason, PSA-based screening is discouraged for screening of PCa because of its low specificity, which means that a high number of PCa cases are of a low-risk phenotype forcing men to undergo painful and repeated biopsies to ensure the tumor has not upstaged (73). Most of the time, PSA acts as a "red flag" that causes considerable anxiety for a patient until the definitive prostate biopsy is taken and examined by a pathologist (3). Prostate biopsy is the gold standard for diagnosis, as it provides very important histological information regarding the 5 different patterns of acinar arrangement and glandular characteristics for grading the tumor with the Gleason Score (GS) system. Gleason grade 1 represents the most well-differentiated lesion, whereas Gleason grade 5 represents the most poorly differentiated lesion, and hence a highly aggressive phenotype of PCa. The most predominant lesion in the specimen also known as the primary pattern or first number of the GS, and the second most common pattern in the specimen (the secondary pattern) becomes the second number of the score. Thus, the Gleason score is the sum of two grades. Only Gleason grade 3, 4, and 5 are considered histologically and clinically relevant, therefore only a GS of 6 and higher is considered to be PCa. However, only GS ≤ 7 is regarded as clinically significant prostate cancer, whereas GS 6 prostate cancer is considered low-risk (73). The recommendation options for most patients with Gleason Score 6 PCa is active surveillance, which requires regular PSA testing, physical examination and periodic biopsy to determine if the cancer has "upstaged" or progressed (74). However, repeated biopsy also submits patients to potential complications such as hematuria, rectal bleeding, and urinary tract infection with rare cases leading to mortality (75). Also, PSA levels do not correlate with the Gleason score of a given cancer (76). Currently, there is a need for new diagnostic tools

to accurately identify patients with aggressive forms of PCa from those with low-risk disease.

1.7 Prostate MPs

The first studies on prostate EVs in 1977 by Ronquist and Hedström (49) described vesicles generated within prostate epithelial cells and released via exocytosis into seminal fluid. These EVs were subsequently termed ‘prostasomes’ (50). In seminal studies comparing prostasomes from both benign and malignant prostate cells, no significant differences were reported regarding synthesis and release of these prostate-derived EVs (51). Although there are few reports describing prostate cell MPs in healthy individuals, the presence of prostasomes in prostate cancer (PCa) patient plasmas continues to be a translational cancer research focus (51).

1.7.1 Prostasomes

These vesicles range in size from about 50–500 nm, originate from prostatic epithelial cells and are present in seminal fluid and post prostatic massage urine (50,51). These EVs have been shown to protect sperm within the female reproductive system, in which cytotoxic interactions between prostasomes and natural killer cells significantly reduce natural killer cells’ activity to prevent immune-mediated sperm destruction (52). Prostasomes represent a novel cancer biomarker platform because of their release by malignant prostate cells into seminal fluid and blood (53).

Tavoosidana *et al.* (54) suggested that the levels of prostasomes reflect disease severity, based on the detection of prostasomes in blood samples from patients with PCa and high Gleason score, whereas levels of prostasomes were reduced in samples from patients with low Gleason score and benign prostatic disease or indolent PCa (54). Despite the small sample size in this study, it demonstrated that prostasomes can be detected in patient blood, and have the potential to distinguish aggressive PCa from low-risk or benign disease (54).

1.7.2 PCa cell fragments

The potential of prostate cancer cell fragments (PCCFs) to serve as a diagnostic biomarker platform for PCa is a topic of intense research effort because they are independent of other serum-based biomarkers currently used for detection of PCa, such as prostate specific membrane antigen (PSA), which is not specific for PCa (4).

Currently, there is a lack of agreement regarding the best purification strategies for PCCFs, as well as which biomarkers should be used to characterize PCCFs. Recent attempts to discover suitable surface markers specific for PCCFs, which relied on proteomic analysis of isolated PCCFs present in the serum of mice grafted with human PCa xenografts, identified putative biomarkers such as RAB5A and RAB11A (55). Other cell-line-dependent studies reveal a higher abundance of proteins such as FASN in cell fragments derived from PC346C and VcaP cells (4). Many of these reported biomarkers have not been clinically validated, either in serum or plasma samples, or cross-referenced with databases, underscoring the need to substantiate biomarkers beyond the initial discovery phase. An approach that enumerates PCCFs based on a multi-parametric technique may also improve sensitivity and accuracy if criteria are based on superimposition of both prostate-specific and cancer-specific biomarkers on the same PCCF. Clearly, PCCFs present an extracellular source of prostate-specific membrane antigen reflecting a prostate cell origin (56,57) and should be the initial ‘capture’ biomarker for assaying other cancer-specific biomarkers. Other antigens specific to prostatic tissue that could potentially be used are STEAP1 (58), STEAP2 (59), and PSCA (60); however, their utility remains unclear owing to the lack of reagents such as flow cytometry (FC)-compatible antibodies available for each of these putative prostate-specific biomarkers.

Aside from their putative abundance in patient biofluids, PCCFs, also termed 'large oncosomes', are also postulated to play a role in disease progression and metastasis (61). Oncosomes, ranging from 1μm to 10μm in size, can be identified histologically in tumor tissue sections. Additionally, they exhibit gelatin-degrading proteolytic activity by the proteases they contain, such as metalloproteinases (MMP9 and MMP2) (61). As these

proteases are commonly associated with tumor cell invasion, oncosomes may serve to concentrate proteases that assist tumor cell migration (61). Provided that oncosomes are stable in the tumor microenvironment and in serum, they in turn could harbor clinically valuable biomarkers to identify patients with intermediate to high-risk PCa in a noninvasive blood-based manner.

Currently superseding PCCFs as biomarkers, are circulating tumor cells (CTC), characterized by co-expression of EpCAM and various cytokeratins in nucleated cells present in a 7–10 mL blood sample collected from patients. CTCs are thought to be generated by the release or entry of tumor cells into circulation during the intravasation step of the metastatic cascade (62). CTC enumeration via the CellSearch Instrument (63,64) is currently the gold standard for prognostication of patients with metastatic PCa (65). However, enumeration of CTCs is not a prognostic tool for localized PCa patients owing to the low CTC counts even in patients undergoing salvage radiation therapy (66). Despite the low abundance of CTCs in patient blood samples (67), several key studies have shown that CTC enumeration can distinguish PCa patients from healthy volunteers (68).

Emerging clinical data suggests that biomarkers derived from plasma exosomes can similarly differentiate PCa patients exhibiting high and low Gleason scores (GS) from those with BPH and healthy individuals. Specifically, exosome-associated Survivin is highly expressed in plasma samples from PCa patients with Gleason score of 6 and 9, whereas the expression of this protein is significantly lower in BPH and healthy donor plasmas (69). However, levels of Survivin were not significantly different between the PCa patients with different GS (6 vs 9), highlighting the need for biomarkers which are Gleason score-specific. Other EV types such as tumor derived microparticles may offer an equivalent, if not improved means of prognosticating PCa recurrence given the large numbers of these submicron entities within patient plasma samples with metastatic disease (68). Clearly, Coumans and co-workers (68) found that tumor cell MPs and tumor cell fragments are other types of extracellular vesicle subclasses that can yield important prognostic information with a large dynamic range, that is highly amenable to blood

based testing. Various genomic tests for prognostication of early biochemical recurrence in localized PCa patients have also prompted the notion that these biomarkers in combination may be present in or on tumor MPs generated by the primary tumor (70). However, transposing transcriptome-based biomarkers into a protein positive EV-based format may be challenging given that some of these biomarkers are downregulated or absent in the target pathology (70).

Alternative, more promising approaches may be based on the presence of microRNAs (miRNAs) within prostate-derived EVs that are specific to each Gleason grade, or associated with early biochemical recurrence in patients post prostatectomy or radiation therapy. Such is the case for miRNA-34a, whose expression within EVs in patient plasma is predictive of sensitivity to first-line treatment with Docetaxel (71). These studies are correlative and although suggestive of a pathogenic mechanism, further investigation is required to conclusively demonstrate compartmentalization of miR-34a within prostate derived EVs or whether they are derived from other non-cancer sources (71). Nonetheless, their promise as biomarkers of cancer progression is tantalizing and reflects a world-wide intensified effort towards understanding EV biogenesis and their ability to mediate intercellular communication during cancer progression.

1.8 Extracellular vesicles such as prostate cancer cell fragments as a fluid biopsy for prostate cancer

Research to discover new diagnostic biomarkers that could differentiate patients with indolent, or low-risk PCa, from those with high-risk disease has not significantly progressed, but the need for a non-invasive test for monitoring PCa patients is of great clinical value. PCCFs are an attractive biomarker platform for detecting PCa, as these fragments originate from prostate epithelium or from malignant cells within the primary tumor and are released into the blood circulation (76). Moreover, it has been previously shown that significant quantities of PCCFs are detectable in samples from PCa patients, but are not detected in healthy individuals (61).

1.9 Thesis hypothesis and objectives

The goal of this project is to find biomarkers on the surface of PPCFs that could differentiate patients with high-grade PCa from those patients with low-grade disease. It is our hypothesis that PCCFs from patients with low grade prostate cancer (GS 6) will express different biomarkers than those found on PCCFs from patients with high grade prostate cancer (GS 8). The following objectives will be pursued in order to reach my goal.

1. To isolate PCCFs from patient plasmas representing low-grade prostate cancer (GS6) and MPs from patient plasmas representing high-grade prostate cancer (GS8) using an immunoaffinity isolation protocol developed by our lab.

2. To assess the enrichment of these isolated PCCFs samples using a nanoscale flow cytometry and atomic force microscopy

3. To perform proteomic and bioinformatics analysis of isolated PCCFs to identify biomarkers that differ between GS6 and GS8 patients, which could help to more accurately diagnose patients with indolent disease from those with an aggressive form of PCa.

Chapter 2

2 Materials and Methods

2.1 Patient plasma

Prostate cancer (PCa) patient plasmas samples were attained through the Ontario Institute for Cancer Research Tumor Bank and the University Health Network Genitourinary BioBank (Toronto, ON) under Western University Research Ethics Board (REB) approved Ethics Applications # 103156 and 103409. Only samples from patients with a minimum of 3 years' follow-up were included to avoid patients that upstaged/upgraded during that time. Whole blood was collected into CellSave vacutainers (10mL volume, Janssen Diagnostics Inc.). To prepare plasma from whole blood for prostate microparticle analysis, whole blood was collected in K2-EDTA Vacutainers (BD Biosciences Inc.) and spun at 1500 × *g* for 10 minutes. The plasma layer was removed, aliquoted and then stored at -80 ˚C.

2.2 Antibodies and isotype controls

Antibodies and isotype controls used in nanoscale flow cytometry and immunoaffinity isolation techniques have been compiled in Table 2.

2.3 Buffers and reagents

Buffers used in the purification of proteins and experiments have been compiled in Table 3.

Table 1: Summary of antibodies and isotype controls used in this study

Antibody	Used in	Isotype Control
STEAP1 clone J2D2 (Abcam; CA# ab117454).	Protein G Immuno-isolation/ Nanoscale flow cytometry/immunostaining	IgG_{2b}
PSMA clone 3/E7 (Dr. Philipp Wolf, University Medical Center Freiburg, Germany)	Magnetic immunoaffinity isolation/ Nanoscale flow cytometry/immunostaining	IgG1κ

Table 2: Summary of buffers used in this study.

Buffer Name	**Used in**
IP Buffer (ThemoFisher CA#: 28379)	Protein G IP
Elution Buffer, (ThermoFisher, CA#: 21004)	Protein G IP
NuPAGE® Sample Reducing Agent (10X) (Life Technologies, CA#: NP0009)	Western blot
NuPAGE® LDS Sample Buffer (4X) (Life Technologies, CA#: NP0008)	Western blot
NuPAGE® MES SDS Running Buffer (20X) (Invitrogen, CA#: NP0002)	Western blot
Chemiluminescence agent Luminata Classico Western HRP substrate (EMD Millipore, CA#: WBLUR0500)	Western blot

2.4 Confirmation of the sizing resolution of the apogee A50-micro nanoscale flow cytometer

Silica microspheres (Apogee FlowSystems Inc.) of varying diameters (110 nm, 179 nm, 235 nm, 304 nm, 585 nm, 880 nm, 1300 nm) were analyzed using the A50-Micro Nanoscale Flow Cytometer (Apogee FlowSystems Inc.). These beads were diluted 1:10000 prior to analysis on the A50-Micro Nanoscale Flow Cytometer.

2.5 Immunoaffinity isolation of prostate cancer cell fragments (PCCFs) from patient plasma with PSMA

To isolate PCCFs from PCa patient plasma (n=10/Gleason score), the Miltenyi Biotec MidiMACS system was used in which 100µL of plasma was incubated at 4 ºC for 30 minutes with 10 µL of biotinylated anti-PSMA antibody. Subsequently, the plasma was diluted in 90 µL of dH_2O and then incubated with 20 µL of Streptavidin microbeads (Miltenyi Biotec; CA#130-048-102) for an additional 20 minutes at 4 ºC. The sample was then diluted in 1 mL of dH_2O, passed through a MACS- LS separation column which was attached to a magnetic field. This step was repeated 3 times (Miltenyi Biotec; CA#130-042-401). The column was then removed from the magnetic field and the PSMA positive PCCFs were eluted twice with 1mL of dH_2O. The eluent was then passed through another magnetic column, and a final elution step was done with a total of 600 µL of dH_2O.

2.6 Tandem immunoaffinity isolation of PCCFs with Protein G agarose beads

The Protein G agarose beads were first to STEAP1 antibody in a microcentrifuge tube. Briefly, 200 µL of Protein G agarose slurry were added to 10 µL of the STEAP1 antibody; the mixed was incubated overnight at 4°C. For the tandem isolation method, 50 µL of Protein G-STEAP1 agarose bead slurry was added to 600 µL of the PCCF samples previously isolated using the biotinylated-PSMA method, and the reaction was incubated with gentle mixing for 1 hour at room temperature. To wash the bead-PCCF immune complex, 100 µL of IP Buffer was added, incubated at room temperature for 5 minutes

and subsequently centrifuged for 5 minutes at 2500×*g*; the supernatant was discarded. The IP Buffer wash step was repeated a total of 3 times. To elute the PCCF's attached to the agarose beads, 100 µL of Elution Buffer was added to the beads and incubated for 5 minutes. The tube was centrifuged for 5 minutes at 2500 × *g* and the supernatant was collected. This step was repeated a total of 2 times and the two supernatant fractions were collected and combined. The pH of the eluate was adjusted to physiological pH by adding ~10 µL of a 1M Tris-HCl (pH 7.5-9), per 100 µL of eluate.

2.7 EV isolation from patient plasma using exosome isolation kits

The EV fraction from PCa patient plasma were purified using the following kits: ExoQuick-TC™ (EQ, System Biosciences Inc.; Mountain View, CA), ExoSpin™ (Cell Guidance Systems LLC.; Carlsbad, CA), and Total Exosome (Life Technologies Inc.; Burlington, ON), with some modification to the manufacturer's recommendations.

2.7.1 ExoQuick-TC™

To prepare the plasma for exosome precipitation, 100 µl of the sample was centrifuged at 3000 × *g* for 15 minutes. The plasma samples were pre-treated with 1 µl of [500U/mL] thrombin to make them compatible with ExoQuick exosome precipitation kit. The mixture was incubated at room temperature for 5 minutes while mixing by gently flicking the tube, then it was centrifuge in a standard microfuge at 10,000 x *g* for 5 minutes. The supernatant was transferred to a new clean tube and treated with 25µl of ExoQuick reagent to precipitate exosomes, and incubated for 60 minutes at 4°C. The ExoQuick/biofluid mixture was centrifuged at 1500 × *g* for 30 minutes, the supernatant was carefully aspirated, and the pellet was resuspended in 100µl of dH_2O and stored at -20°C.

2.7.2 ExoSpin™

100µl of plasma was centrifuged at 300 × *g* for 10 minutes to remove cell debris. The supernatant was transferred to a new microcentrifuge tube and spun at 20,000 × *g* for 30 minutes. The supernatant was transferred to a new microcentrifuge tube and 50µl of Buffer A was added and incubated at 4°C for 5 minutes, and then centrifuged at 20,000 x *g* for 30 minutes. The supernatant was carefully removed and discarded, and the exosome-containing pellet was resuspended in 50 µl of dH_2O and stored at -20°C. The supplied column was prepared by spinning it down at 50 x *g* for 30 seconds to remove buffer from the top of the column and allowing it to enter the column bed. To wash the column, 200µl of dH_2O were added to the top, and spun down again at 50 x *g* for 30 seconds. The exosome-containing sample was added to the column and centrifuged at 50 x *g* for 60 seconds. This step was repeated once more, and the resulting eluate containing the purified exosomes was stored at -20°C.

2.7.3 Total Exosome™

100µl of plasma was centrifuged at 2000 × *g* for 20 minutes at room temperature. The supernatant containing partially clarified plasma was transferred to a new tube without disturbing the pellet, and centrifuged at 10,000 × *g* for 20 minutes at room temperature. The clarified plasma was placed in a new tube without disturbing the pellet, 50 µL of dH_2O was added and mixed thoroughly by vortexing. 30 µL of the Exosome Precipitation Reagent (from plasma) was added to the sample, mixed by vortexing, and incubated at room temperature for 10 minutes. The sample was centrifuged at 10,000 × *g* for 5 minutes at room temperature. The supernatant was removed and discarded and the remaining exosome pellet was resuspended with 50 µL of dH_2O, and stored at -20°C.

2.8 Enumerating the PSMA positive populations of PCCFs

To enumerate the populations of PCCFs in patient plasma, a phycoerythrin (PE) labelled antibody directed against PSMA (PSMA-PE) was incubated with the plasma samples. To

stain for detection of the PCCFs, 1 µL of the antibody was added to 10 µl of plasma, incubated in the dark for 30 minutes, then diluted with 290 µL of PBS and analyzed on the Apogee A50-Micro nanoscale flow cytometer. The negative isotype control mouse IgG-PE was performed in parallel following the same incubation conditions. Gates for the PCCF population were established by analyzing the isotype control first, and then analyzing the antibody labeled samples.

2.9 Nanoscale flow cytometric detection of dual positive PCCF populations

For detection of dual positive PCCF populations, the same protocol as section 2.8 was followed with some modifications. In brief, 10µl of patient plasma was incubated with 1µl of anti-PSMA-PE and 2 µL of anti-STEAP1-Alexa 647 antibody at room temperature in the dark for 30 minutes. The negative isotype controls were utilized in parallel following the same incubation conditions. Samples were diluted with 290 µL of PBS and analyzed on the Apogee A50-Micro nanoscale flow cytometer. Gates for each microparticle population were established by analyzing the isotype control first, modifying the gains for each PMT as necessary, and then analyzing the antibody labeled samples.

2.10 Atomic force microscopy

Exosome suspensions and PCCFs were diluted in dH_2O ratios of 1:10, 1:1000, and 1: 10,000. From these diluted samples, a volume of 2 µL was placed and adsorbed to a freshly cleaved mica coverslip (Ted Pella, Inc.; Redding, California) and dried in an oven at 60ºC for 5 minutes. Samples were analyzed with the Veeco Dimension 3100 Nanoman AFM (Veeco Metrology, LLC; Santa Barbara, California) in tapping mode. Topographic height and phase images were recorded at 256×256 pixels at a scan rate of 1 Hz. Image processing was performed with Gwyddion Data Processing software, version 2.40 (Department of Nanometrology, Czech Metrology Institute; Brno, Czech Republic).

2.11 Western blotting

For protein extraction, isolated PCCFs were lysed in a master mix of reducing sample buffer at a 10X concentration, and LDS sample loading buffer at a 4X concentration. Samples were boiled for ~10 minutes at 90 ºC. Cellular proteins from LNCaP and PC-3M-LN4 cell lysate were also extracted following the previously described steps. To separate the PCCF and cellular proteins, 10 µg were loaded onto a NuPAGE® Novex® 4-12% Bis-Tris Gels (Invitrogen, CA#: NP0321BOX) and electrophoresed at 200V for 1 hour. Transfer of the gels to a polyvinylidene difluoride transfer membrane (Thermo Scientific, CA#: 88518) was done at 30V for 1 hour. Blocking of the membrane was done in 5% powdered milk in TBS-T for 1 hour at room temperature. Membranes were probed using primary antibody STEA1 or PSMA, overnight in 4°C at a dilution ratio: 1:500, and then with horseradish peroxidase conjugated-second antibody for 1 hour at room temperature (Sigma Aldridge, CA#: NXA931-1ML) at a ratio of 1:2000. Protein bands were detected by using an enhanced chemiluminescence HRP substrate, incubated for 5 minutes at room temperature, and the membrane was developed using the Bio-Rad ChemiDoc™ MP System (Bio-Rad Laboratories Inc., Hercules, CA).

2.12 Mass spectrometry and proteomic analysis of PSMA isolated samples

This process was contracted out to the Campus Chemical Instrument Center (CCIC) Mass Spectrometry and Proteomics Facility at The Ohio State University (Arpad Somogyi, PhD - Associate MS&P Facility Director; http://www.ccic.ohio-state.edu/msp)

2.13 In-solution digestion

2.13.1 List of solution

Solutions prepared for in-solution digestion have been compiled in Table 4.

Table 3: Summary of solutions used for in-solution digestion.

Concentration	Preparation
200 mM Dithiothreitol (DTT)	0.03086 g of DTT in 1000 µL of 100mM NH4HCO3
1M iodoacetamide	Add 0.037 g of iodoacetamide to 200 µL of 100mM NH4HCO3
Buffer A	25 µL of Acetonitrile + 50 µL 0.1% formic acid + 25 µL ddH_2O
Buffer B:	1 µL formic acid + 1000 µL ddH_2O

2.13.2 Sample preparation and disulfide reduction

Samples were first prepared by adding 1 uL of a 100mM NH_4HCO_3. In order to bring samples to 100 µL, dH_2O was added if needed. To reduce the sample, 5 µL of 200mM DTT were added to the sample, which was subsequently boiled for ten minutes.

2.13.1 Sulfhydryl alkylation

To alkylate the sample, 4 uL of the iodoacetamide stock was added to the sample and vortexed, followed by brief centrifugation in a microcentrifuge to get the sample to the bottom of the tube. The sample was incubated 1 hour at room temperature.

2.13.2 Stopping alkylation

To neutralize the remaining iodoacetamide, 20 µL of DTT stock was added to each sample, which was then vortexed and incubated at room temperature for 1hour.

2.13.3 Trypsin digest

For trypic digestion, each sample was gently vortexed and trypsin was added at a 1:20 ratio (1mg of trypsin for every 20mg of sample). To allow complete digestion, the sample was placed in a 37°C water bath overnight.

2.13.4 Sample clean-up

The SPE cartridges (HyperSep™ C18 columns - 50mg resin, Thermofisher CA: #60108-390) were prepared by first washing the column 3 times with 1mL of Buffer A, then 3 times with 1 mL Buffer B, eluting the flow through into a waste beaker. Subsequently, the samples were acidified with 0.2% formic acid and passed over the SPE cartridge twice. The unbound components were washed off the column with 1 mL of Buffer B 3 times. The peptides were then eluted off of the column with 400 µL of Buffer A. To reduce the volume of the samples and remove the acetonitrile, samples were concentrated using a Speed-Vac.

2.14 Mass spectrometry and proteomic analysis of tandem isolated samples

This process was contracted out to the Biological Mass Spectrometry Laboratory at the University of Western Ontario (Director: Prof. Gilles A. Lajoie; http://www.uwo.ca/biochem/bmsl/)

Chapter 3

3 « Results»

3.1 The A50-micro nanoscale flow cytometer analyzes events within the submicron size range, and detects PSMA positive extracellular vesicles

The A50-Micro nanoscale flow cytometer (NFC; Apogee Flow Systems, Hertfordshire, UK) is reported by the manufacturer to be capable of high-throughput and multi-parametric analysis of events between 100-1000 nm, resolving various sizes of calibration beads based on large angle light scatter (LALS) and small angle light scatter (SALS). We ran silica beads of various diameters, 110 nm, 179 nm, 235 nm, 304 nm, 585 nm, 880 nm, 1300 nm (Fig. 3A-B), though the A50-Micro NFC. The analysis of these beads show that the A50-Micro has the ability to analyze events within the submicron size range, resolving discrete subpopulations when analyzed together.

The corresponding analysis of PCa patient plasma with the A50-Micro nanoscale flow cytometer (Fig. 3C) demonstrate that when the plasma is incubated with an anti-PSMA-PE antibody, a subpopulation of prostate cancer cell fragments (PSMA positive PCCFs) is observed and determined to be within the 110-304 nm diameter size range (red box). This population is distinct from other particles in the sample, which are PSMA negative (blue box), in both size and immunofluorescence. When the isotype control mouse IgG1$_{\kappa}$-PE was incubated with PCa patient plasma, a minimal number of events were recorded (Fig. 3D, red box).

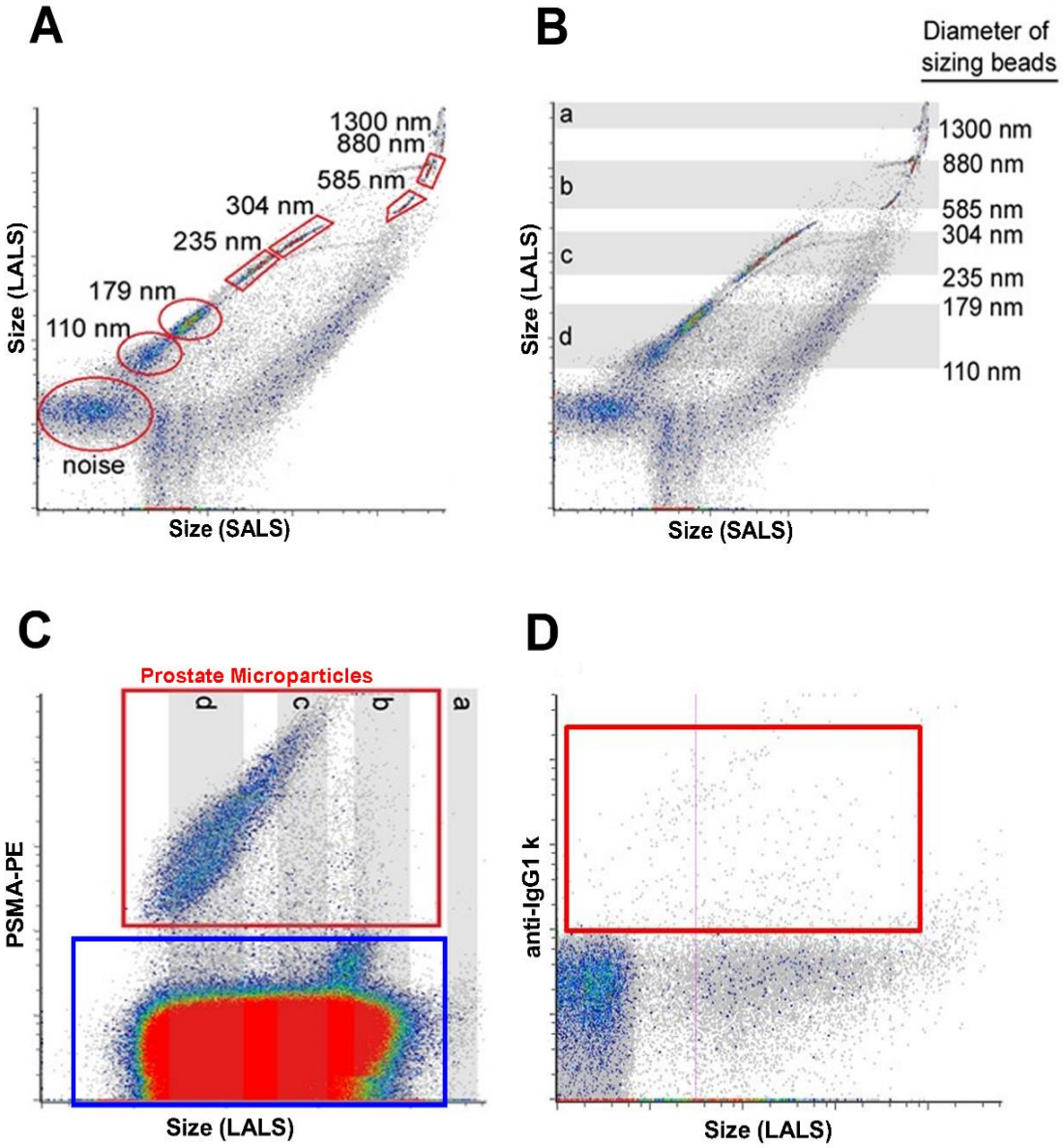
A
1300 nm
880 nm
585 nm
304 nm
235 nm
179 nm
110 nm
noise
Size (LALS)
Size (SALS)
B
Diameter of sizing beads
a
b
c
d
1300 nm
880 nm
585 nm
304 nm
235 nm
179 nm
110 nm
Size (LALS)
Size (SALS)
C
Prostate Microparticles
d
c
b
a
PSMA-PE
Size (LALS)
D
anti-IgG1 k
Size (LALS)

Figure 3. Nanoscale flow cytometry analysis of sizing beads and PCa patient plasma measure events within the submicron range.

The Apogee A50-Micro nanoscale flow cytometer is able to readily analyze events within the submicron range based on the analysis of silica beads of various diameters (A and B). When patient plasma is incubated with anti-PSMA-PE antibodies, a subpopulation of PSMA positive PCCFs are observed within the 110-304 nm diameter size range (C). Isotype control IgG1$_{\kappa}$-PE incubated with patient plasma does not detect a significant number of events (D).

3.2 Immunoaffinity isolation using PSMA antibodies enriches extracellular vesicles from prostate cancer patient plasma

The immunoaffinity method for PCCF isolation (Fig. 4A) utilizes a biotinylated PSMA antibody and a streptavidin conjugated magnetic bead to separate PSMA positive PCCF's from other plasma components, such as cell debris and non-target MP's. When patient plasma is incubated with the biotinylated PSMA antibody and streptavidin beads and subsequently passed through a magnetic field, the magnet attracts the PSMA positive PCCFs, while other plasma components which are PSMA negative are not retained, resulting in concentration and recovery of PSMA positive PCCFs.

The enrichment evaluation of immunoaffinity purified PCCFs from patient plasma shows the relative abundance of PSMA-PE positive PCCF's (red box) compared to the total events of other non-target MPs (grey shaded areas) in plasma before PSMA immunoaffinity isolation (Fig. 4B), within the first elution fraction (Fig. 4C), and within the second elution fraction (Fig. 4D) from the same plasma sample. The population events of non-target MP's and other cell debris is greater in plasma samples before immunoaffinity purification, when compared to PSMA positive PCCFs. After the first elution, the non-target MP population is significantly reduced relative to the PSMA positive PCCFs. After the second elution, a greater reduction of non-target MPs is observed, and PCCF events. The relative abundance of PSMA positive PCCFs shows the enrichment of this populations after isolation. In patient plasma (B), PSMA positive events account for 1.1% of all events. After the last elution fraction (D), 21.5% of the overall events are PSMA positive PCCFs.

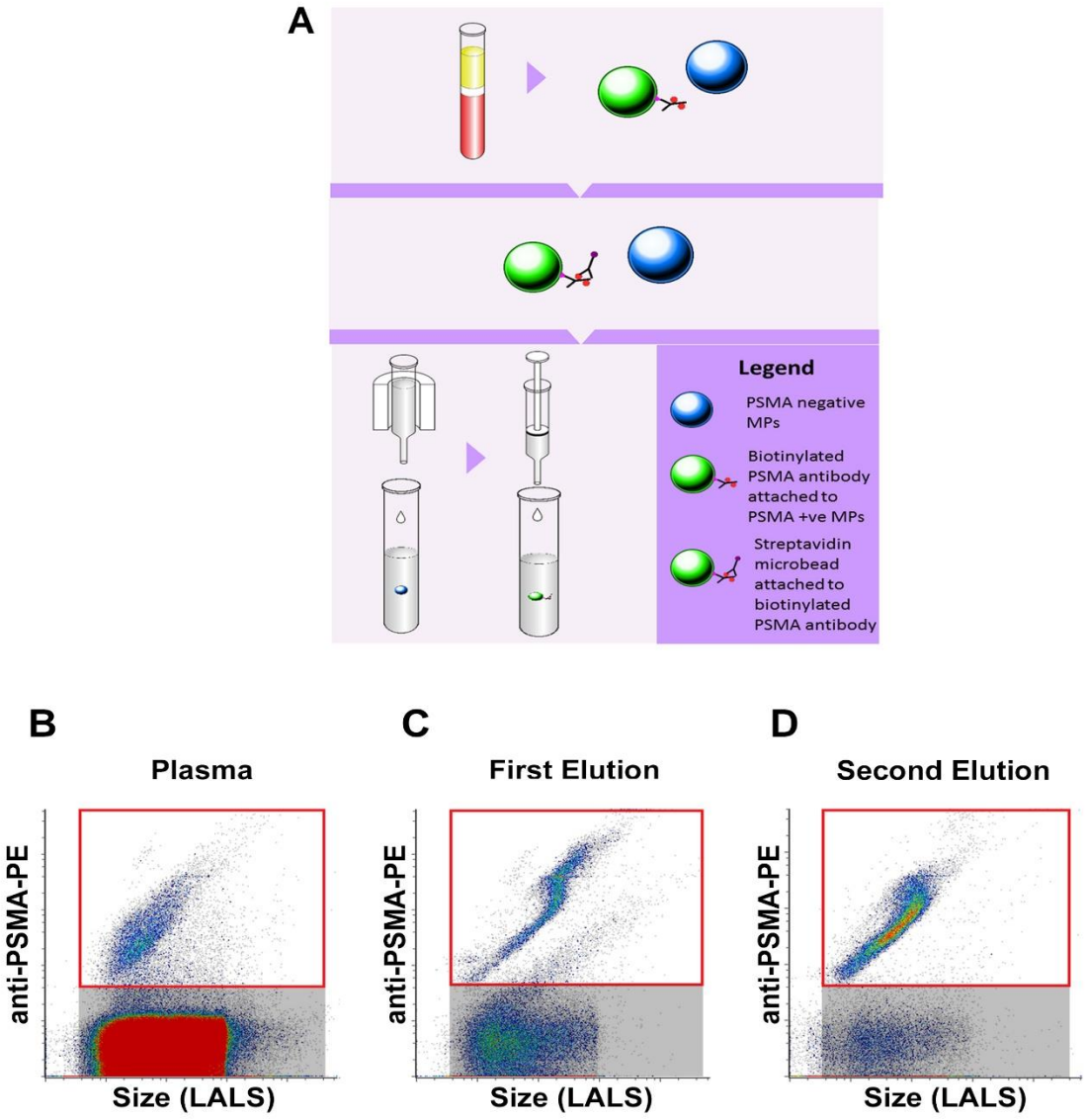
A
Legend
PSMA negative MPs
Biotinylated PSMA antibody attached to PSMA +ve MPs
Streptavidin microbead attached to biotinylated PSMA antibody
B
Plasma
anti-PSMA-PE
Size (LALS)
C
First Elution
anti-PSMA-PE
Size (LALS)
D
Second Elution
anti-PSMA-PE
Size (LALS)

Figure 4. Working model of biotinylated-PSMA technique enriches PCCFs from patient plasma and are quantified using nanoscale flow cytometry.

The biotinylated PSMA immunoaffinity method targets PCCFs from prostate cancer patient plasma that are positive for PSMA, and washes out EVs which do not express PSMA (A). Enrichment of PCCF populations (red gates) compared to total non-target EV populations (shaded areas in histoplot) in patient plasma (B), first elution fraction (C), and second elution fraction (D).

3.3 Atomic force microscopy (AFM) evaluation of controls shows size distribution of soluble proteins

Standard controls, including bovine serum albumin (BSA) and platelet poor plasma (PPP) at varying concentrations, were used to help identify protein content in a sample and measure the height and distribution of contaminating protein in the PCCF preparations. Atomic force microscopy (AFM) analysis performed at 5 µm ×5 µm and at dilution factors of 10X (Fig. 5A), 1000X (Fig. 5B), and 100,000X (Fig. 5C), shows the capability of AFM to measure events in the submicron size. In the images representing both BSA and PPP (diluted 10X), the samples are dominated by smaller events (~5-10 nanometers high), which reflects the small monomeric proteins that are abundant in the BSA and PPP controls. Some larger events, between 30-60 nm in height and ~800nm in diameter may represent extracellular vesicles in the samples. As samples were further diluted to achieve lower concentrations of both BSA and PPP (1,000X and 100,000X dilution factors), the images reveal the magnitude of plasma protein depletion, with a corresponding decrease in particles visible in the field of view of the AFM. Fig. 5D depicts AFM analysis performed at 1 µm by 1 µm of both the BSA and PPP samples.

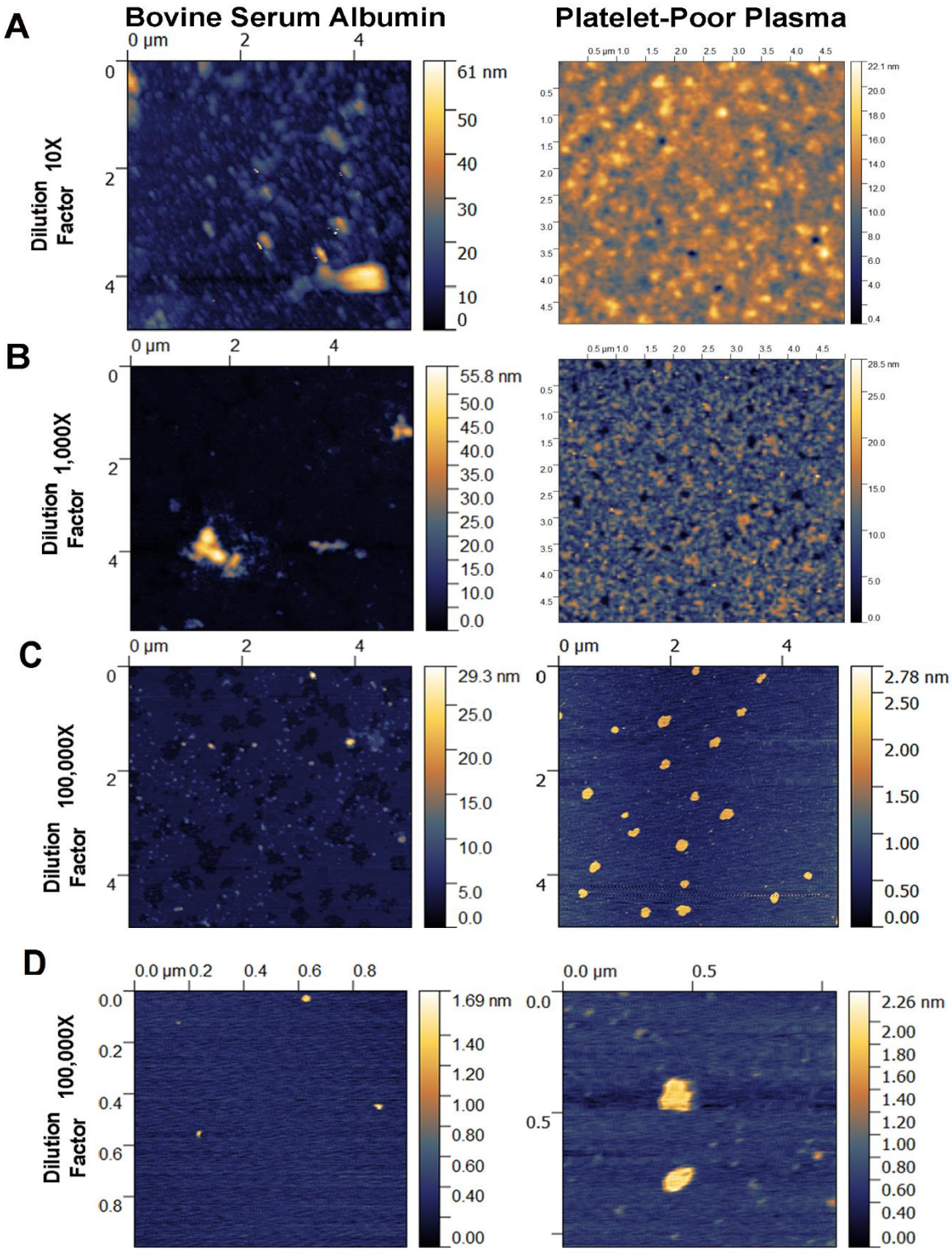
A
Bovine Serum Albumin
Platelet-Poor Plasma
Dilution Factor 10X
B
Dilution Factor 1,000X
C
Dilution Factor 100,000X
D
Dilution Factor 100,000X

Figure 5. Atomic force microscopy images of bovine serum albumin and platelet-poor plasma reveal size and distribution of proteins at varying concentrations.

Height channel of AFM images from BSA and PPP reveal the size and distribution of proteins and other particles in these samples. As expected, diluting the samples reduces the concentration of particles in the samples, confirming that the detected signal is sample specific.

3.4 Multimodal characterization of PCCFs isolated using different techniques reveals that the immunoaffinity method is the most efficient at eliminating background proteins

Prostate cancer cell fragments from patient plasma were isolated using PSMA immunoaffinity-based purification and 3 commercially available extracellular vesicle purification kits. A total of 10 samples per isolation method were submitted to NFC and AFM; the images in Fig.6 represent the analysis of one sample per isolation method. Sample purified using the immunoaffinity method (Fig. 6A) show the presence of extracellular vesicles with a small amount of proteins in the background.

Images of the samples isolated with Total Exosome (Fig. 6B) and Exo Spin (Fig. 6C) kits show the presence of isolated extracellular vesicles; however, most of the sample is dominated by co-isolated contaminating protein. The purification of extracellular vesicles with the Exo Quick kit (Fig. 6D) resulted in the highest concentration of co-isolated contaminant proteins, as illustrated in the AFM image of this sample.

Flow cytometry analysis of isolated PCCFs depicts the enrichment of PSMA positive particles (red box) compared to the total amount of other MPs and co-isolated particles (shaded areas in histoplot). The sample purified by immunoaffinity shows the greatest reduction of non-target MP's population relative to the dense population PSMA positive PCCFs (Fig. 6A). In contrast, the scatterplots representing the three isolation kits contains a larger population of non-target MP's (Fig. 6B, C, D). The relative abundance of PSMA positive PCCFs shows the enrichment of achieved after each isolation method. The highest percentage of PSMA positive PCCFs was achieved with the immunoaffinity isolation method (Fig. 6A), with 49.7% of all events being PSMA positive. For the isolation kits, the overall PSMA events were much lower. Total Exosome (Fig. 6B) had a relative abundance of 38% PSMA positive events; Exo Spin (Fig. 6D) showed a 30% of all events were PSMA positive; and lastly the lowest PSMA abundance was from the Exo Quick kit (Fig. 6C), with 14% of all events being PSMA positive PCCF.

Assessment of PCCF volumetric data shows the differences between the vesicles isolated using the isolation kits and those isolated with the PSMA immunoaffinity technique (Fig.

6E). The particles measured were from one individual sample per isolation method, and one sample of bovine serum albumin (BSA). The BSA volumetric data was used as a control. Volumetric measurement of EV provide useful information regarding sizing, with the majority of all objects imaged exhibiting particle volumes below 1.0×10^{-18} m^3; this is consistent with previous studies of EV volumetric data (23). PCCFs measures from the PSMA isolation group (Fig. 6E, PMP34) shows to have a mean volume of 1.0×10^{-19} m^3. The mean volume of particles in BSA is below 1.0×10^{-22} m^3, due to the high quantity of proteins in the sample. From the isolation kits, the volume of particles was mostly below 1.0×10^{-20} m^3, with many events close to the volume of particles found in BSA, showing that these kits are co-isolating a high quantity of proteins. Volume of the particles isolated with PSMA was significantly different than particle volume in BSA and from Total Exo kit (both $P = 0.0001$; Kruskal-Wallis Test), but not from Exo Quick and Exo Spin kits ($P =$ NS; Kruskal-Wallis Test). All volume mesurements obtained from the exosome kits were not significantly different from particle volume in BSA ($P =$ NS; Kruskal-Wallis Test).

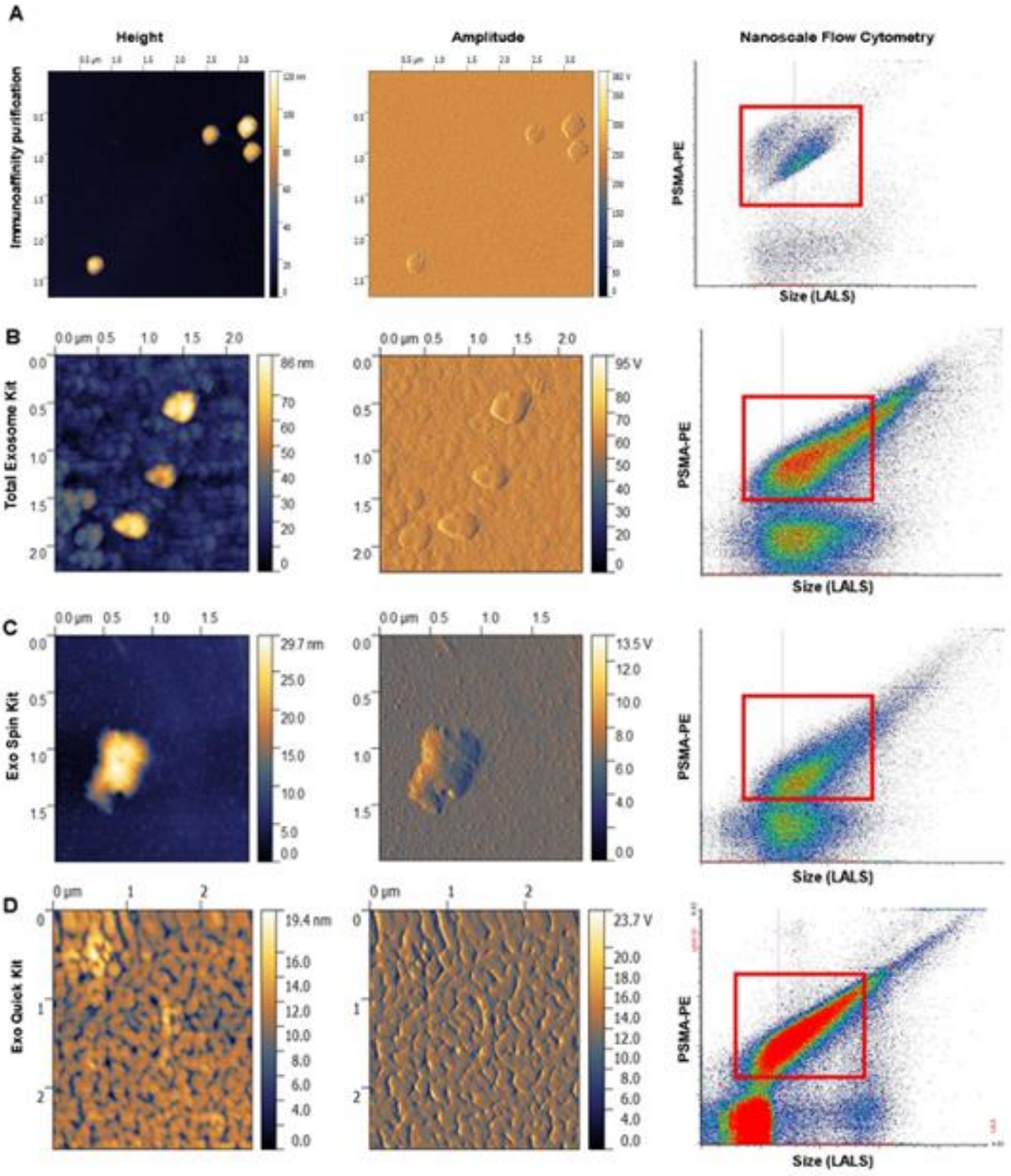
A
Height
Amplitude
Nanoscale Flow Cytometry
Immunoaffinity purification
PSMA-PE
Size (LALS)
B
Total Exosome Kit
86 nm
95 V
PSMA-PE
Size (LALS)
C
Exo Spin Kit
29.7 nm
13.5 V
PSMA-PE
Size (LALS)
D
Exo Quick Kit
19.4 nm
23.7 V
PSMA-PE
Size (LALS)

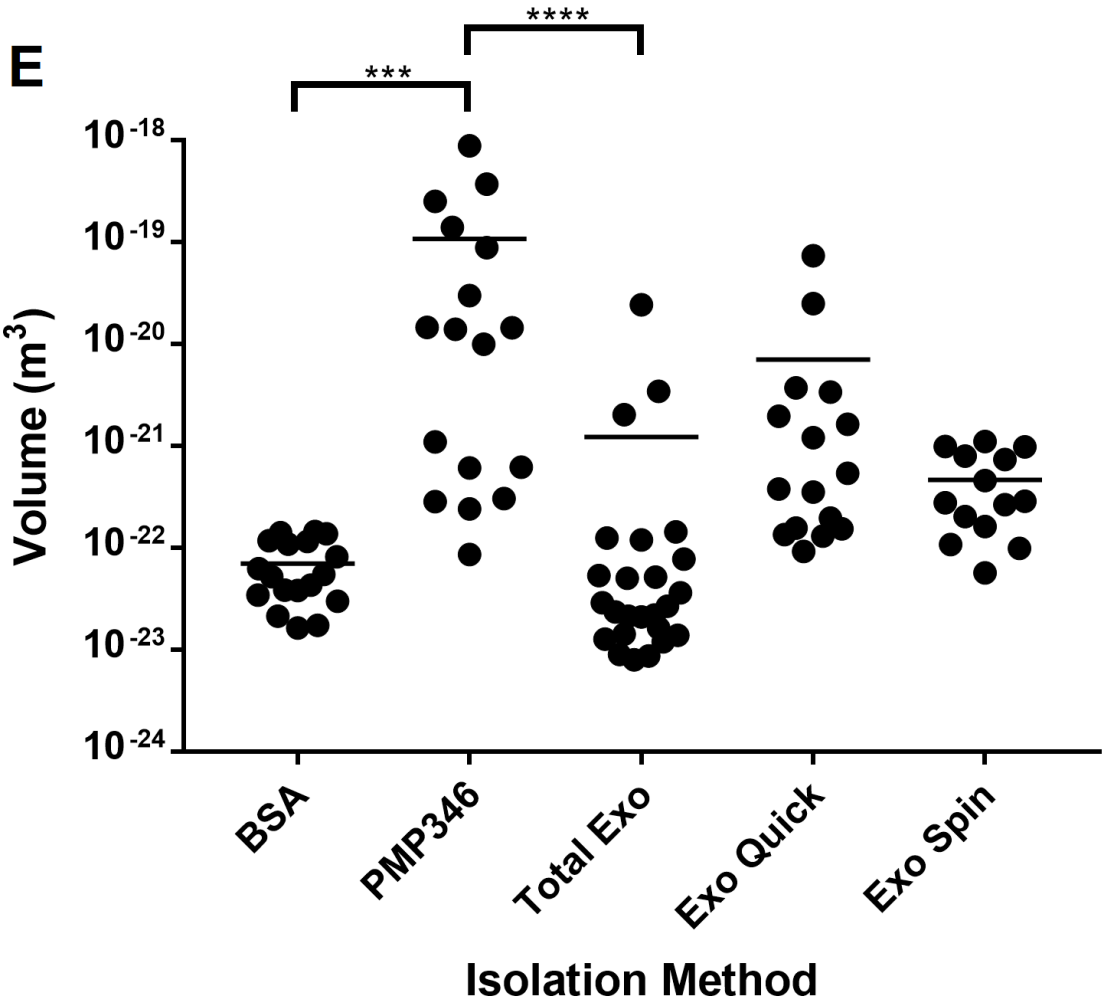

Figure 6. Atomic force microscopy and nanoscale flow cytometry reveal differences in particle size and distribution in PCCF samples obtained using different isolation methods.

AFM images representing the height and amplitude of isolated EVs demonstrate the differences in content of extracellular vesicles versus co-isolated contaminant protein and non-target particles. NFC of all samples also demonstrates the differences between all methods in depleting 'noise' populations (outside red boxes) (A, B, C, D). Volumetric data of PCCFs isolate with PSMA immunoaffinity and three isolation kits; BSA used as a control (E). ****P*= 0.0001, *****P*= 0.0001; Kruskal-Wallis Test.

3.5 Atomic force microscopy resolves three dimensional surface characteristics of isolated PCCFs

Atomic force microscopy evaluation of PCCFs isolated with the PSMA immunoaffinity approach detects individual PCCFs measuring ~110nm in height (Fig. 7A). AFM imaging also shows that the background of the sample contains minimal amounts of co-isolated proteins and other EVs from the plasma samples. The height of isolated PCCFs are within the range previously determined with NFC. I used the Gwyddion software to analyze the PCCF in the inset, both in 2 and 3 dimensional planes. The 2 dimensional image of the inset reveals that at a closer magnification (1 µm × 1 µm), the surface of this individual PCCF contains areas with higher peaks (Fig. 7A-inset). The 3 dimensional image (Fig. 7B) allows for superior resolution of peaks observed in the previous image. When one individual peak is measured, it was shown to be ~14 nm in height (Fig. 7C). These peaks could represent receptors or other membrane associated proteins on the surface of the PCCFs.

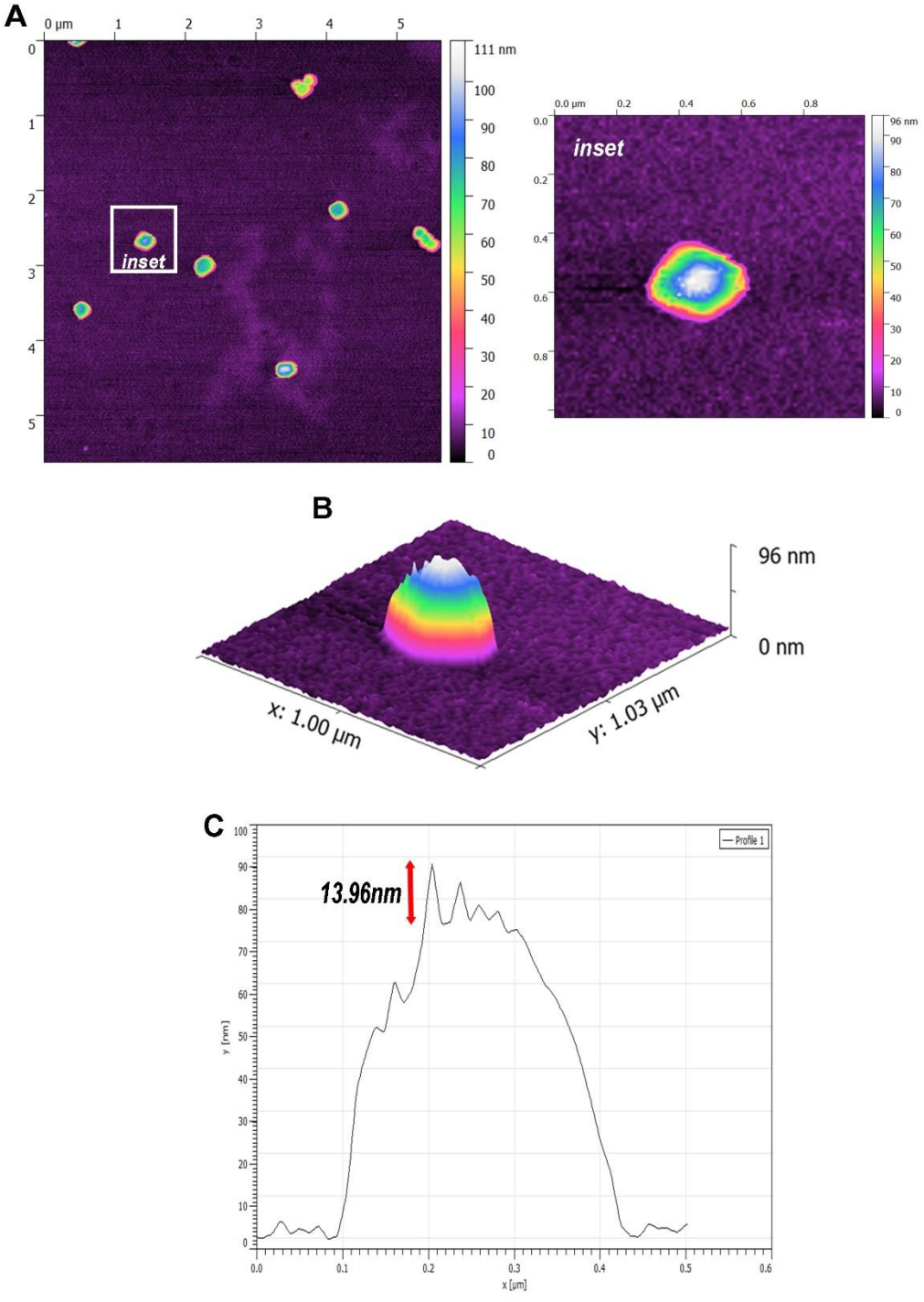
A
inset
111 nm
96 nm
B
96 nm
0 nm
x: 1.00 µm
y: 1.03 µm
C
13.96nm
Profile 1
y [nm]
x [µm]

Figure 7. Atomic force microscopy resolves three-dimensional structures of PCCF isolated from patient plasma and reveals small peaks in PCCF surface.

AFM images of multiple PCCFs in one sample show their distribution, as well as the background of the sample to detect co-isolated proteins, which in this case are virtually depleted (A). Individual PCCFs can be imaged in 2 (inset) and 3 (B) dimensional planes. A profile of an individual PCCF can be plotted to accurately measure peaks on the surface of the particle, which may correspond to membrane associated protein (C).

3.6 Mass spectrometry analysis of PSMA-isolated PCCFs identifies an abundance of albumin and protein peptides from tissues other than prostate

Prostate cancer cell fragments isolated with the PSMA immunoaffinity method were submitted for mass spectrometry analysis in order to find proteins which differ from each Gleason score group (N=2; one sample belonging to Gleason score 6 and one sample to Gleason score 8). Sample preparation and LC-MS/MS was performed by the Ohio State University Mass Spectrometry and Proteomics Facility. Consensus lists containing all protein hits from each of the samples were provided from this analysis (Appendix A and B).

Analysis revealed a total of 158 proteins identified for the Gleason score 6 sample, and 209 proteins identified for the Gleason score 8 sample. In both types of samples, there was an abundance of plasma proteins, such as albumin and immunoglobulins. Other abundant proteins include components of the coagulation and complement cascades, cytoskeleton-associated proteins, enzymes, and signaling molecules. Keratins and other skin related proteins were found in abundance in both sets of samples, indicating the possibility of contamination of the samples. We were not able to find any prostate specific proteins which we could use as potential biomakers.

3.7 Nanoscale flow cytometry detects STEAP1 positive events in prostate cancer patient plasma as well as dual positive PSMA-STEAP1 PCCF events

Analysis of PCa patient plasma with the A50-Micro nanoscale flow cytometer demonstrates that events in plasma are within the 110-800 nm diameter size range (Fig. 8A), with a large population of 'noise' particles which are smaller (red oval). When analyzing PCa patient plasma samples with the isotype control IgG_{2b}-Alexa647 (Fig. 8B, red box), a very small number of events were detected by the NFC, allowing us to determine the placement of gates to identify positive events. When plasma is incubated with an anti-STEAP1 Alexa647 antibody, a subpopulation of PCCFs which express STEAP1 is detected within the previously set gate (Fig. 8B, red box). This population is distinct in both size and immunofluorescence from other particles in the sample (Fig. 8B, blue box).

The A50-Micro NFC also has the capability to measure events which are positive for two antibodies. Dual positive assessment of PCa patient plasma shows events which are recognized by both PSMA-PE and STEAP1-Alexa647 antibodies. Indeed, a large population of dual positive PCCFs is detected (Fig. 8D, top right quadrant). This scatterplot also shows the events that are negative for both antibodies (Fig. 8D, bottom left quadrant).

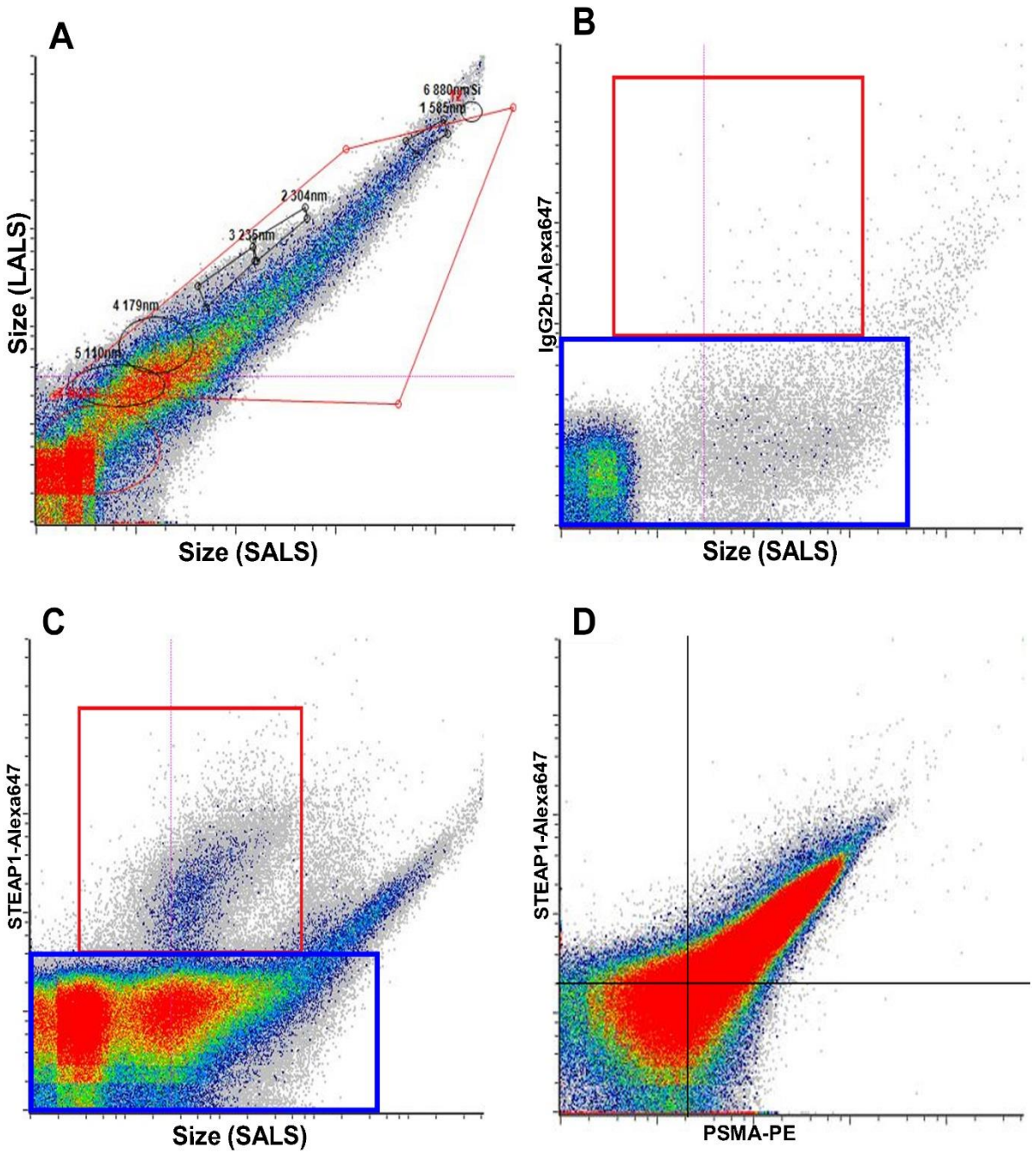
A
6 880nm Si
1 585nm
2 304nm
3 235nm
4 179nm
5 110nm
Size (LALS)
Size (SALS)
B
IgG2b-Alexa647
Size (SALS)
C
STEAP1-Alexa647
Size (SALS)
D
STEAP1-Alexa647
PSMA-PE

Figure 8. Nanoscale flow cytometry reveals the incidence of STEAP1 positive PCCF events in PCa patient plasma samples, and also detects dual PSMA-STEAP1 positive events in PCa patient plasma samples.

NFC analysis of patient plasma reveals that samples contain EV populations of varying sizes, as well as a large population of ‘noise’ particles (A). The isotype control allows for the placement of gates as a threshold for negative events (B). The NFC detects clear subpopulations of STEAP1 positive (C) as well as dual PSMA-STEAP1 positive (D) PCCFs.

3.8 Tandem immunoaffinity isolation of PCCFs significantly reduces non-target MP populations, while maintaining PSMA+STEAP1 dual events

Tandem immunoaffinity isolation of PCCFs consists of an initial isolation of the fragments from patient plasma using the biotinylated-PSMA method. A second immunoisolation technique is then performed, using the STEAP1 antibody (Fig. 9A). In other words, the PCCFs isolated using the PSMA method are then incubated with the Protein G-SEAP1 immune complex. In this way, the non-target PCCFs that are STEAP1 negative are washed form the sample, and the PSMA-STEAP1 dual positive PCCFs are eluted for subsequent analysis.

PCCFs isolated with the tandem immunoaffinity method were evaluated using NFC to assess the efficiency of this technique at enriching PCCFs populations. Individual scatterplot for PSMA-PE, STEAP1-Alexa647, and dual positive PCCF events were measured to determine the number of PCCFs that are recognized by one, or both antibodies. Individually, the expression of PSMA (Fig. 9B, red gates) and STEAP1 (Fig. 9C, red gates) was detected in a significant number of events in isolated PCCFs. Correspondingly, a high number of dual-positive events were detected as observed on the top-right quadrant of the scatterplot, and this was determined to be ~40% of all events measured (Fig. 9D, top right quadrant). This is an ~11-fold enrichment from the PCCF population detected in samples of plasma only. The ‘noise’ population, which is negative for both PSMA and STEAP1, was significantly reduced after tandem isolation (Fig. 9, bottom left quadrant).

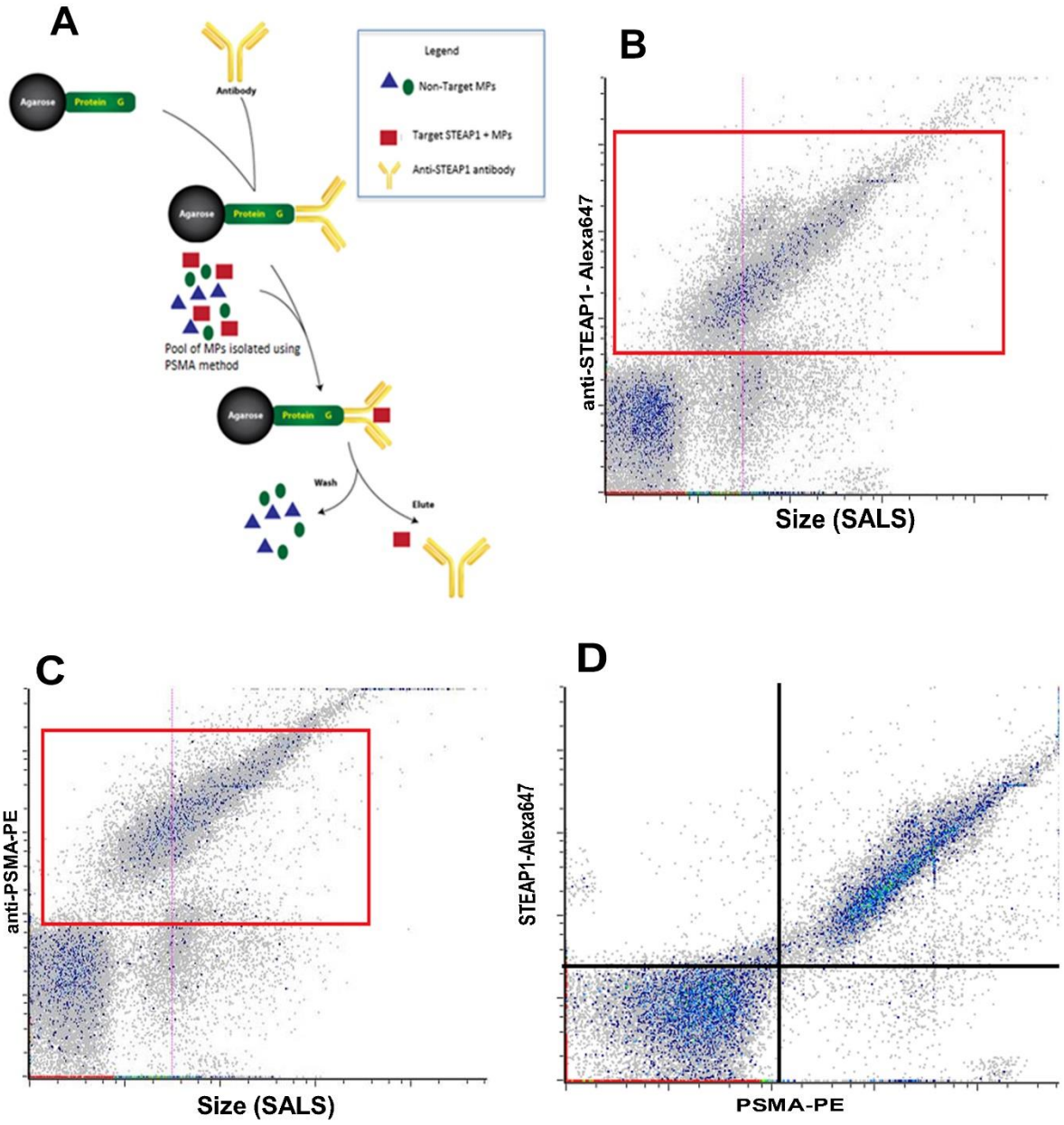
A
Agarose
Protein G
Antibody
Legend
Non-Target MPs
Target STEAP1 + MPs
Anti-STEAP1 antibody
Pool of MPs isolated using PSMA method
Wash
Elute
B
anti-STEAP1- Alexa647
Size (SALS)
C
anti-PSMA-PE
Size (SALS)
D
STEAP1-Alexa647
PSMA-PE

Figure 9. Nanoscale flow cytometry analysis of tandem immunoaffinity isolated PCCFs from patient plasma show the enrichment of STEAP1 positive as well as dual PSMA-STEAP1 positive events.

This method of PCCF isolation utilizes Protein G agarose beads and STEAP1 antibody, which are incubated with the pooled PCCFs previously isolated with PSMA (A). NFC analysis shows that this tandem immunoaffinity isolation yields a sample containing PCCF populations which are positive for PSMA (B) and STEAP1 (C), and a double positive population of PCCFs which expresses both antigens (D).

3.9 Western blot detection of prostate proteins in prostate cell lysate and PSMA immuno-purified PCCFs, but not in tandem isolated PCCF samples

Western blot analysis was performed to measure PSMA and STEAP1 protein expression in PCCFs isolated using the PSMA technique only, as well as PCCFs isolated using the tandem technique. Cell lysate from LNCAP and PC-3M-LN4 cells (10 μg) were also loaded onto gels as controls for PSMA and STEAP1 protein expression (Fig. 10).

Protein bands for STEAP1 are clearly seen in PC-3M-LN4 cell lysate at 47 kDa, which is the expected molecular mass of STEAP1 (Fig. 10A). In the LNCaP cell lysate, the STEAP1 protein band is less prominent than in PC3 lysate; however, a faint band is also detected at 47 kDa (Fig. 10A). PSMA protein bands are clearly seen in PC-3M-LN4 and LNCaP cell lysate at ~110 kDa.

Samples containing PCCFs isolated using the biotinylated-PSMA technique show the presence of a ~110 kDa band corresponding to PSMA, and a band at ~47 kDa corresponding to STEAP1 when ~10μg of protein are also loaded onto the gels (Fig. 10B; N=5, S1-S5). Both proteins are differentially expressed in individual samples, possibly due to the high variances in protein content from one sample to another. ß-actin bands were not detected in these samples.

After tandem isolation, the protein concentration of the PCCF is extremely low and I could not load 10 μg as done previously. Consequently, I could not perform western blot analysis to detect PSMA or STEAP1.

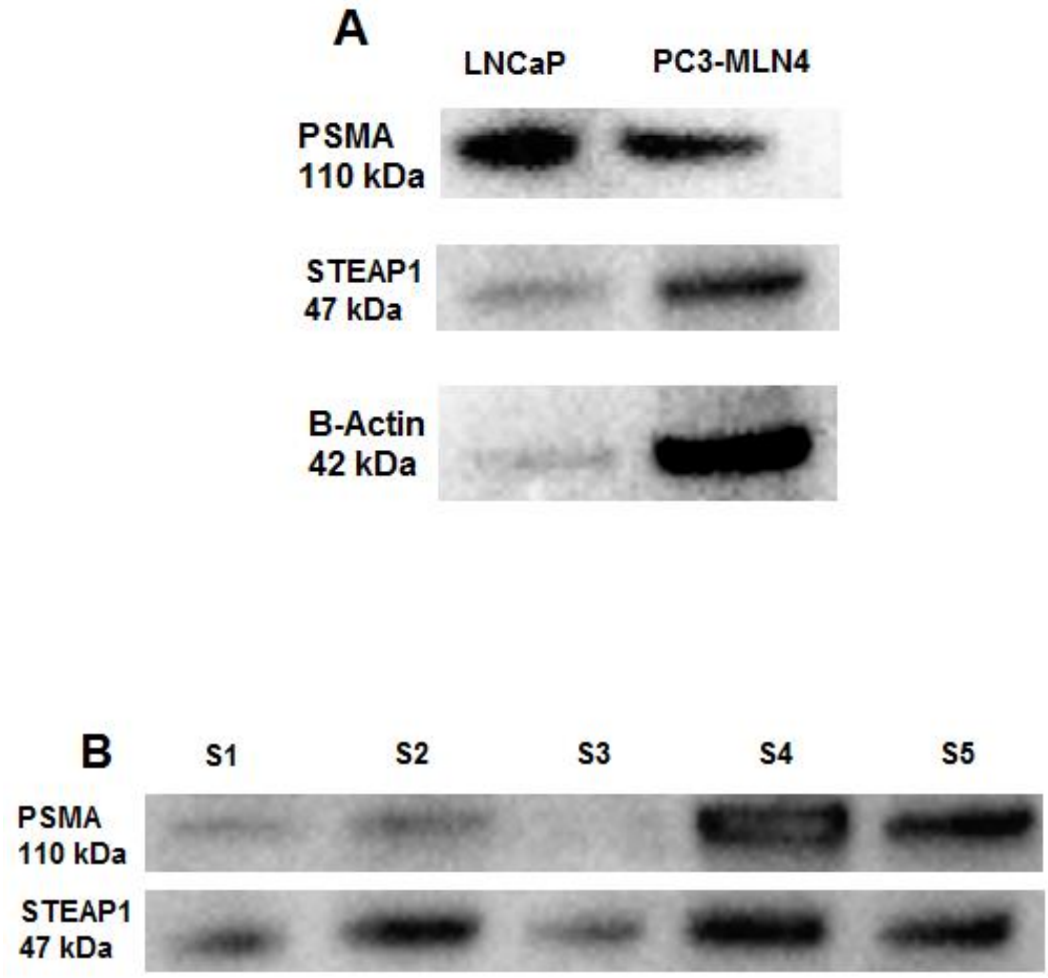

Figure 10. PSMA and STEAP1 protein expression in LNCaP and PC-3M-LN4 prostate cancer cell lines and PCCFs isolated with biotinylated-PSMA method.

Western blot analysis PSMA and STEAP1 protein levels of in LNCaP and PC-3M-LN4 cell lysate (A), as well as in PCCFs isolated using the biotinylated-PSMA immunoaffinity isolation from 5 different patient plasma samples (B; S1-S5). Neither PSMA nor STEAP1 were detected in the tandem immunoaffinity isolated samples, likely because insufficient protein was recovered (data not shown). ß-actin was detected in cell lysate for LNCaP and PC-3M-LN4; however, it was not detected in both isolated samples (data not shown).

3.10 Mass spectrometry results of tandem isolated samples reveal abundance of plasma and cytoskeletal proteins.

To obtain detailed information on the identities of the proteins contained in the plasma isolated PCCFs, we submitted the samples for LC–MS/MS proteomic analysis. Initial sample preparation for proteomic analysis was done by in-gel digestion of the samples. An image of SDS-PAGE gel from one tandem isolated sample (sample ID: PMP-324) reveals the absence of any visible protein bands on the gel, when compared to a loading control which shows an array of bands (Fig. 11A; courtesy of Campus Chemical Instrument Center (CCIC) Mass Spectrometry and Proteomics Facility at The Ohio State University). Mass spectrometry was not conducted after in-gel digestion, due to the absence of protein bands to pick for digest.

Subsequently, proteins in the PCCF samples (N=10 per Gleason score group) were submitted for in-solution digestion. Mass spectrometry output lists were obtained identifying proteins by abundance, in PCCFs from Gleason score 6 (Appendix C) and 8 (Appendix D) patients. Interestingly, a higher number of proteins were detected in Gleason 6 samples totaling 203 proteins; while from the Gleason 8 samples a total of 80 proteins were detected. The majority of proteins identified, and those with the largest number of peptides found in the sample, were serum albumin, immunoglobulins, and components of the coagulation and complement cascades, as well as cytoskeleton-associated proteins, enzymes, and signaling molecules. The abundance of keratins and collagens in both groups of PCCF samples could be due to contamination during handling of the samples.

In the analysis of protein differences between Gleason 6 and 8, one prostate protein was found in a single Gleason 8 sample from one individual patient, and not found in any of the Gleason 6 samples. This protein was Prostasin (PRSS8_HUMAN), a glycosylphosphatidylinositol-anchored serine protease involved in epithelial Na channel activation (77). However, this protein was only detected in one patient, and in low abundance.

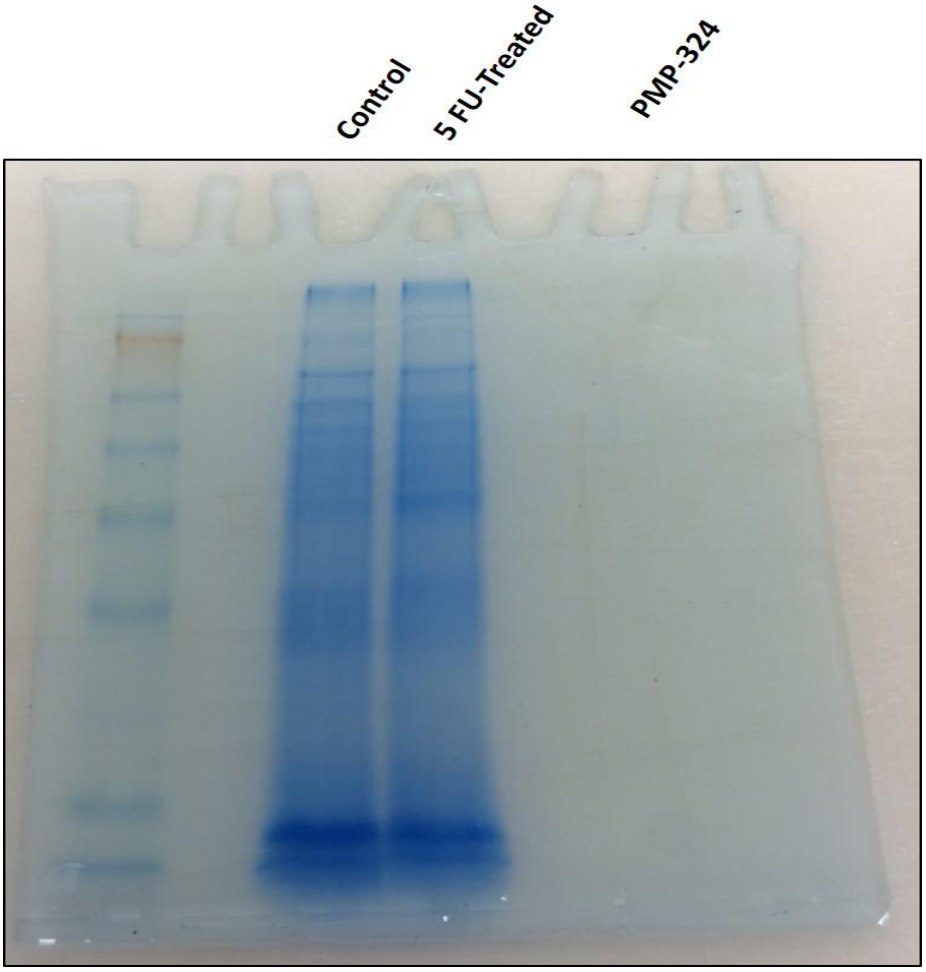

Figure 11. SDS-PAGE gel show the difference in protein band identification between loading controls and a sample consisting of tandem isolated PCCF.

SDS-PAGE gel of controls and tandem isolated PCCF from patient PMP-324. Gel was stained with coomassie brilliant blue (performed by our Ohio State collaborators), which reveals clearly visible protein bands in both controls, but no bands in the PMP-324 lane were detected.

Chapter 4

4 Discussion

In this study, we isolated prostate cancer cell fragments (PCCFs) from the plasma of prostate cancer patients with Gleason scores of 6 and 8, which indicates low and high-grade PCa respectively, in order to assess the protein content of these PCFFs. The goal was to find a protein specific for each of these PCa grades, which could be used to discriminate between these two clinically distinct patient cohorts. We created a novel tandem immunoaffinity isolation technique using two prostate-specific antigens, PSMA and STEAP1, to separate PCCF from other non-prostate EVs and plasma proteins. The purity of the samples, assessed by the reduction of background cellular material and plasma protein, as well as the morphological features of the isolated EVs, were analyzed with atomic force microscopy and nanoscale flow cytometry.

4.1 Extracellular vesicles such as prostate cancer cell fragments as a fluid biopsy for prostate cancer

Research on EVs began in 1967, when Peter Wolf discovered platelet MPs, but many regarded EVs as simply ‘cellular debris’. Currently, research in EVs has increased our understanding of the mechanisms of vesicle production, their role as modulators of normal physiological processes, as well as in cancer progression and other disease states (10). It is now known that during microvesicle biogenesis, cell fragments retain membrane proteins and nucleic acid originally found within the parent cell (78). Furthermore, studies have confirmed that release of EV is accelerated in cancer (9) and other diseases (10), feeding interest for their role in mediating cell-to-cell communication, and as a biomarker platform for improved screening and prognosis of diseases.

The promise of EVs in PCa may be more suited for biomarker development, considering that PCCFs are endowed with portions of membrane proteins from the parent cell (78). Attempts to discover PCCFs-associated biomarkers specific for PCa are limited to

proteomic analysis of isolated PCCFs from *in vitro* studies (4), or from human PCa xenografts in mice (55). However, these reported biomarkers have not been clinically validated, either in serum or plasma samples, underscoring the need to substantiate biomarkers beyond the initial discovery phase.

4.2 Immunoaffinity isolation of PCCFs

The ability to isolate and enrich EVs, such as exosomes or microparticles, is a highly important method that is currently not standardized. A significant barrier in discovering biomarkers associated with EV samples is due to the lack of robust platforms for isolation of EV populations, with the samples mostly dominated by co-isolated soluble proteins that may also contain the biomarker of interest (79). As the majority of studies have failed to evaluate the purity of isolated EV populations before performing downstream analytical assays, the sample may be a misrepresentation of the EV population of interest, consequently leading to erroneous conclusions.

A key step in the isolation of EVs from bodily fluids is the reduction of other non-target factors such as proteins, circulating nucleic acids, and non-target EVs in order to demonstrate that factors within the target EVs are specific effectors during intercellular communication (80). The most commonly used method for EV purification is differential ultracentrifugation (4,31), a practice that many consider the “gold standard” for purification of EVs (81). However, ultracentrifugation does not guarantee complete elimination of non-target EVs, resulting in enrichment as opposed to the purification of the desired EV population (42). Moreover, this technique involves lengthy periods of centrifugation and requires expensive specialized equipment for ultracentrifugation of the sample.

As interest in EVs has intensified, so has the demand for procedures which are rapid and more user-friendly. This has resulted in the creation of several kits which act by separating exosomes through sedimentation from other factors within the sample; in particular, ExoQuick (System Bioscience), Total Exosome (Life Technologies) and ExoSpin (Cell Guidance Systems), which are all commercially available. While these kits

minimize the time spent performing EV isolation, little is known about their purification efficacy. Newly published data shows that although the precipitation techniques yield a higher protein content, this is not an indication of high exosome purification, but rather a consequence of contaminating non-exosomal proteins (82).

In comparison with the other methods of EV isolation, immunoaffinity-based isolation methods provide a high level of specificity for selecting EVs from the tissue of interest. The ability to select a subpopulation of EVs from biological fluids is an essential requirement for studies focusing on the diagnostic potential of EV (83). In this thesis, we developed an immunoaffinity isolation protocol using the PSMA antigen, which proved to be efficient at separating PCCFs from other small vesicles present in plasma samples. This technique proved to be more effective than all previously mentioned commercially available kits at removing background subpopulations (Fig. 6A-D). We also created a tandem isolation method to further eliminate plasma and other contaminating proteins. Moreover, the use of two prostate antigens (PSMA and STEAP1) was helpful in further selecting EVs that were prostate specific.

4.3 Multi-modal nano-characterization of purified extracellular vesicles from biological samples

The field of EVs is rapidly evolving in terms of the techniques used for characterizing vesicles isolated from different sources. In EV characterization, is important to use several techniques in combination for quantifying and visually analyzing the features of the vesicles (81). We present here the combined use of nanoscale flow cytometry and atomic force microscopy as a means to quantify prostate cancer cell fragment events, to measure them to the atomic level, and visualize their topographical morphology.

4.3.1 Nanoscale flow cytometry for quantification of PCCFs in plasma and isolated samples

The emergence of nanoscale flow cytometry (NFC) has made high-throughput, multi-parametric analysis of all events between 110 and 880 nm possible regardless of the incident wavelength of light used (46). Using the Apogee A50-Micro nanoscale flow cytometer, polystyrene microspheres and silica-based beads can be size-resolved up to differences of 100 nm (47), revealing the potential of this instrumentation to become widely used for the analysis of EVs in complex biological mixtures (48).

In the present study, we used the NFC to successfully quantify PCCF events in both plasma and isolated samples, which expressed the prostate antigens PSMA (Fig. and STEAP1 (Fig. 8C). The Apogee A50-Micro NFC was also useful in validating the efficiency of our tandem immunoaffinity method to reduce the population of non-target EVs and other noise particles from the starting plasma sample (Fig. 9B-D).

4.3.2 Atomic force microscopy for visual characterization and validation of the isolated PCCFs

Microscopy continues to be a common approach to assessing the efficacy of EV isolation from a given sample, as well as to characterize the structure and relative size of these vesicles (42,48). Most publications have reported the use of transmission electron microscopy (TEM) and scanning electron microscopy (SEM) as key modalities to visually characterize and evaluate the ratio of EVs to soluble protein and other cellular debris (42). However, these techniques are not quantitative, as they do not allow for the atomic measurement of components in the sample, which is important for distinguishing exosomes (50-100 nm) from microparticles (100-1000 nm).

The atomic force microscope (AFM) has been recently reported to be a valuable tool for the nanoscale measurement of EVs at atomic resolution (23). This instrument allows for the topographical imaging of EV surfaces, as well as offering information regarding protein contamination in purified EVs preparations (84). Moreover, sample preparation for AFM analysis is rapid and does not alter the native state of the target EV, which is

substantially different from the lengthy and harsh sample processing required for electron microscopy (85).

We have shown that AFM is an idea promising imaging modality for the measurement of small vesicles with a mean diameter of ~100 nm and for the detection of protein complexes co-isolated with the target population of EVs (Fig. 7A). Images of isolated PCCFs obtained with AFM also allowed for the 3-dimensional rendering of the particles (Fig. 7B); depicting the surface of the particles in a 3-dimensional plane led us to visualize small peaks (Fig. 7C), which we speculate could be protein receptors inherited from the parental cell.

4.4 Mass spectrometry

The great interest in EV as protein carriers is evident in the literature, with a large number of publications focusing on characterizing the proteome of EVs derived from cell culture media (14,86) and biological fluids (4,87). Currently, discovery of disease biomarkers from EVs using mass spectrometry (MS) is mostly from cell culture media samples. Moreover, the information gained from proteomic analysis of EVs from biological fluids is limited in the literature. This could be due to the complexity of proteins that are present in biological fluids. The greatest challenge of performing MS analysis from blood serum or plasma samples vs. tissue culture is the vast difference in the dynamic range of proteins. Even with attempts to remove abundant proteins such as albumin and immunoglobulins, small amounts of impurities can have a significant effect in MS analysis of isolated EVs, making the identification of low abundance proteins difficult (87).

In agreement with previous reports, Bastos-Amador *et al.* (88) showed that plasma proteins such as albumin, and cytosolic proteins like heat shock proteins were among the most abundant protein present after EV isolation from plasma samples. They also reported a high proportion of immunoglobulins co-isolated with their EV preparations. However, some of these generally co-isolated proteins may be difficult to remove from

the samples, as they may be purposely packaged in EVs to maintain membrane and protein integrity (89).

In the present study, the MS results (Appendix A-D) we obtained from isolated PCCFs are consistent with the literature in regards to the majority of proteins detected by MS being albumin and immunoglobulins Moreover, the MS output data shows an abundance of keratins and collagen, which could be due to contamination caused by handling of the sample during the isolation process, or while preparing the samples for in-solution digestion. The aim of this part of the study was to find possible protein biomarkers uniformly expressed in all the PCCF samples from one Gleason score group that were not expressed in the other Gleason score group. Although there were some proteins which were differentially expressed between these two Gleason scores, these were found in only one or two of the samples, but not the rest. In addition, only a small number of peptides from some of these proteins were identified. Like our results, another group has similarly reported that they were able to identify a small number of proteins in EVs isolated from plasma (90).

The inability to detect the expected quantity of proteins in our PCCF samples could be due to intrinsic issues with the tandem immunoaffinity method we developed. This technique requires the use of elution buffers that modify the pH of the sample. Although physiological pH was restored immediately, exposing the PCCFs to the conditions of the eluting buffer could have affected the three-dimensional structure of proteins assembled on the PCCF surface (91). Consequently, alteration of the biological properties of proteins in the isolated PCCF could have resulted in inability to detect these proteins with MS.

4.5 Significance

Currently, there is a need for new diagnostic tools to accurately identify patients with aggressive or high-risk PCa from those with low-risk disease. Prostate specific antigen (PSA) testing continues to be employed as a monitoring and prognostication tool;

however, PSA is produced and secreted by both normal prostate epithelium and PCa into the circulation (4). The low specificity and high false-positive rate of PSA have resulted in many men without PCa having to undergo painful and unnecessary biopsies and risk the possibility of infections post-biopsy. As a result, PSA is no longer recommended as the leading test for PCa screening (73).

Research to discover new diagnostic biomarkers that could differentiate low-risk from high-risk PCa has not significantly progressed, but the need for a non-invasive test in monitoring PCa patients is clearly of great clinical value. PCCFs are an attractive biomarker platform for detecting PCa, as these fragments originate from prostate epithelium or from malignant cells within the primary tumor and are released into the blood circulation (76). Moreover, it has been previously shown that significant quantities of PCCFs are detectable in samples from PCa patients, but are not detected in healthy individuals (92).

In general, the PCa research community must double its efforts to understand extracellular vesicles like PCCFs in order to apply these fragments as a novel non-invasive biomarker-based test. Biomarkers that arise out of these studies could eventually become clinically validated. Upon development of biomarkers specific to PCCFs from Gleason score 6 and 8 lesions, a "liquid biopsy" format of the Gleason score could be established to evaluate patients prior to biopsy, and determine the stage of cancer. This is a major clinically unmet need, which may aid clinicians towards a more precise means of managing PCa. Such a test would also provide major health costs savings, as well as minimize patient morbidity and anxiety related to the biopsy procedure.

4.6 Future directions and conclusions

Future studies will need to focus on further optimizing the tandem isolation protocol to allow for the maximum collection of PCCFs to produce a higher yield of prostate-specific proteins. This may be partially overcome by scaling up the isolation with a higher volume

of initial plasma. Previously, an initial volume of <1 mL has been used for the isolation of EV from complex biological fluids (81), which is a feasible volume of starting sample to collect from patients.

To further support future efforts in finding independent biomarkers for each Gleason score (GS 6 and 8), the small sample size in this study (N=10 per Gleason score cohort) should be significantly increased. A larger sample size could guarantee a better representation of the population, as well as detection of low-abundance proteins in additional samples.

In addition, using antibodies with higher affinity for the target populations could potentially have utility, as we only tested one antibody for each target antigen (PSMA and STEAP1). Using a cocktail of l antibodies could be better if the target epitope is not always available.

Although we proved with NFC and AFM that there is a significant reduction of the noise population when using our tandem isolation method, we still detected co-isolated plasma and cytosolic proteins. These co-isolated proteins could be masking the expression of other, less abundant proteins. Therefore, it is important to effectively separate the target EV, in order to avoid the background caused by these co-isolated protein aggregates (91). The use of albumin/IgG removal kits has been previously proposed in order to achieve the depletion of plasma and cytosolic proteins (81). This step could be introduced prior to the tandem immunoaffinity isolation technique.

To our knowledge, this is the first evidence that the tandem affinity methodology is effective at reducing other non-target EVs and proteins from PCa patient samples while keeping a significant number of PCCFs. We showed that using our tandem affinity technique is more efficient than other isolation methods - such as commercial EV purification kits - in removing soluble proteins and other debris from the sample. Moreover, we also showed that the combined use of nanoscale flow cytometry and

atomic force microscopy has a great potential to become a widely used technique to analyze extracellular vesicle enrichment.

In the current study, we were not able to identify protein biomarkers for differentiating the two patient cohorts (Gleason score 6 and 8), which was the principal goal of this thesis. However, future efforts in optimizing the protocols we have developed in this project could help in the identification of protein biomarkers for better and faster diagnosis and staging of prostate cancer.

References

1. Lee TH, D'Asti E, Magnus N, Al-Nedawi K, Meehan B, Rak J. Microvesicles as mediators of intercellular communication in cancer--the emerging science of cellular "debris". Semin Immunopathol [Internet]. 2011 Sep [cited 2014 Sep 17];33(5):455–67. Available from: http://www.ncbi.nlm.nih.gov/pubmed/21318413

2. Wang W, Li H, Zhou Y, Jie S. Peripheral blood microvesicles are potential biomarkers for hepatocellular carcinoma. Cancer Biomark [Internet]. 2013 Jan [cited 2014 Oct 25];13(5):351–7. Available from: http://www.ncbi.nlm.nih.gov/pubmed/24440975

3. Sahlén GE, Egevad L, Ahlander A, Norlén BJ, Ronquist G, Nilsson BO. Ultrastructure of the secretion of prostasomes from benign and malignant epithelial cells in the prostate. Prostate [Internet]. 2002 Nov 1 [cited 2014 Sep 30];53(3):192–9. Available from: http://www.ncbi.nlm.nih.gov/pubmed/12386919

4. Duijvesz D, Burnum-Johnson KE, Gritsenko MA, Hoogland AM, Vredenbregt-van den Berg MS, Willemsen R, et al. Proteomic profiling of exosomes leads to the identification of novel biomarkers for prostate cancer. PLoS One [Internet]. 2013 Jan [cited 2014 Oct 8];8(12):e82589. Available from: http://www.pubmedcentral.nih.gov/articlerender.fcgi?artid=3876995&tool=pmcentrez&rendertype=abstract

5. Théry C, Zitvogel L, Amigorena S. Exosomes: composition, biogenesis and function. Nat Rev Immunol [Internet]. 2002 Aug [cited 2014 Oct 23];2(8):569–79. Available from: http://www.ncbi.nlm.nih.gov/pubmed/12154376

6. Berda-Haddad Y, Robert S, Salers P, Zekraoui L, Farnarier C, Dinarello CA, et al. Sterile inflammation of endothelial cell-derived apoptotic bodies is mediated by interleukin-1α. Proc Natl Acad Sci U S A [Internet]. 2011 Dec 20 [cited 2014 Oct 25];108(51):20684–9. Available from: http://www.pubmedcentral.nih.gov/articlerender.fcgi?artid=3251090&tool=pmcentrez&rendertype=abstract

7. George JN, Thoi LL, McManus LM, Reimann TA. Isolation of human platelet membrane microparticles from plasma and serum. Blood [Internet]. 1982 Oct [cited 2014 Oct 26];60(4):834–40. Available from: http://www.ncbi.nlm.nih.gov/pubmed/7115953

8. Leong HS, Mahesh BM, Day JR, Smith JD, McCormack AD, Ghimire G, et al. Vimentin autoantibodies induce platelet activation and formation of platelet-leukocyte conjugates via platelet-activating factor. J Leukoc Biol [Internet]. 2008 Feb [cited 2014 Oct 21];83(2):263–71. Available from: http://www.ncbi.nlm.nih.gov/pubmed/17974709

9. Al-Nedawi K, Meehan B, Rak J. Microvesicles: messengers and mediators of tumor progression. Cell Cycle [Internet]. 2009 Jul 1 [cited 2014 Oct 29];8(13):2014–8. Available from: http://www.ncbi.nlm.nih.gov/pubmed/19535896

10. Martínez MC, Tesse A, Zobairi F, Andriantsitohaina R. Shed membrane microparticles from circulating and vascular cells in regulating vascular function. Am J Physiol Heart Circ Physiol [Internet]. 2005 Mar [cited 2014 Sep 20];288(3):H1004-9. Available from: http://www.ncbi.nlm.nih.gov/pubmed/15706036

11. Kooijmans SAA, Vader P, van Dommelen SM, van Solinge WW, Schiffelers RM. Exosome mimetics: a novel class of drug delivery systems. Int J Nanomedicine [Internet]. 2012;7:1525–41. Available from: http://www.ncbi.nlm.nih.gov/pubmed/22619510

12. Mesri M, Altieri DC. Endothelial cell activation by leukocyte microparticles. J Immunol [Internet]. 1998 Oct 15 [cited 2014 Oct 2];161(8):4382–7. Available from: http://www.ncbi.nlm.nih.gov/pubmed/9780216

13. Al-Nedawi K, Meehan B, Micallef J, Lhotak V, May L, Guha A, et al. Intercellular transfer of the oncogenic receptor EGFRvIII by microvesicles derived from tumour cells. Nat Cell Biol [Internet]. 2008 May [cited 2014 Sep 17];10(5):619–24. Available from: http://www.ncbi.nlm.nih.gov/pubmed/18425114

14. Peinado H, Alečković M, Lavotshkin S, Matei I, Costa-Silva B, Moreno-Bueno G, et al. Melanoma exosomes educate bone marrow progenitor cells toward a pro-metastatic phenotype through MET. Nat Med [Internet]. 2012 Jun [cited 2014 Aug 12];18(6):883–91. Available from: http://www.pubmedcentral.nih.gov/articlerender.fcgi?artid=3645291&tool=pmcentrez&rendertype=abstract

15. Valadi H, Ekström K, Bossios A, Sjöstrand M, Lee JJ, Lötvall JO. Exosome-mediated transfer of mRNAs and microRNAs is a novel mechanism of genetic exchange between cells. Nat Cell Biol [Internet]. 2007 Jun [cited 2014 Aug 6];9(6):654–9. Available from: http://www.ncbi.nlm.nih.gov/pubmed/17486113

16. Ji H, Greening DW, Barnes TW, Lim JW, Tauro BJ, Rai A, et al. Proteome profiling of exosomes derived from human primary and metastatic colorectal cancer cells reveal differential expression of key metastatic factors and signal transduction components. Proteomics [Internet]. 2013 May;13(10–11):1672–86. Available from: http://www.ncbi.nlm.nih.gov/pubmed/23585443

17. Bartels CL, Tsongalis GJ. MicroRNAs: novel biomarkers for human cancer. Clin Chem [Internet]. 2009 Apr [cited 2014 Oct 7];55(4):623–31. Available from: http://www.ncbi.nlm.nih.gov/pubmed/19246618

18. Selth LA, Townley S, Gillis JL, Ochnik AM, Murti K, Macfarlane RJ, et al. Discovery of circulating microRNAs associated with human prostate cancer using a mouse model of disease. Int J Cancer [Internet]. 2012 Aug 1 [cited 2014 Sep 20];131(3):652–61. Available from: http://www.ncbi.nlm.nih.gov/pubmed/22052531

19. Taylor DD, Gercel-Taylor C. MicroRNA signatures of tumor-derived exosomes as diagnostic biomarkers of ovarian cancer. Gynecol Oncol [Internet]. 2008 Jul [cited 2015 Feb 6];110(1):13–21. Available from: http://www.ncbi.nlm.nih.gov/pubmed/18589210

20. Rabinowits G, Gerçel-Taylor C, Day JM, Taylor DD, Kloecker GH. Exosomal microRNA: a diagnostic marker for lung cancer. Clin Lung Cancer [Internet]. 2009 Jan [cited 2014 Sep 25];10(1):42–6. Available from: http://www.ncbi.nlm.nih.gov/pubmed/19289371

21. Melo SA, Sugimoto H, O'Connell JT, Kato N, Villanueva A, Vidal A, et al. Cancer Exosomes Perform Cell-Independent MicroRNA Biogenesis and Promote Tumorigenesis. Cancer Cell [Internet]. 2014 Nov 10 [cited 2014 Dec 3];26(5):707–21. Available from: http://www.ncbi.nlm.nih.gov/pubmed/25446899

22. Utleg AG, Yi EC, Xie T, Shannon P, White JT, Goodlett DR, et al. Proteomic analysis of human prostasomes. Prostate [Internet]. 2003 Jul 1 [cited 2015 Jan 15];56(2):150–61. Available from: http://www.ncbi.nlm.nih.gov/pubmed/12746840

23. Leong HS, Podor TJ, Manocha B, Lewis JD. Validation of flow cytometric detection of platelet microparticles and liposomes by atomic force microscopy. J Thromb Haemost [Internet]. 2011 Dec [cited 2014 Sep 8];9(12):2466–76. Available from: http://www.ncbi.nlm.nih.gov/pubmed/21981726

24. Wickman G, Julian L, Olson MF. How apoptotic cells aid in the removal of their own cold dead bodies. Cell Death Differ [Internet]. 2012 May;19(5):735–42. Available from: http://www.ncbi.nlm.nih.gov/pubmed/22421963

25. Parrish AB, Freel CD, Kornbluth S. Cellular mechanisms controlling caspase activation and function. Cold Spring Harb Perspect Biol [Internet]. 2013 Jun;5(6). Available from: http://www.ncbi.nlm.nih.gov/pubmed/23732469

26. Taylor RC, Cullen SP, Martin SJ. Apoptosis: controlled demolition at the cellular level. Nat Rev Mol Cell Biol [Internet]. 2008 Mar;9(3):231–41. Available from: http://www.ncbi.nlm.nih.gov/pubmed/18073771

27. Ravichandran KS. Find-me and eat-me signals in apoptotic cell clearance: progress and conundrums. J Exp Med [Internet]. 2010 Aug 30;207(9):1807–17. Available from: http://www.ncbi.nlm.nih.gov/pubmed/20805564

28. Bergsmedh A, Szeles A, Henriksson M, Bratt A, Folkman MJ, Spetz AL, et al. Horizontal transfer of oncogenes by uptake of apoptotic bodies. Proc Natl Acad Sci U S A [Internet]. 2001 May 22;98(11):6407–11. Available from: http://www.ncbi.nlm.nih.gov/pubmed/11353826

29. Xie Y, Bai O, Yuan J, Chibbar R, Slattery K, Wei Y, et al. Tumor apoptotic bodies inhibit CTL responses and antitumor immunity via membrane-bound transforming growth factor-beta1 inducing CD8+ T-cell anergy and CD4+ Tr1 cell responses. Cancer Res [Internet]. 2009 Oct 1;69(19):7756–66. Available from: http://www.ncbi.nlm.nih.gov/pubmed/19789353

30. Hargett LA, Bauer NN. On the origin of microparticles: From "platelet dust" to mediators of intercellular communication. Pulm Circ [Internet]. 2013 Apr [cited 2014 Sep 20];3(2):329–40. Available from: http://www.pubmedcentral.nih.gov/articlerender.fcgi?artid=3757826&tool=pmcentrez&rendertype=abstract

31. Wolf P. The nature and significance of platelet products in human plasma. Br J Haematol [Internet]. 1967 May [cited 2015 Apr 30];13(3):269–88. Available from: http://www.ncbi.nlm.nih.gov/pubmed/6025241

32. Wang C-C, Tseng C-C, Hsiao C-C, Chang H-C, Chang L-T, Fang W-F, et al. Circulating endothelial-derived activated microparticle: a useful biomarker for predicting one-year mortality in patients with advanced non-small cell lung cancer. Biomed Res Int [Internet]. 2014 Jan [cited 2014 Oct 9];2014:173401. Available from: http://www.pubmedcentral.nih.gov/articlerender.fcgi?artid=4100353&tool=pmcentrez&rendertype=abstract

33. Mesri M, Altieri DC. Leukocyte microparticles stimulate endothelial cell cytokine release and tissue factor induction in a JNK1 signaling pathway. J Biol Chem [Internet]. 1999 Aug 13 [cited 2014 Sep 9];274(33):23111–8. Available from: http://www.ncbi.nlm.nih.gov/pubmed/10438480

34. Heijnen HF, Schiel AE, Fijnheer R, Geuze HJ, Sixma JJ. Activated platelets release two types of membrane vesicles: microvesicles by surface shedding and exosomes derived from exocytosis of multivesicular bodies and alpha-granules. Blood [Internet]. 1999 Dec 1 [cited 2014 Oct 23];94(11):3791–9. Available from: http://www.ncbi.nlm.nih.gov/pubmed/10572093

35. Podor TJ, Singh D, Chindemi P, Foulon DM, McKelvie R, Weitz JI, et al. Vimentin exposed on activated platelets and platelet microparticles localizes vitronectin and plasminogen activator inhibitor complexes on their surface. J Biol Chem [Internet]. 2002 Mar 1 [cited 2014 Oct 21];277(9):7529–39. Available from: http://www.ncbi.nlm.nih.gov/pubmed/11744725

36. Dashevsky O, Varon D, Brill A. Platelet-derived microparticles promote invasiveness of prostate cancer cells via upregulation of MMP-2 production. Int J Cancer [Internet]. 2009 Apr 15 [cited 2014 Oct 26];124(8):1773–7. Available from: http://www.ncbi.nlm.nih.gov/pubmed/19101987

37. Chironi G, Simon A, Hugel B, Del Pino M, Gariepy J, Freyssinet J-M, et al. Circulating leukocyte-derived microparticles predict subclinical atherosclerosis burden in asymptomatic subjects. Arterioscler Thromb Vasc Biol [Internet]. 2006 Dec [cited 2014 Oct 9];26(12):2775–80. Available from: http://www.ncbi.nlm.nih.gov/pubmed/17038634

38. Combes V, Simon AC, Grau GE, Arnoux D, Camoin L, Sabatier F, et al. In vitro generation of endothelial microparticles and possible prothrombotic activity in patients with lupus anticoagulant. J Clin Invest [Internet]. 1999 Jul;104(1):93–102. Available from: http://www.ncbi.nlm.nih.gov/pubmed/10393703

39. Tseng C-C, Wang C-C, Chang H-C, Tsai T-H, Chang L-T, Huang K-T, et al. Levels of circulating microparticles in lung cancer patients and possible prognostic value. Dis Markers [Internet]. 2013 Jan [cited 2014 Oct 23];35(5):301–10. Available from: http://www.pubmedcentral.nih.gov/articlerender.fcgi?artid=3787568&tool=pmcentrez&rendertype=abstract

40. Mitchell PS, Parkin RK, Kroh EM, Fritz BR, Wyman SK, Pogosova-Agadjanyan EL, et al. Circulating microRNAs as stable blood-based markers for cancer detection. Proc Natl Acad Sci U S A [Internet]. 2008 Jul 29 [cited 2014 Jul 20];105(30):10513–8. Available from: http://www.pubmedcentral.nih.gov/articlerender.fcgi?artid=2492472&tool=pmcentrez&rendertype=abstract

41. Crawford N. The presence of contractile proteins in platelet microparticles isolated from human and animal platelet-free plasma. Br J Haematol [Internet]. 1971 Jul;21(1):53–69. Available from: http://www.ncbi.nlm.nih.gov/pubmed/4254312

42. Mrvar-Brecko A, Sustar V, Jansa V, Stukelj R, Jansa R, Mujagić E, et al. Isolated microvesicles from peripheral blood and body fluids as observed by scanning electron microscope. Blood Cells Mol Dis [Internet]. 2010 Apr 15 [cited 2015 May 7];44(4):307–12. Available from: http://www.ncbi.nlm.nih.gov/pubmed/20199878

43. Ellis WJ, Pfitzenmaier J, Colli J, Arfman E, Lange PH, Vessella RL. Detection and isolation of prostate cancer cells from peripheral blood and bone marrow. Urology [Internet]. 2003 Feb;61(2):277–81. Available from: http://www.ncbi.nlm.nih.gov/pubmed/12597930

44. Mizutani K, Terazawa R, Kameyama K, Kato T, Horie K, Tsuchiya T, et al. Isolation of prostate cancer-related exosomes. Anticancer Res [Internet]. 2014 Jul [cited 2014 Oct 8];34(7):3419–23. Available from: http://www.ncbi.nlm.nih.gov/pubmed/24982349

45. Sims PJ, Faioni EM, Wiedmer T, Shattil SJ. Complement proteins C5b-9 cause release of membrane vesicles from the platelet surface that are enriched in the membrane receptor for coagulation factor Va and express prothrombinase activity. J Biol Chem [Internet]. 1988 Dec 5 [cited 2014 Oct 24];263(34):18205–12. Available from: http://www.ncbi.nlm.nih.gov/pubmed/2848029

46. Chandler WL, Yeung W, Tait JF. A new microparticle size calibration standard for use in measuring smaller microparticles using a new flow cytometer. J Thromb Haemost [Internet]. 2011 Jun [cited 2014 Oct 6];9(6):1216–24. Available from: http://www.ncbi.nlm.nih.gov/pubmed/21481178

47. Montoro-García S, Shantsila E, Orenes-Piñero E, Lozano ML, Lip GYH. An innovative flow cytometric approach for small-size platelet microparticles: influence of calcium. Thromb Haemost [Internet]. 2012 Aug [cited 2014 Oct 14];108(2):373–83. Available from: http://www.ncbi.nlm.nih.gov/pubmed/22740162

48. van der Pol E, Coumans FAW, Grootemaat AE, Gardiner C, Sargent IL, Harrison P, et al. Particle size distribution of exosomes and microvesicles determined by transmission electron microscopy, flow cytometry, nanoparticle tracking analysis, and resistive pulse sensing. J Thromb Haemost [Internet]. 2014 Jul [cited 2014 Nov 29];12(7):1182–92. Available from: http://www.ncbi.nlm.nih.gov/pubmed/24818656

49. Ronquist G, Hedström M. Restoration of detergent-inactivated adenosine triphosphatase activity of human prostatic fluid with concanavalin A. Biochim

Biophys Acta [Internet]. 1977 Aug 11 [cited 2014 Oct 29];483(2):483–6. Available from: http://www.ncbi.nlm.nih.gov/pubmed/142513

50. Brody I, Ronquist G, Gottfries A. Ultrastructural localization of the prostasome - an organelle in human seminal plasma. Ups J Med Sci [Internet]. 1983 Jan [cited 2014 Oct 7];88(2):63–80. Available from: http://www.ncbi.nlm.nih.gov/pubmed/6649193

51. Sahlén G, Ahlander A, Frost A, Ronquist G, Norlén BJ, Nilsson BO. Prostasomes are secreted from poorly differentiated cells of prostate cancer metastases. Prostate [Internet]. 2004 Nov 1 [cited 2015 Jan 20];61(3):291–7. Available from: http://www.ncbi.nlm.nih.gov/pubmed/15368476

52. Tarazona R, Delgado E, Guarnizo MC, Roncero RG, Morgado S, Sánchez-Correa B, et al. Human prostasomes express CD48 and interfere with NK cell function. Immunobiology [Internet]. [cited 2014 Nov 20];216(1–2):41–6. Available from: http://www.ncbi.nlm.nih.gov/pubmed/20382443

53. Nilsson BO, Carlsson L, Larsson A, Ronquist G. Autoantibodies to prostasomes as new markers for prostate cancer. Ups J Med Sci [Internet]. 2001 Jan [cited 2014 Oct 9];106(1):43–9. Available from: http://www.ncbi.nlm.nih.gov/pubmed/11817562

54. Tavoosidana G, Ronquist G, Darmanis S, Yan J, Carlsson L, Wu D, et al. Multiple recognition assay reveals prostasomes as promising plasma biomarkers for prostate cancer. Proc Natl Acad Sci U S A [Internet]. 2011 May 24 [cited 2014 Oct 4];108(21):8809–14. Available from: http://www.pubmedcentral.nih.gov/articlerender.fcgi?artid=3102389&tool=pmcentrez&rendertype=abstract

55. Jansen FH, Krijgsveld J, van Rijswijk A, van den Bemd G-J, van den Berg MS, van Weerden WM, et al. Exosomal secretion of cytoplasmic prostate cancer xenograft-derived proteins. Mol Cell Proteomics [Internet]. 2009 Jun [cited 2014 Oct 15];8(6):1192–205. Available from: http://www.pubmedcentral.nih.gov/articlerender.fcgi?artid=2690478&tool=pmcentrez&rendertype=abstract

56. Liu T, Mendes DE, Berkman CE. Functional prostate-specific membrane antigen is enriched in exosomes from prostate cancer cells. Int J Oncol [Internet]. 2014 Mar [cited 2015 Jan 15];44(3):918–22. Available from: http://www.pubmedcentral.nih.gov/articlerender.fcgi?artid=3928468&tool=pmcentrez&rendertype=abstract

57. Ronquist GK, Larsson A, Stavreus-Evers A, Ronquist G. Prostasomes are heterogeneous regarding size and appearance but affiliated to one DNA-containing exosome family. Prostate [Internet]. 2012 Dec 1 [cited 2015 Jan 15];72(16):1736–45. Available from: http://www.ncbi.nlm.nih.gov/pubmed/22539202

58. Ihlaseh-Catalano SM, Drigo SA, de Jesus CMN, Domingues MAC, Trindade Filho JCS, de Camargo JL V, et al. STEAP1 protein overexpression is an independent marker for biochemical recurrence in prostate carcinoma. Histopathology [Internet]. 2013 Nov [cited 2015 Jan 15];63(5):678–85. Available from:

http://www.ncbi.nlm.nih.gov/pubmed/24025158

59. Porkka KP, Helenius MA, Visakorpi T. Cloning and characterization of a novel six-transmembrane protein STEAP2, expressed in normal and malignant prostate. Lab Invest [Internet]. 2002 Nov [cited 2015 Jan 15];82(11):1573–82. Available from: http://www.ncbi.nlm.nih.gov/pubmed/12429817

60. Zhigang Z, Wenlv S. Prostate stem cell antigen (PSCA) expression in human prostate cancer tissues and its potential role in prostate carcinogenesis and progression of prostate cancer. World J Surg Oncol [Internet]. 2004 Jan [cited 2015 Jan 20];2:13. Available from: http://www.pubmedcentral.nih.gov/articlerender.fcgi?artid=420493&tool=pmcentrez&rendertype=abstract

61. Di Vizio D, Morello M, Dudley AC, Schow PW, Adam RM, Morley S, et al. Large oncosomes in human prostate cancer tissues and in the circulation of mice with metastatic disease. Am J Pathol [Internet]. 2012 Nov [cited 2015 Jan 16];181(5):1573–84. Available from: http://www.pubmedcentral.nih.gov/articlerender.fcgi?artid=3483805&tool=pmcentrez&rendertype=abstract

62. Chambers AF, Groom AC, MacDonald IC. Dissemination and growth of cancer cells in metastatic sites. Nat Rev Cancer [Internet]. 2002 Aug [cited 2015 Jan 20];2(8):563–72. Available from: http://www.ncbi.nlm.nih.gov/pubmed/12154349

63. Ligthart ST, Coumans FAW, Attard G, Cassidy AM, de Bono JS, Terstappen LWMM. Unbiased and automated identification of a circulating tumour cell definition that associates with overall survival. PLoS One [Internet]. 2011 Jan [cited 2015 Jan 20];6(11):e27419. Available from: http://www.pubmedcentral.nih.gov/articlerender.fcgi?artid=3210171&tool=pmcentrez&rendertype=abstract

64. Goodman OB, Symanowski JT, Loudyi A, Fink LM, Ward DC, Vogelzang NJ. Circulating tumor cells as a predictive biomarker in patients with hormone-sensitive prostate cancer. Clin Genitourin Cancer [Internet]. 2011 Sep [cited 2015 Jan 20];9(1):31–8. Available from: http://www.ncbi.nlm.nih.gov/pubmed/21705286

65. Adams DL, Stefansson S, Haudenschild C, Martin SS, Charpentier M, Chumsri S, et al. Cytometric characterization of Circulating Tumor Cells captured by microfiltration and their correlation to the CellSearch(®) CTC test. Cytometry A [Internet]. 2014 Dec 16 [cited 2015 Jan 16]; Available from: http://www.ncbi.nlm.nih.gov/pubmed/25515318

66. Lowes LE, Lock M, Rodrigues G, D'Souza D, Bauman G, Ahmad B, et al. Circulating tumour cells in prostate cancer patients receiving salvage radiotherapy. Clin Transl Oncol [Internet]. 2012 Feb [cited 2015 Jan 21];14(2):150–6. Available from: http://www.ncbi.nlm.nih.gov/pubmed/22301405

67. Cristofanilli M, Budd GT, Ellis MJ, Stopeck A, Matera J, Miller MC, et al. Circulating tumor cells, disease progression, and survival in metastatic breast cancer. N Engl J Med [Internet]. 2004 Aug 19 [cited 2015 Jan 19];351(8):781–91.

Available from: http://www.ncbi.nlm.nih.gov/pubmed/15317891

68. Coumans FAW, Doggen CJM, Attard G, de Bono JS, Terstappen LWMM. All circulating EpCAM+CK+CD45- objects predict overall survival in castration-resistant prostate cancer. Ann Oncol [Internet]. 2010 Sep [cited 2015 Jan 19];21(9):1851–7. Available from: http://www.ncbi.nlm.nih.gov/pubmed/20147742

69. Khan S, Jutzy JMS, Valenzuela MMA, Turay D, Aspe JR, Ashok A, et al. Plasma-derived exosomal survivin, a plausible biomarker for early detection of prostate cancer. PLoS One [Internet]. 2012 Jan [cited 2015 Jan 15];7(10):e46737. Available from: http://www.pubmedcentral.nih.gov/articlerender.fcgi?artid=3473028&tool=pmcentrez&rendertype=abstract

70. Klein EA, Cooperberg MR, Magi-Galluzzi C, Simko JP, Falzarano SM, Maddala T, et al. A 17-gene assay to predict prostate cancer aggressiveness in the context of Gleason grade heterogeneity, tumor multifocality, and biopsy undersampling. Eur Urol [Internet]. 2014 Sep [cited 2015 Jan 20];66(3):550–60. Available from: http://www.ncbi.nlm.nih.gov/pubmed/24836057

71. Corcoran C, Rani S, O'Driscoll L. miR-34a is an intracellular and exosomal predictive biomarker for response to docetaxel with clinical relevance to prostate cancer progression. Prostate [Internet]. 2014 Sep [cited 2015 Jan 20];74(13):1320–34. Available from: http://www.ncbi.nlm.nih.gov/pubmed/25053345

72. Siegel RL, Miller KD, Jemal A. Cancer statistics, 2016. CA Cancer J Clin [Internet]. 66(1):7–30. Available from: http://www.ncbi.nlm.nih.gov/pubmed/26742998

73. Klotz L, Emberton M. Management of low risk prostate cancer-active surveillance and focal therapy. Nat Rev Clin Oncol [Internet]. 2014 Jun [cited 2014 Oct 30];11(6):324–34. Available from: http://www.ncbi.nlm.nih.gov/pubmed/24821214

74. Klotz L, Zhang L, Lam A, Nam R, Mamedov A, Loblaw A. Clinical results of long-term follow-up of a large, active surveillance cohort with localized prostate cancer. J Clin Oncol [Internet]. 2010 Jan 1 [cited 2014 Oct 30];28(1):126–31. Available from: http://www.ncbi.nlm.nih.gov/pubmed/19917860

75. Loeb S, Carter HB, Berndt SI, Ricker W, Schaeffer EM. Complications after prostate biopsy: data from SEER-Medicare. J Urol [Internet]. 2011 Nov;186(5):1830–4. Available from: http://www.ncbi.nlm.nih.gov/pubmed/21944136

76. Sardana G, Diamandis EP. Biomarkers for the diagnosis of new and recurrent prostate cancer. Biomark Med [Internet]. 2012 Oct [cited 2014 Sep 17];6(5):587–96. Available from: http://www.ncbi.nlm.nih.gov/pubmed/23075237

77. Pizzolo F, Chiecchi L, Morandini F, Castagna A, Zorzi F, Zaltron C, et al. Increased urinary excretion of the epithelial Na channel activator prostasin in patients with primary aldosteronism. J Hypertens [Internet]. 2016 Nov 10;

Available from: http://www.ncbi.nlm.nih.gov/pubmed/27841781

78. Hannafon BN, Ding W-Q. Intercellular Communication by Exosome-Derived microRNAs in Cancer. Int J Mol Sci [Internet]. 2013 Jan [cited 2014 Sep 21];14(7):14240–69. Available from: http://www.pubmedcentral.nih.gov/articlerender.fcgi?artid=3742242&tool=pmcentrez&rendertype=abstract

79. Rood IM, Deegens JKJ, Merchant ML, Tamboer WPM, Wilkey DW, Wetzels JFM, et al. Comparison of three methods for isolation of urinary microvesicles to identify biomarkers of nephrotic syndrome. Kidney Int [Internet]. 2010 Oct [cited 2015 May 11];78(8):810–6. Available from: http://www.ncbi.nlm.nih.gov/pubmed/20686450

80. Szatanek R, Baran J, Siedlar M, Baj-Krzyworzeka M. Isolation of extracellular vesicles: Determining the correct approach (Review). Int J Mol Med [Internet]. 2015 Apr 22 [cited 2015 May 11]; Available from: http://www.ncbi.nlm.nih.gov/pubmed/25902369

81. Gardiner C, Di Vizio D, Sahoo S, Théry C, Witwer KW, Wauben M, et al. Techniques used for the isolation and characterization of extracellular vesicles: results of a worldwide survey. J Extracell vesicles [Internet]. 2016;5:32945. Available from: http://www.ncbi.nlm.nih.gov/pubmed/27802845

82. Van Deun J, Mestdagh P, Sormunen R, Cocquyt V, Vermaelen K, Vandesompele J, et al. The impact of disparate isolation methods for extracellular vesicles on downstream RNA profiling. J Extracell vesicles [Internet]. 2014 Jan [cited 2015 Apr 26];3. Available from: http://www.pubmedcentral.nih.gov/articlerender.fcgi?artid=4169610&tool=pmcentrez&rendertype=abstract

83. Abramowicz A, Widlak P, Pietrowska M. Proteomic analysis of exosomal cargo: the challenge of high purity vesicle isolation. Mol BioSyst [Internet]. 2016;12(5):1407–19. Available from: http://xlink.rsc.org/?DOI=C6MB00082G

84. Mukherjee R, Saha M, Routray A, Chakraborty C. Nano-Scale Surface Characterization of Human Erythrocytes by Atomic Force Microscopy: A Critical Review. IEEE Trans Nanobioscience [Internet]. 2015 Apr 28 [cited 2015 May 11]; Available from: http://www.ncbi.nlm.nih.gov/pubmed/25935044

85. Ruozi B, Tosi G, Leo E, Vandelli MA. Application of atomic force microscopy to characterize liposomes as drug and gene carriers. Talanta [Internet]. 2007 Aug 15 [cited 2015 May 12];73(1):12–22. Available from: http://www.ncbi.nlm.nih.gov/pubmed/19071844

86. Roccaro AM, Sacco A, Maiso P, Azab AK, Tai Y-T, Reagan M, et al. BM mesenchymal stromal cell-derived exosomes facilitate multiple myeloma progression. J Clin Invest [Internet]. 2013 Apr;123(4):1542–55. Available from: http://www.ncbi.nlm.nih.gov/pubmed/23454749

87. Øverbye A, Skotland T, Koehler CJ, Thiede B, Seierstad T, Berge V, et al. Identification of prostate cancer biomarkers in urinary exosomes. Oncotarget

[Internet]. 2015 Oct 6;6(30):30357–76. Available from: http://www.ncbi.nlm.nih.gov/pubmed/26196085

88. Bastos-Amador P, Royo F, Gonzalez E, Conde-Vancells J, Palomo-Diez L, Borras FE, et al. Proteomic analysis of microvesicles from plasma of healthy donors reveals high individual variability. J Proteomics [Internet]. 2012 Jun;75(12):3574–84. Available from: http://linkinghub.elsevier.com/retrieve/pii/S1874391912002059

89. Simpson RJ, Lim JW, Moritz RL, Mathivanan S. Exosomes: proteomic insights and diagnostic potential. Expert Rev Proteomics [Internet]. 2009 Jun;6(3):267–83. Available from: http://www.ncbi.nlm.nih.gov/pubmed/19489699

90. Kreimer S, Belov AM, Ghiran I, Murthy SK, Frank DA, Ivanov AR. Mass-spectrometry-based molecular characterization of extracellular vesicles: lipidomics and proteomics. J Proteome Res [Internet]. 2015 Jun 5 [cited 2015 Oct 20];14(6):2367–84. Available from: http://www.ncbi.nlm.nih.gov/pubmed/25927954

91. Abramowicz A, Widlak P, Pietrowska M. Proteomic analysis of exosomal cargo: the challenge of high purity vesicle isolation. Mol Biosyst [Internet]. 2016 Apr 26;12(5):1407–19. Available from: http://www.ncbi.nlm.nih.gov/pubmed/27030573

92. Di Vizio D, Morello M, Dudley AC, Schow PW, Adam RM, Morley S, et al. Large oncosomes in human prostate cancer tissues and in the circulation of mice with metastatic disease. Am J Pathol [Internet]. 2012 Nov [cited 2014 Oct 23];181(5):1573–84. Available from: http://www.pubmedcentral.nih.gov/articlerender.fcgi?artid=3483805&tool=pmcentrez&rendertype=abstract

Appendices

Appendix A: List of proteins identified in PCCF isolated using biotinylated PSMA immunoaffinity method from plasma of patients with Gleason score 6.

Accession	Description
ALBU_HUMAN	Serum albumin OS=Homo sapiens GN=ALB PE=1 SV=2
CO3_HUMAN	Complement C3 OS=Homo sapiens GN=C3 PE=1 SV=2
CFAH_HUMAN	Complement factor H OS=Homo sapiens GN=CFH PE=1 SV=4
A2MG_HUMAN	Alpha-2-macroglobulin OS=Homo sapiens GN=A2M PE=1 SV=3
APOB_HUMAN	Apolipoprotein B-100 OS=Homo sapiens GN=APOB PE=1 SV=2
CO4A_HUMAN	Complement C4-A OS=Homo sapiens GN=C4A PE=1 SV=2
CO4B_HUMAN	Complement C4-B OS=Homo sapiens GN=C4B PE=1 SV=2
TRFE_HUMAN	Serotransferrin OS=Homo sapiens GN=TF PE=1 SV=3
FINC_HUMAN	Fibronectin OS=Homo sapiens GN=FN1 PE=1 SV=4
HPT_HUMAN	Haptoglobin OS=Homo sapiens GN=HP PE=1 SV=1
CFAB_HUMAN	Complement factor B OS=Homo sapiens GN=CFB PE=1 SV=2
PLMN_HUMAN	Plasminogen OS=Homo sapiens GN=PLG PE=1 SV=2
K2C1_HUMAN	Keratin, type II cytoskeletal 1 OS=Homo sapiens GN=KRT1 PE=1 SV=6
VTDB_HUMAN	Vitamin D-binding protein OS=Homo sapiens GN=GC PE=1 SV=1
K1C10_HUMAN	Keratin, type I cytoskeletal 10 OS=Homo sapiens GN=KRT10 PE=1 SV=6
IGHG3_HUMAN	Ig gamma-3 chain C region OS=Homo sapiens GN=IGHG3 PE=1 SV=2
IGHM_HUMAN	Ig mu chain C region OS=Homo sapiens GN=IGHM PE=1 SV=3

ITIH4_HUMAN	Inter-alpha-trypsin inhibitor heavy chain H4 OS=Homo sapiens GN=ITIH4 PE=1 SV=4
A1BG_HUMAN	Alpha-1B-glycoprotein OS=Homo sapiens GN=A1BG PE=1 SV=4
FETUA_HUMAN	Alpha-2-HS-glycoprotein OS=Homo sapiens GN=AHSG PE=1 SV=1
K22E_HUMAN	Keratin, type II cytoskeletal 2 epidermal OS=Homo sapiens GN=KRT2 PE=1 SV=2
HPTR_HUMAN	Haptoglobin-related protein OS=Homo sapiens GN=HPR PE=2 SV=2
C4BPA_HUMAN	C4b-binding protein alpha chain OS=Homo sapiens GN=C4BPA PE=1 SV=2
K1C9_HUMAN	Keratin, type I cytoskeletal 9 OS=Homo sapiens GN=KRT9 PE=1 SV=3
CERU_HUMAN	Ceruloplasmin OS=Homo sapiens GN=CP PE=1 SV=1
IGHG4_HUMAN	Ig gamma-4 chain C region OS=Homo sapiens GN=IGHG4 PE=1 SV=1
KNG1_HUMAN	Kininogen-1 OS=Homo sapiens GN=KNG1 PE=1 SV=2
THRB_HUMAN	Prothrombin OS=Homo sapiens GN=F2 PE=1 SV=2
IGHG1_HUMAN	Ig gamma-1 chain C region OS=Homo sapiens GN=IGHG1 PE=1 SV=1
A1AG1_HUMAN	Alpha-1-acid glycoprotein 1 OS=Homo sapiens GN=ORM1 PE=1 SV=1
CO5_HUMAN	Complement C5 OS=Homo sapiens GN=C5 PE=1 SV=4
IGKC_HUMAN	Ig kappa chain C region OS=Homo sapiens GN=IGKC PE=1 SV=1

IGHG2_HUMAN	Ig gamma-2 chain C region OS=Homo sapiens GN=IGHG2 PE=1 SV=2
CO8B_HUMAN	Complement component C8 beta chain OS=Homo sapiens GN=C8B PE=1 SV=3
AFAM_HUMAN	Afamin OS=Homo sapiens GN=AFM PE=1 SV=1
AMBP_HUMAN	Protein AMBP OS=Homo sapiens GN=AMBP PE=1 SV=1
CO7_HUMAN	Complement component C7 OS=Homo sapiens GN=C7 PE=1 SV=2
VWF_HUMAN	von Willebrand factor OS=Homo sapiens GN=VWF PE=1 SV=4
MUCB_HUMAN	Ig mu heavy chain disease protein OS=Homo sapiens PE=1 SV=1
IGJ_HUMAN	Immunoglobulin J chain OS=Homo sapiens GN=JCHAIN PE=1 SV=4
APOH_HUMAN	Beta-2-glycoprotein 1 OS=Homo sapiens GN=APOH PE=1 SV=3
A1AG2_HUMAN	Alpha-1-acid glycoprotein 2 OS=Homo sapiens GN=ORM2 PE=1 SV=2
IGHA1_HUMAN	Ig alpha-1 chain C region OS=Homo sapiens GN=IGHA1 PE=1 SV=2
CO6_HUMAN	Complement component C6 OS=Homo sapiens GN=C6 PE=1 SV=3

APOA1_HUMAN	Apolipoprotein A-I OS=Homo sapiens GN=APOA1 PE=1 SV=1
C1S_HUMAN	Complement C1s subcomponent OS=Homo sapiens GN=C1S PE=1 SV=1
C1R_HUMAN	Complement C1r subcomponent OS=Homo sapiens GN=C1R PE=1 SV=2
CD5L_HUMAN	CD5 antigen-like OS=Homo sapiens GN=CD5L PE=1 SV=1
CO9_HUMAN	Complement component C9 OS=Homo sapiens GN=C9 PE=1 SV=2
LAC2_HUMAN	Ig lambda-2 chain C regions OS=Homo sapiens GN=IGLC2 PE=1 SV=1
A1AT_HUMAN	Alpha-1-antitrypsin OS=Homo sapiens GN=SERPINA1 PE=1 SV=3
GELS_HUMAN	Gelsolin OS=Homo sapiens GN=GSN PE=1 SV=1
K2C6B_HUMAN	Keratin, type II cytoskeletal 6B OS=Homo sapiens GN=KRT6B PE=1 SV=5
CFAI_HUMAN	Complement factor I OS=Homo sapiens GN=CFI PE=1 SV=2
ITIH1_HUMAN	Inter-alpha-trypsin inhibitor heavy chain H1 OS=Homo sapiens GN=ITIH1 PE=1 SV=3
AACT_HUMAN	Alpha-1-antichymotrypsin OS=Homo sapiens GN=SERPINA3 PE=1 SV=2

LAC3_HUMAN	Ig lambda-3 chain C regions OS=Homo sapiens GN=IGLC3 PE=1 SV=1
CO2_HUMAN	Complement C2 OS=Homo sapiens GN=C2 PE=1 SV=2
ITIH2_HUMAN	Inter-alpha-trypsin inhibitor heavy chain H2 OS=Homo sapiens GN=ITIH2 PE=1 SV=2
CO8A_HUMAN	Complement component C8 alpha chain OS=Homo sapiens GN=C8A PE=1 SV=2
PROS_HUMAN	Vitamin K-dependent protein S OS=Homo sapiens GN=PROS1 PE=1 SV=1
K1C14_HUMAN	Keratin, type I cytoskeletal 14 OS=Homo sapiens GN=KRT14 PE=1 SV=4
ACTB_HUMAN	Actin, cytoplasmic 1 OS=Homo sapiens GN=ACTB PE=1 SV=1
CLUS_HUMAN	Clusterin OS=Homo sapiens GN=CLU PE=1 SV=1
PON1_HUMAN	Serum paraoxonase/arylesterase 1 OS=Homo sapiens GN=PON1 PE=1 SV=3
HEP2_HUMAN	Heparin cofactor 2 OS=Homo sapiens GN=SERPIND1 PE=1 SV=3
PZP_HUMAN	Pregnancy zone protein OS=Homo sapiens GN=PZP PE=1 SV=4
K2C5_HUMAN	Keratin, type II cytoskeletal 5 OS=Homo sapiens GN=KRT5 PE=1 SV=3
VTNC_HUMAN	Vitronectin OS=Homo sapiens GN=VTN PE=1 SV=1

IGLL5_HUMAN	Immunoglobulin lambda-like polypeptide 5 OS=Homo sapiens GN=IGLL5 PE=2 SV=2
IGHA2_HUMAN	Ig alpha-2 chain C region OS=Homo sapiens GN=IGHA2 PE=1 SV=3
ANT3_HUMAN	Antithrombin-III OS=Homo sapiens GN=SERPINC1 PE=1 SV=1
HEMO_HUMAN	Hemopexin OS=Homo sapiens GN=HPX PE=1 SV=2
APOE_HUMAN	Apolipoprotein E OS=Homo sapiens GN=APOE PE=1 SV=1
KLKB1_HUMAN	Plasma kallikrein OS=Homo sapiens GN=KLKB1 PE=1 SV=1
A2GL_HUMAN	Leucine-rich alpha-2-glycoprotein OS=Homo sapiens GN=LRG1 PE=1 SV=2
FHR1_HUMAN	Complement factor H-related protein 1 OS=Homo sapiens GN=CFHR1 PE=1 SV=2
POTEF_HUMAN	POTE ankyrin domain family member F OS=Homo sapiens GN=POTEF PE=1 SV=2
ANXA2_HUMAN	Annexin A2 OS=Homo sapiens GN=ANXA2 PE=1 SV=2
KV305_HUMAN	Ig kappa chain V-III region WOL OS=Homo sapiens PE=1 SV=1

1433S_HUMAN	14-3-3 protein sigma OS=Homo sapiens GN=SFN PE=1 SV=1
C1QC_HUMAN	Complement C1q subcomponent subunit C OS=Homo sapiens GN=C1QC PE=1 SV=3
APOA4_HUMAN	Apolipoprotein A-IV OS=Homo sapiens GN=APOA4 PE=1 SV=3
FHR4_HUMAN	Complement factor H-related protein 4 OS=Homo sapiens GN=CFHR4 PE=1 SV=3
FIBA_HUMAN	Fibrinogen alpha chain OS=Homo sapiens GN=FGA PE=1 SV=2
FBLN1_HUMAN	Fibulin-1 OS=Homo sapiens GN=FBLN1 PE=1 SV=4
APOL1_HUMAN	Apolipoprotein L1 OS=Homo sapiens GN=APOL1 PE=1 SV=5
TTHY_HUMAN	Transthyretin OS=Homo sapiens GN=TTR PE=1 SV=1
HBB_HUMAN	Hemoglobin subunit beta OS=Homo sapiens GN=HBB PE=1 SV=2
KPYM_HUMAN	Pyruvate kinase PKM OS=Homo sapiens GN=PKM PE=1 SV=4
ITIH3_HUMAN	Inter-alpha-trypsin inhibitor heavy chain H3 OS=Homo sapiens GN=ITIH3 PE=1 SV=2
HABP2_HUMAN	Hyaluronan-binding protein 2 OS=Homo sapiens GN=HABP2 PE=1 SV=1

PEDF_HUMAN	Pigment epithelium-derived factor OS=Homo sapiens GN=SERPINF1 PE=1 SV=4
KR510_HUMAN	Keratin-associated protein 5-10 OS=Homo sapiens GN=KRTAP5-10 PE=2 SV=1
KRA54_HUMAN	Keratin-associated protein 5-4 OS=Homo sapiens GN=KRTAP5-4 PE=2 SV=1
KRA53_HUMAN	Keratin-associated protein 5-3 OS=Homo sapiens GN=KRTAP5-3 PE=2 SV=1
FHR2_HUMAN	Complement factor H-related protein 2 OS=Homo sapiens GN=CFHR2 PE=1 SV=1
K1C16_HUMAN	Keratin, type I cytoskeletal 16 OS=Homo sapiens GN=KRT16 PE=1 SV=4
LDHA_HUMAN	L-lactate dehydrogenase A chain OS=Homo sapiens GN=LDHA PE=1 SV=2
LV302_HUMAN	Ig lambda chain V-III region LOI OS=Homo sapiens PE=1 SV=1
KV301_HUMAN	Ig kappa chain V-III region B6 OS=Homo sapiens PE=1 SV=1
HRG_HUMAN	Histidine-rich glycoprotein OS=Homo sapiens GN=HRG PE=1 SV=1
CO8G_HUMAN	Complement component C8 gamma chain OS=Homo sapiens GN=C8G PE=1 SV=3
SAMP_HUMAN	Serum amyloid P-component OS=Homo sapiens GN=APCS PE=1 SV=2
KV204_HUMAN	Ig kappa chain V-II region TEW OS=Homo sapiens PE=1 SV=1
KV203_HUMAN	Ig kappa chain V-II region MIL OS=Homo sapiens PE=1 SV=1
ATRN_HUMAN	Attractin OS=Homo sapiens GN=ATRN PE=1 SV=2
DCD_HUMAN	Dermcidin OS=Homo sapiens GN=DCD PE=1 SV=2

G3P_HUMAN	Glyceraldehyde-3-phosphate dehydrogenase OS=Homo sapiens GN=GAPDH PE=1 SV=3
FCN3_HUMAN	Ficolin-3 OS=Homo sapiens GN=FCN3 PE=1 SV=2
APOA_HUMAN	Apolipoprotein(a) OS=Homo sapiens GN=LPA PE=1 SV=1
ALDOA_HUMAN	Fructose-bisphosphate aldolase A OS=Homo sapiens GN=ALDOA PE=1 SV=2
FA12_HUMAN	Coagulation factor XII OS=Homo sapiens GN=F12 PE=1 SV=3
C1QB_HUMAN	Complement C1q subcomponent subunit B OS=Homo sapiens GN=C1QB PE=1 SV=3
TBA1A_HUMAN	Tubulin alpha-1A chain OS=Homo sapiens GN=TUBA1A PE=1 SV=1
TETN_HUMAN	Tetranectin OS=Homo sapiens GN=CLEC3B PE=1 SV=3
LRP1_HUMAN	Prolow-density lipoprotein receptor-related protein 1 OS=Homo sapiens GN=LRP1 PE=1 SV=2
KRA44_HUMAN	Keratin-associated protein 4-4 OS=Homo sapiens GN=KRTAP4-4 PE=2 SV=1
HV301_HUMAN	Ig heavy chain V-III region TRO OS=Homo sapiens PE=1 SV=1
MYH9_HUMAN	Myosin-9 OS=Homo sapiens GN=MYH9 PE=1 SV=4
VIME_HUMAN	Vimentin OS=Homo sapiens GN=VIM PE=1 SV=4
MBL2_HUMAN	Mannose-binding protein C OS=Homo sapiens GN=MBL2 PE=1 SV=2
HSPB1_HUMAN	Heat shock protein beta-1 OS=Homo sapiens GN=HSPB1 PE=1 SV=2

CBPB2_HUMAN	Carboxypeptidase B2 OS=Homo sapiens GN=CPB2 PE=1 SV=2
SEPP1_HUMAN	Selenoprotein P OS=Homo sapiens GN=SEPP1 PE=1 SV=3
HBA_HUMAN	Hemoglobin subunit alpha OS=Homo sapiens GN=HBA1 PE=1 SV=2
LG3BP_HUMAN	Galectin-3-binding protein OS=Homo sapiens GN=LGALS3BP PE=1 SV=1
APOD_HUMAN	Apolipoprotein D OS=Homo sapiens GN=APOD PE=1 SV=1
FETUB_HUMAN	Fetuin-B OS=Homo sapiens GN=FETUB PE=1 SV=2
ANXA1_HUMAN	Annexin A1 OS=Homo sapiens GN=ANXA1 PE=1 SV=2
A2AP_HUMAN	Alpha-2-antiplasmin OS=Homo sapiens GN=SERPINF2 PE=1 SV=3
APOM_HUMAN	Apolipoprotein M OS=Homo sapiens GN=APOM PE=1 SV=2
HV101_HUMAN	Ig heavy chain V-I region EU OS=Homo sapiens PE=1 SV=1
TSP1_HUMAN	Thrombospondin-1 OS=Homo sapiens GN=THBS1 PE=1 SV=2
KV101_HUMAN	Ig kappa chain V-I region AG OS=Homo sapiens PE=1 SV=1
KV111_HUMAN	Ig kappa chain V-I region Ka OS=Homo sapiens PE=1 SV=1

GSTP1_HUMAN	Glutathione S-transferase P OS=Homo sapiens GN=GSTP1 PE=1 SV=2
KV310_HUMAN	Ig kappa chain V-III region VH (Fragment) OS=Homo sapiens PE=4 SV=1
KV306_HUMAN	Ig kappa chain V-III region POM OS=Homo sapiens PE=1 SV=1
KV308_HUMAN	Ig kappa chain V-III region CLL OS=Homo sapiens PE=4 SV=2
ECM1_HUMAN	Extracellular matrix protein 1 OS=Homo sapiens GN=ECM1 PE=1 SV=2
DESP_HUMAN	Desmoplakin OS=Homo sapiens GN=DSP PE=1 SV=3
CALM_HUMAN	Calmodulin OS=Homo sapiens GN=CALM1 PE=1 SV=2
SAA1_HUMAN	Serum amyloid A-1 protein OS=Homo sapiens GN=SAA1 PE=1 SV=1
FA10_HUMAN	Coagulation factor X OS=Homo sapiens GN=F10 PE=1 SV=2
SHBG_HUMAN	Sex hormone-binding globulin OS=Homo sapiens GN=SHBG PE=1 SV=2
EF1A1_HUMAN	Elongation factor 1-alpha 1 OS=Homo sapiens GN=EEF1A1 PE=1 SV=1
LCE2B_HUMAN	Late cornified envelope protein 2B OS=Homo sapiens GN=LCE2B PE=2 SV=1
KRA59_HUMAN	Keratin-associated protein 5-9 OS=Homo sapiens GN=KRTAP5-9 PE=1 SV=1

LAMC1_HUMAN	Laminin subunit gamma-1 OS=Homo sapiens GN=LAMC1 PE=1 SV=3
MT2_HUMAN	Metallothionein-2 OS=Homo sapiens GN=MT2A PE=1 SV=1
KRA51_HUMAN	Keratin-associated protein 5-1 OS=Homo sapiens GN=KRTAP5-1 PE=2 SV=1
FA9_HUMAN	Coagulation factor IX OS=Homo sapiens GN=F9 PE=1 SV=2
TENX_HUMAN	Tenascin-X OS=Homo sapiens GN=TNXB PE=1 SV=4
MT1L_HUMAN	Metallothionein-1L OS=Homo sapiens GN=MT1L PE=2 SV=1
STAB1_HUMAN	Stabilin-1 OS=Homo sapiens GN=STAB1 PE=1 SV=3
KRA57_HUMAN	Keratin-associated protein 5-7 OS=Homo sapiens GN=KRTAP5-7 PE=2 SV=1
MT1DP_HUMAN	Putative metallothionein MT1DP OS=Homo sapiens GN=MT1DP PE=5 SV=1

Appendix B: List of proteins identified in PCCF isolated using tandem immunoaffinity method from plasma of patients with Gleason score 8.

Accession	Description
APOB_HUMAN	Apolipoprotein B-100 OS=Homo sapiens GN=APOB PE=1 SV=2
CO3_HUMAN	Complement C3 OS=Homo sapiens GN=C3 PE=1 SV=2
MYH9_HUMAN	Myosin-9 OS=Homo sapiens GN=MYH9 PE=1 SV=4
FLNA_HUMAN	Filamin-A OS=Homo sapiens GN=FLNA PE=1 SV=4
TLN1_HUMAN	Talin-1 OS=Homo sapiens GN=TLN1 PE=1 SV=3
CO4A_HUMAN	Complement C4-A OS=Homo sapiens GN=C4A PE=1 SV=2
CO4B_HUMAN	Complement C4-B OS=Homo sapiens GN=C4B PE=1 SV=2
A2MG_HUMAN	Alpha-2-macroglobulin OS=Homo sapiens GN=A2M PE=1 SV=3
ALBU_HUMAN	Serum albumin OS=Homo sapiens GN=ALB PE=1 SV=2
A1AT_HUMAN	Alpha-1-antitrypsin OS=Homo sapiens GN=SERPINA1 PE=1 SV=3
FIBB_HUMAN	Fibrinogen beta chain OS=Homo sapiens GN=FGB PE=1 SV=2
FIBA_HUMAN	Fibrinogen alpha chain OS=Homo sapiens GN=FGA PE=1 SV=2
CERU_HUMAN	Ceruloplasmin OS=Homo sapiens GN=CP PE=1 SV=1
APOA1_HUMAN	Apolipoprotein A-I OS=Homo sapiens GN=APOA1 PE=1 SV=1
ITIH4_HUMAN	Inter-alpha-trypsin inhibitor heavy chain H4 OS=Homo sapiens GN=ITIH4 PE=1 SV=4
ITIH2_HUMAN	Inter-alpha-trypsin inhibitor heavy chain H2 OS=Homo sapiens GN=ITIH2 PE=1 SV=2
TSP1_HUMAN	Thrombospondin-1 OS=Homo sapiens GN=THBS1 PE=1 SV=2
GELS_HUMAN	Gelsolin OS=Homo sapiens GN=GSN PE=1 SV=1
TRFE_HUMAN	Serotransferrin OS=Homo sapiens GN=TF PE=1 SV=3
ITA2B_HUMAN	Integrin alpha-IIb OS=Homo sapiens GN=ITGA2B PE=1 SV=3

CFAB_HUMAN	Complement factor B OS=Homo sapiens GN=CFB PE=1 SV=2
ACTB_HUMAN	Actin, cytoplasmic 1 OS=Homo sapiens GN=ACTB PE=1 SV=1
AACT_HUMAN	Alpha-1-antichymotrypsin OS=Homo sapiens GN=SERPINA3 PE=1 SV=2
K2C1_HUMAN	Keratin, type II cytoskeletal 1 OS=Homo sapiens GN=KRT1 PE=1 SV=6
FIBG_HUMAN	Fibrinogen gamma chain OS=Homo sapiens GN=FGG PE=1 SV=3
K22E_HUMAN	Keratin, type II cytoskeletal 2 epidermal OS=Homo sapiens GN=KRT2 PE=1 SV=2
FA5_HUMAN	Coagulation factor V OS=Homo sapiens GN=F5 PE=1 SV=4
HPT_HUMAN	Haptoglobin OS=Homo sapiens GN=HP PE=1 SV=1
ITIH1_HUMAN	Inter-alpha-trypsin inhibitor heavy chain H1 OS=Homo sapiens GN=ITIH1 PE=1 SV=3
ANT3_HUMAN	Antithrombin-III OS=Homo sapiens GN=SERPINC1 PE=1 SV=1
CFAH_HUMAN	Complement factor H OS=Homo sapiens GN=CFH PE=1 SV=4
CO5_HUMAN	Complement C5 OS=Homo sapiens GN=C5 PE=1 SV=4
K1C10_HUMAN	Keratin, type I cytoskeletal 10 OS=Homo sapiens GN=KRT10 PE=1 SV=6
FINC_HUMAN	Fibronectin OS=Homo sapiens GN=FN1 PE=1 SV=4
APOA4_HUMAN	Apolipoprotein A-IV OS=Homo sapiens GN=APOA4 PE=1 SV=3
MMRN1_HUMAN	Multimerin-1 OS=Homo sapiens GN=MMRN1 PE=1 SV=3
TPM4_HUMAN	Tropomyosin alpha-4 chain OS=Homo sapiens GN=TPM4 PE=1 SV=3
ACTN1_HUMAN	Alpha-actinin-1 OS=Homo sapiens GN=ACTN1 PE=1 SV=2
HPTR_HUMAN	Haptoglobin-related protein OS=Homo sapiens GN=HPR PE=2 SV=2
A1BG_HUMAN	Alpha-1B-glycoprotein OS=Homo sapiens GN=A1BG PE=1 SV=4
TBB1_HUMAN	Tubulin beta-1 chain OS=Homo sapiens GN=TUBB1 PE=1 SV=1
VINC_HUMAN	Vinculin OS=Homo sapiens GN=VCL PE=1 SV=4

ACTC_HUMAN	Actin, alpha cardiac muscle 1 OS=Homo sapiens GN=ACTC1 PE=1 SV=1
IGHG1_HUMAN	Ig gamma-1 chain C region OS=Homo sapiens GN=IGHG1 PE=1 SV=1
CO9_HUMAN	Complement component C9 OS=Homo sapiens GN=C9 PE=1 SV=2
APOE_HUMAN	Apolipoprotein E OS=Homo sapiens GN=APOE PE=1 SV=1
K1C9_HUMAN	Keratin, type I cytoskeletal 9 OS=Homo sapiens GN=KRT9 PE=1 SV=3
CO6_HUMAN	Complement component C6 OS=Homo sapiens GN=C6 PE=1 SV=3
IGHA1_HUMAN	Ig alpha-1 chain C region OS=Homo sapiens GN=IGHA1 PE=1 SV=2
IGHM_HUMAN	Ig mu chain C region OS=Homo sapiens GN=IGHM PE=1 SV=3
ANGT_HUMAN	Angiotensinogen OS=Homo sapiens GN=AGT PE=1 SV=1
IGHG3_HUMAN	Ig gamma-3 chain C region OS=Homo sapiens GN=IGHG3 PE=1 SV=2
HEMO_HUMAN	Hemopexin OS=Homo sapiens GN=HPX PE=1 SV=2
IGHA2_HUMAN	Ig alpha-2 chain C region OS=Homo sapiens GN=IGHA2 PE=1 SV=3
TTHY_HUMAN	Transthyretin OS=Homo sapiens GN=TTR PE=1 SV=1
HEP2_HUMAN	Heparin cofactor 2 OS=Homo sapiens GN=SERPIND1 PE=1 SV=3
CBG_HUMAN	Corticosteroid-binding globulin OS=Homo sapiens GN=SERPINA6 PE=1 SV=1
TBA4A_HUMAN	Tubulin alpha-4A chain OS=Homo sapiens GN=TUBA4A PE=1 SV=1
IC1_HUMAN	Plasma protease C1 inhibitor OS=Homo sapiens GN=SERPING1 PE=1 SV=2
HBB_HUMAN	Hemoglobin subunit beta OS=Homo sapiens GN=HBB PE=1 SV=2
CLUS_HUMAN	Clusterin OS=Homo sapiens GN=CLU PE=1 SV=1
HRG_HUMAN	Histidine-rich glycoprotein OS=Homo sapiens GN=HRG PE=1 SV=1
VTDB_HUMAN	Vitamin D-binding protein OS=Homo sapiens GN=GC PE=1 SV=1

THBG_HUMAN	Thyroxine-binding globulin OS=Homo sapiens GN=SERPINA7 PE=1 SV=2
C1S_HUMAN	Complement C1s subcomponent OS=Homo sapiens GN=C1S PE=1 SV=1
CO8B_HUMAN	Complement component C8 beta chain OS=Homo sapiens GN=C8B PE=1 SV=3
STOM_HUMAN	Erythrocyte band 7 integral membrane protein OS=Homo sapiens GN=STOM PE=1 SV=3
ATPB_HUMAN	ATP synthase subunit beta, mitochondrial OS=Homo sapiens GN=ATP5B PE=1 SV=3
GRP78_HUMAN	78 kDa glucose-regulated protein OS=Homo sapiens GN=HSPA5 PE=1 SV=2
IGHG4_HUMAN	Ig gamma-4 chain C region OS=Homo sapiens GN=IGHG4 PE=1 SV=1
IGHG2_HUMAN	Ig gamma-2 chain C region OS=Homo sapiens GN=IGHG2 PE=1 SV=2
K2C5_HUMAN	Keratin, type II cytoskeletal 5 OS=Homo sapiens GN=KRT5 PE=1 SV=3
SAMP_HUMAN	Serum amyloid P-component OS=Homo sapiens GN=APCS PE=1 SV=2
1433Z_HUMAN	14-3-3 protein zeta/delta OS=Homo sapiens GN=YWHAZ PE=1 SV=1
APOA2_HUMAN	Apolipoprotein A-II OS=Homo sapiens GN=APOA2 PE=1 SV=1
ITB3_HUMAN	Integrin beta-3 OS=Homo sapiens GN=ITGB3 PE=1 SV=2
TBA1A_HUMAN	Tubulin alpha-1A chain OS=Homo sapiens GN=TUBA1A PE=1 SV=1
KNG1_HUMAN	Kininogen-1 OS=Homo sapiens GN=KNG1 PE=1 SV=2
PLMN_HUMAN	Plasminogen OS=Homo sapiens GN=PLG PE=1 SV=2
GP1BA_HUMAN	Platelet glycoprotein Ib alpha chain OS=Homo sapiens GN=GP1BA PE=1 SV=2
APOL1_HUMAN	Apolipoprotein L1 OS=Homo sapiens GN=APOL1 PE=1 SV=5
PROS_HUMAN	Vitamin K-dependent protein S OS=Homo sapiens GN=PROS1 PE=1 SV=1
A2AP_HUMAN	Alpha-2-antiplasmin OS=Homo sapiens GN=SERPINF2 PE=1 SV=3
IGLL5_HUMAN	Immunoglobulin lambda-like polypeptide 5 OS=Homo sapiens GN=IGLL5 PE=2 SV=2

LAC7_HUMAN	Ig lambda-7 chain C region OS=Homo sapiens GN=IGLC7 PE=4 SV=2
VTNC_HUMAN	Vitronectin OS=Homo sapiens GN=VTN PE=1 SV=1
MYL6_HUMAN	Myosin light polypeptide 6 OS=Homo sapiens GN=MYL6 PE=1 SV=2
ML12A_HUMAN	Myosin regulatory light chain 12A OS=Homo sapiens GN=MYL12A PE=1 SV=2
RET4_HUMAN	Retinol-binding protein 4 OS=Homo sapiens GN=RBP4 PE=1 SV=3
SDPR_HUMAN	Serum deprivation-response protein OS=Homo sapiens GN=SDPR PE=1 SV=3
CO7_HUMAN	Complement component C7 OS=Homo sapiens GN=C7 PE=1 SV=2
AT2A3_HUMAN	Sarcoplasmic/endoplasmic reticulum calcium ATPase 3 OS=Homo sapiens GN=ATP2A3 PE=1 SV=2
IDHP_HUMAN	Isocitrate dehydrogenase [NADP], mitochondrial OS=Homo sapiens GN=IDH2 PE=1 SV=2
A2GL_HUMAN	Leucine-rich alpha-2-glycoprotein OS=Homo sapiens GN=LRG1 PE=1 SV=2
C1R_HUMAN	Complement C1r subcomponent OS=Homo sapiens GN=C1R PE=1 SV=2
F13A_HUMAN	Coagulation factor XIII A chain OS=Homo sapiens GN=F13A1 PE=1 SV=4
IGKC_HUMAN	Ig kappa chain C region OS=Homo sapiens GN=IGKC PE=1 SV=1
TBB5_HUMAN	Tubulin beta chain OS=Homo sapiens GN=TUBB PE=1 SV=2
LAC2_HUMAN	Ig lambda-2 chain C regions OS=Homo sapiens GN=IGLC2 PE=1 SV=1
PON1_HUMAN	Serum paraoxonase/arylesterase 1 OS=Homo sapiens GN=PON1 PE=1 SV=3
HBA_HUMAN	Hemoglobin subunit alpha OS=Homo sapiens GN=HBA1 PE=1 SV=2
TBA8_HUMAN	Tubulin alpha-8 chain OS=Homo sapiens GN=TUBA8 PE=1 SV=1
MYL9_HUMAN	Myosin regulatory light polypeptide 9 OS=Homo sapiens GN=MYL9 PE=1 SV=4
THRB_HUMAN	Prothrombin OS=Homo sapiens GN=F2 PE=1 SV=2
RAB1B_HUMAN	Ras-related protein Rab-1B OS=Homo sapiens GN=RAB1B PE=1 SV=1
RAB1A_HUMAN	Ras-related protein Rab-1A OS=Homo sapiens GN=RAB1A PE=1 SV=3

PEDF_HUMAN	Pigment epithelium-derived factor OS=Homo sapiens GN=SERPINF1 PE=1 SV=4
G3P_HUMAN	Glyceraldehyde-3-phosphate dehydrogenase OS=Homo sapiens GN=GAPDH PE=1 SV=3
LTBP1_HUMAN	Latent-transforming growth factor beta-binding protein 1 OS=Homo sapiens GN=LTBP1 PE=1 SV=4
CALX_HUMAN	Calnexin OS=Homo sapiens GN=CANX PE=1 SV=2
VDAC3_HUMAN	Voltage-dependent anion-selective channel protein 3 OS=Homo sapiens GN=VDAC3 PE=1 SV=1
KPYM_HUMAN	Pyruvate kinase PKM OS=Homo sapiens GN=PKM PE=1 SV=4
ALDOA_HUMAN	Fructose-bisphosphate aldolase A OS=Homo sapiens GN=ALDOA PE=1 SV=2
HSP72_HUMAN	Heat shock-related 70 kDa protein 2 OS=Homo sapiens GN=HSPA2 PE=1 SV=1
C4BPA_HUMAN	C4b-binding protein alpha chain OS=Homo sapiens GN=C4BPA PE=1 SV=2
CALD1_HUMAN	Caldesmon OS=Homo sapiens GN=CALD1 PE=1 SV=3
CO8A_HUMAN	Complement component C8 alpha chain OS=Homo sapiens GN=C8A PE=1 SV=2
AFAM_HUMAN	Afamin OS=Homo sapiens GN=AFM PE=1 SV=1
LUM_HUMAN	Lumican OS=Homo sapiens GN=LUM PE=1 SV=2
ITIH3_HUMAN	Inter-alpha-trypsin inhibitor heavy chain H3 OS=Homo sapiens GN=ITIH3 PE=1 SV=2
1B07_HUMAN	HLA class I histocompatibility antigen, B-7 alpha chain OS=Homo sapiens GN=HLA-B PE=1 SV=3
1A68_HUMAN	HLA class I histocompatibility antigen, A-68 alpha chain OS=Homo sapiens GN=HLA-A PE=1 SV=4
PHLD_HUMAN	Phosphatidylinositol-glycan-specific phospholipase D OS=Homo sapiens GN=GPLD1 PE=1 SV=3
K1C13_HUMAN	Keratin, type I cytoskeletal 13 OS=Homo sapiens GN=KRT13 PE=1 SV=4
KV312_HUMAN	Ig kappa chain V-III region HAH OS=Homo sapiens PE=2 SV=1
FETUA_HUMAN	Alpha-2-HS-glycoprotein OS=Homo sapiens GN=AHSG PE=1 SV=1
1433G_HUMAN	14-3-3 protein gamma OS=Homo sapiens GN=YWHAG PE=1 SV=2
1433E_HUMAN	14-3-3 protein epsilon OS=Homo sapiens GN=YWHAE PE=1 SV=1

1433F_HUMAN	14-3-3 protein eta OS=Homo sapiens GN=YWHAH PE=1 SV=4
C1QB_HUMAN	Complement C1q subcomponent subunit B OS=Homo sapiens GN=C1QB PE=1 SV=3
CXCL7_HUMAN	Platelet basic protein OS=Homo sapiens GN=PPBP PE=1 SV=3
C1QC_HUMAN	Complement C1q subcomponent subunit C OS=Homo sapiens GN=C1QC PE=1 SV=3
AMBP_HUMAN	Protein AMBP OS=Homo sapiens GN=AMBP PE=1 SV=1
RAB10_HUMAN	Ras-related protein Rab-10 OS=Homo sapiens GN=RAB10 PE=1 SV=1
CH60_HUMAN	60 kDa heat shock protein, mitochondrial OS=Homo sapiens GN=HSPD1 PE=1 SV=2
KAIN_HUMAN	Kallistatin OS=Homo sapiens GN=SERPINA4 PE=1 SV=3
GTR3_HUMAN	Solute carrier family 2, facilitated glucose transporter member 3 OS=Homo sapiens GN=SLC2A3 PE=2 SV=1
PLEK_HUMAN	Pleckstrin OS=Homo sapiens GN=PLEK PE=1 SV=3
SAA4_HUMAN	Serum amyloid A-4 protein OS=Homo sapiens GN=SAA4 PE=1 SV=2
HS71L_HUMAN	Heat shock 70 kDa protein 1-like OS=Homo sapiens GN=HSPA1L PE=1 SV=2
ZA2G_HUMAN	Zinc-alpha-2-glycoprotein OS=Homo sapiens GN=AZGP1 PE=1 SV=2
HV306_HUMAN	Ig heavy chain V-III region BUT OS=Homo sapiens PE=1 SV=1
ATPA_HUMAN	ATP synthase subunit alpha, mitochondrial OS=Homo sapiens GN=ATP5A1 PE=1 SV=1
APOC2_HUMAN	Apolipoprotein C-II OS=Homo sapiens GN=APOC2 PE=1 SV=1
KLKB1_HUMAN	Plasma kallikrein OS=Homo sapiens GN=KLKB1 PE=1 SV=1
FA10_HUMAN	Coagulation factor X OS=Homo sapiens GN=F10 PE=1 SV=2
CPN2_HUMAN	Carboxypeptidase N subunit 2 OS=Homo sapiens GN=CPN2 PE=1 SV=3
HXK1_HUMAN	Hexokinase-1 OS=Homo sapiens GN=HK1 PE=1 SV=3
GNAI2_HUMAN	Guanine nucleotide-binding protein G(i) subunit alpha-2 OS=Homo sapiens GN=GNAI2 PE=1 SV=3

PECA1_HUMAN	Platelet endothelial cell adhesion molecule OS=Homo sapiens GN=PECAM1 PE=1 SV=1
ITB1_HUMAN	Integrin beta-1 OS=Homo sapiens GN=ITGB1 PE=1 SV=2
BIN2_HUMAN	Bridging integrator 2 OS=Homo sapiens GN=BIN2 PE=1 SV=3
URP2_HUMAN	Fermitin family homolog 3 OS=Homo sapiens GN=FERMT3 PE=1 SV=1
FHR1_HUMAN	Complement factor H-related protein 1 OS=Homo sapiens GN=CFHR1 PE=1 SV=2
K2C4_HUMAN	Keratin, type II cytoskeletal 4 OS=Homo sapiens GN=KRT4 PE=1 SV=4
KV301_HUMAN	Ig kappa chain V-III region B6 OS=Homo sapiens PE=1 SV=1
KV118_HUMAN	Ig kappa chain V-I region WEA OS=Homo sapiens PE=1 SV=1
KV105_HUMAN	Ig kappa chain V-I region DEE OS=Homo sapiens PE=1 SV=1
KV121_HUMAN	Ig kappa chain V-I region Ni OS=Homo sapiens PE=1 SV=1
KV106_HUMAN	Ig kappa chain V-I region EU OS=Homo sapiens PE=1 SV=1
LV302_HUMAN	Ig lambda chain V-III region LOI OS=Homo sapiens PE=1 SV=1
APOH_HUMAN	Beta-2-glycoprotein 1 OS=Homo sapiens GN=APOH PE=1 SV=3
TETN_HUMAN	Tetranectin OS=Homo sapiens GN=CLEC3B PE=1 SV=3
CD36_HUMAN	Platelet glycoprotein 4 OS=Homo sapiens GN=CD36 PE=1 SV=2
FBLN1_HUMAN	Fibulin-1 OS=Homo sapiens GN=FBLN1 PE=1 SV=4
FCN3_HUMAN	Ficolin-3 OS=Homo sapiens GN=FCN3 PE=1 SV=2
HV320_HUMAN	Ig heavy chain V-III region GAL OS=Homo sapiens PE=1 SV=1
C1QA_HUMAN	Complement C1q subcomponent subunit A OS=Homo sapiens GN=C1QA PE=1 SV=2
LV106_HUMAN	Ig lambda chain V-I region WAH OS=Homo sapiens PE=1 SV=1
PROF1_HUMAN	Profilin-1 OS=Homo sapiens GN=PFN1 PE=1 SV=2
RAP1B_HUMAN	Ras-related protein Rap-1b OS=Homo sapiens GN=RAP1B PE=1 SV=1

RTN4_HUMAN	Reticulon-4 OS=Homo sapiens GN=RTN4 PE=1 SV=2
COF1_HUMAN	Cofilin-1 OS=Homo sapiens GN=CFL1 PE=1 SV=3
MDHM_HUMAN	Malate dehydrogenase, mitochondrial OS=Homo sapiens GN=MDH2 PE=1 SV=3
ADT2_HUMAN	ADP/ATP translocase 2 OS=Homo sapiens GN=SLC25A5 PE=1 SV=7
AT5F1_HUMAN	ATP synthase F(0) complex subunit B1, mitochondrial OS=Homo sapiens GN=ATP5F1 PE=1 SV=2
KV309_HUMAN	Ig kappa chain V-III region VG (Fragment) OS=Homo sapiens PE=1 SV=1
MBL2_HUMAN	Mannose-binding protein C OS=Homo sapiens GN=MBL2 PE=1 SV=2
RB27B_HUMAN	Ras-related protein Rab-27B OS=Homo sapiens GN=RAB27B PE=1 SV=4
VDAC2_HUMAN	Voltage-dependent anion-selective channel protein 2 OS=Homo sapiens GN=VDAC2 PE=1 SV=2
CKLF5_HUMAN	CKLF-like MARVEL transmembrane domain-containing protein 5 OS=Homo sapiens GN=CMTM5 PE=1 SV=2
LYSC_HUMAN	Lysozyme C OS=Homo sapiens GN=LYZ PE=1 SV=1
THAS_HUMAN	Thromboxane-A synthase OS=Homo sapiens GN=TBXAS1 PE=1 SV=3
CISY_HUMAN	Citrate synthase, mitochondrial OS=Homo sapiens GN=CS PE=1 SV=2
TAGL2_HUMAN	Transgelin-2 OS=Homo sapiens GN=TAGLN2 PE=1 SV=3
COR1C_HUMAN	Coronin-1C OS=Homo sapiens GN=CORO1C PE=1 SV=1
CBPN_HUMAN	Carboxypeptidase N catalytic chain OS=Homo sapiens GN=CPN1 PE=1 SV=1
ZYX_HUMAN	Zyxin OS=Homo sapiens GN=ZYX PE=1 SV=1
CAP1_HUMAN	Adenylyl cyclase-associated protein 1 OS=Homo sapiens GN=CAP1 PE=1 SV=5
GBG5_HUMAN	Guanine nucleotide-binding protein G(I)/G(S)/G(O) subunit gamma-5 OS=Homo sapiens GN=GNG5 PE=1 SV=3
PGRP2_HUMAN	N-acetylmuramoyl-L-alanine amidase OS=Homo sapiens GN=PGLYRP2 PE=1 SV=1
INF2_HUMAN	Inverted formin-2 OS=Homo sapiens GN=INF2 PE=1 SV=2

SEPP1_HUMAN	Selenoprotein P OS=Homo sapiens GN=SEPP1 PE=1 SV=3
LYAM3_HUMAN	P-selectin OS=Homo sapiens GN=SELP PE=1 SV=3
LCAT_HUMAN	Phosphatidylcholine-sterol acyltransferase OS=Homo sapiens GN=LCAT PE=1 SV=1
COR1A_HUMAN	Coronin-1A OS=Homo sapiens GN=CORO1A PE=1 SV=4
ALS_HUMAN	Insulin-like growth factor-binding protein complex acid labile subunit OS=Homo sapiens GN=IGFALS PE=1 SV=1
MPCP_HUMAN	Phosphate carrier protein, mitochondrial OS=Homo sapiens GN=SLC25A3 PE=1 SV=2
CO8G_HUMAN	Complement component C8 gamma chain OS=Homo sapiens GN=C8G PE=1 SV=3
CSRP1_HUMAN	Cysteine and glycine-rich protein 1 OS=Homo sapiens GN=CSRP1 PE=1 SV=3
CAZA1_HUMAN	F-actin-capping protein subunit alpha-1 OS=Homo sapiens GN=CAPZA1 PE=1 SV=3

Appendix C: List of proteins identified in PCCF isolated using tandem immunoaffinity method from plasma of patients with Gleason score 6.

Accession	Description	#Peptides
P01834|IGKC_HUMAN	Ig kappa chain C region OS=Homo sapiens GN=IGKC PE=1 SV=1	7
P01834|IGKC_HUMAN	Ig kappa chain C region OS=Homo sapiens GN=IGKC PE=1 SV=1	8
P01834|IGKC_HUMAN	Ig kappa chain C region OS=Homo sapiens GN=IGKC PE=1 SV=1	12
P02768|ALBU_HUMAN	Serum albumin OS=Homo sapiens GN=ALB PE=1 SV=2	57
P02768|ALBU_HUMAN	Serum albumin OS=Homo sapiens GN=ALB PE=1 SV=2	60
P02768|ALBU_HUMAN	Serum albumin OS=Homo sapiens GN=ALB PE=1 SV=2	60
P0CG05|LAC2_HUMAN	Ig lambda-2 chain C regions OS=Homo sapiens GN=IGLC2 PE=1 SV=1	5
P0CG06|LAC3_HUMAN	Ig lambda-3 chain C regions OS=Homo sapiens GN=IGLC3 PE=1 SV=1	5
P01857|IGHG1_HUMAN	Ig gamma-1 chain C region OS=Homo sapiens GN=IGHG1 PE=1 SV=1	24
P01857|IGHG1_HUMAN	Ig gamma-1 chain C region OS=Homo sapiens GN=IGHG1 PE=1 SV=1	29
P13645|K1C10_HUMAN	Keratin, type I cytoskeletal 10 OS=Homo sapiens GN=KRT10 PE=1 SV=6	33
P13645|K1C10_HUMAN	Keratin, type I cytoskeletal 10 OS=Homo sapiens GN=KRT10 PE=1 SV=6	31
P01857|IGHG1_HUMAN	Ig gamma-1 chain C region OS=Homo sapiens GN=IGHG1 PE=1 SV=1	18
P01859|IGHG2_HUMAN	Ig gamma-2 chain C region OS=Homo sapiens GN=IGHG2 PE=1 SV=2	19
P35908|K22E_HUMAN	Keratin, type II cytoskeletal 2 epidermal OS=Homo sapiens GN=KRT2 PE=1 SV=2	28
P01859|IGHG2_HUMAN	Ig gamma-2 chain C region OS=Homo sapiens GN=IGHG2 PE=1 SV=2	18

P01861|IGHG4_HUMAN	Ig gamma-4 chain C region OS=Homo sapiens GN=IGHG4 PE=1 SV=1	17
P01860|IGHG3_HUMAN	Ig gamma-3 chain C region OS=Homo sapiens GN=IGHG3 PE=1 SV=2	17
P04264|K2C1_HUMAN	Keratin, type II cytoskeletal 1 OS=Homo sapiens GN=KRT1 PE=1 SV=6	32
P02763|A1AG1_HUMAN	Alpha-1-acid glycoprotein 1 OS=Homo sapiens GN=ORM1 PE=1 SV=1	7
P01861|IGHG4_HUMAN	Ig gamma-4 chain C region OS=Homo sapiens GN=IGHG4 PE=1 SV=1	14
P13645|K1C10_HUMAN	Keratin, type I cytoskeletal 10 OS=Homo sapiens GN=KRT10 PE=1 SV=6	22
P35527|K1C9_HUMAN	Keratin, type I cytoskeletal 9 OS=Homo sapiens GN=KRT9 PE=1 SV=3	24
P04264|K2C1_HUMAN	Keratin, type II cytoskeletal 1 OS=Homo sapiens GN=KRT1 PE=1 SV=6	27
P04206|KV307_HUMAN	Ig kappa chain V-III region GOL OS=Homo sapiens PE=1 SV=1	3
P02452|CO1A1_HUMAN	Collagen alpha-1(I) chain OS=Homo sapiens GN=COL1A1 PE=1 SV=5	133
P80748|LV302_HUMAN	Ig lambda chain V-III region LOI OS=Homo sapiens PE=1 SV=1	3
B9A064|IGLL5_HUMAN	Immunoglobulin lambda-like polypeptide 5 OS=Homo sapiens GN=IGLL5 PE=2 SV=2	6
P02763|A1AG1_HUMAN	Alpha-1-acid glycoprotein 1 OS=Homo sapiens GN=ORM1 PE=1 SV=1	6
P04264|K2C1_HUMAN	Keratin, type II cytoskeletal 1 OS=Homo sapiens GN=KRT1 PE=1 SV=6	20
P35908|K22E_HUMAN	Keratin, type II cytoskeletal 2 epidermal OS=Homo sapiens GN=KRT2 PE=1 SV=2	20
P81605|DCD_HUMAN	Dermcidin OS=Homo sapiens GN=DCD PE=1 SV=2	2

P01859|IGHG2_HUMAN	Ig gamma-2 chain C region OS=Homo sapiens GN=IGHG2 PE=1 SV=2	16
P01860|IGHG3_HUMAN	Ig gamma-3 chain C region OS=Homo sapiens GN=IGHG3 PE=1 SV=2	16
P01860|IGHG3_HUMAN	Ig gamma-3 chain C region OS=Homo sapiens GN=IGHG3 PE=1 SV=2	18
P02452|CO1A1_HUMAN	Collagen alpha-1(I) chain OS=Homo sapiens GN=COL1A1 PE=1 SV=5	92
P0CG05|LAC2_HUMAN	Ig lambda-2 chain C regions OS=Homo sapiens GN=IGLC2 PE=1 SV=1	3
P0CG06|LAC3_HUMAN	Ig lambda-3 chain C regions OS=Homo sapiens GN=IGLC3 PE=1 SV=1	3
P13647|K2C5_HUMAN	Keratin, type II cytoskeletal 5 OS=Homo sapiens GN=KRT5 PE=1 SV=3	19
P04206|KV307_HUMAN	Ig kappa chain V-III region GOL OS=Homo sapiens PE=1 SV=1	2
P02452|CO1A1_HUMAN	Collagen alpha-1(I) chain OS=Homo sapiens GN=COL1A1 PE=1 SV=5	82
P08123|CO1A2_HUMAN	Collagen alpha-2(I) chain OS=Homo sapiens GN=COL1A2 PE=1 SV=7	57
P02452|CO1A1_HUMAN	Collagen alpha-1(I) chain OS=Homo sapiens GN=COL1A1 PE=1 SV=5	64
P08123|CO1A2_HUMAN	Collagen alpha-2(I) chain OS=Homo sapiens GN=COL1A2 PE=1 SV=7	80
P35527|K1C9_HUMAN	Keratin, type I cytoskeletal 9 OS=Homo sapiens GN=KRT9 PE=1 SV=3	15
P08123|CO1A2_HUMAN	Collagen alpha-2(I) chain OS=Homo sapiens GN=COL1A2 PE=1 SV=7	66
P01598|KV106_HUMAN	Ig kappa chain V-I region EU OS=Homo sapiens PE=1 SV=1	2
B9A064|IGLL5_HUMAN	Immunoglobulin lambda-like polypeptide 5 OS=Homo sapiens GN=IGLL5 PE=2 SV=2	5
P02763|A1AG1_HUMAN	Alpha-1-acid glycoprotein 1 OS=Homo sapiens GN=ORM1 PE=1 SV=1	5

P02533|K1C14_HUMAN	Keratin, type I cytoskeletal 14 OS=Homo sapiens GN=KRT14 PE=1 SV=4	12
P07478|TRY2_HUMAN	Trypsin-2 OS=Homo sapiens GN=PRSS2 PE=1 SV=1	20
P02647|APOA1_HUMAN	Apolipoprotein A-I OS=Homo sapiens GN=APOA1 PE=1 SV=1	5
P02461|CO3A1_HUMAN	Collagen alpha-1(III) chain OS=Homo sapiens GN=COL3A1 PE=1 SV=4	37
P08123|CO1A2_HUMAN	Collagen alpha-2(I) chain OS=Homo sapiens GN=COL1A2 PE=1 SV=7	34
P04433|KV309_HUMAN	Ig kappa chain V-III region VG (Fragment) OS=Homo sapiens PE=1 SV=1	2
P04433|KV309_HUMAN	Ig kappa chain V-III region VG (Fragment) OS=Homo sapiens PE=1 SV=1	2
P19652|A1AG2_HUMAN	Alpha-1-acid glycoprotein 2 OS=Homo sapiens GN=ORM2 PE=1 SV=2	4
P35030|TRY3_HUMAN	Trypsin-3 OS=Homo sapiens GN=PRSS3 PE=1 SV=2	8
P02458|CO2A1_HUMAN	Collagen alpha-1(II) chain OS=Homo sapiens GN=COL2A1 PE=1 SV=3	19
P02461|CO3A1_HUMAN	Collagen alpha-1(III) chain OS=Homo sapiens GN=COL3A1 PE=1 SV=4	44
P81605|DCD_HUMAN	Dermcidin OS=Homo sapiens GN=DCD PE=1 SV=2	2
B9A064|IGLL5_HUMAN	Immunoglobulin lambda-like polypeptide 5 OS=Homo sapiens GN=IGLL5 PE=2 SV=2	4
P35527|K1C9_HUMAN	Keratin, type I cytoskeletal 9 OS=Homo sapiens GN=KRT9 PE=1 SV=3	10
P13647|K2C5_HUMAN	Keratin, type II cytoskeletal 5 OS=Homo sapiens GN=KRT5 PE=1 SV=3	12
P35030|TRY3_HUMAN	Trypsin-3 OS=Homo sapiens GN=PRSS3 PE=1 SV=2	12
Q8NHM4|TRY6_HUMAN	Putative trypsin-6 OS=Homo sapiens GN=TRY6 PE=5 SV=1	7

P01765|HV304_HUMAN	Ig heavy chain V-III region TIL OS=Homo sapiens PE=1 SV=1	1
P01596|KV104_HUMAN	Ig kappa chain V-I region CAR OS=Homo sapiens PE=1 SV=1	1
P01598|KV106_HUMAN	Ig kappa chain V-I region EU OS=Homo sapiens PE=1 SV=1	1
P02787|TRFE_HUMAN	Serotransferrin OS=Homo sapiens GN=TF PE=1 SV=3	9
P07477|TRY1_HUMAN	Trypsin-1 OS=Homo sapiens GN=PRSS1 PE=1 SV=1	12
P02747|C1QC_HUMAN	Complement C1q subcomponent subunit C OS=Homo sapiens GN=C1QC PE=1 SV=3	3
P01766|HV305_HUMAN	Ig heavy chain V-III region BRO OS=Homo sapiens PE=1 SV=1	5
P01766|HV305_HUMAN	Ig heavy chain V-III region BRO OS=Homo sapiens PE=1 SV=1	1
P01774|HV313_HUMAN	Ig heavy chain V-III region POM OS=Homo sapiens PE=1 SV=1	1
P01774|HV313_HUMAN	Ig heavy chain V-III region POM OS=Homo sapiens PE=1 SV=1	1
P01777|HV316_HUMAN	Ig heavy chain V-III region TEI OS=Homo sapiens PE=1 SV=1	3
P01762|HV301_HUMAN	Ig heavy chain V-III region TRO OS=Homo sapiens PE=1 SV=1	1
P01762|HV301_HUMAN	Ig heavy chain V-III region TRO OS=Homo sapiens PE=1 SV=1	1
P01779|HV318_HUMAN	Ig heavy chain V-III region TUR OS=Homo sapiens PE=1 SV=1	1
P01764|HV303_HUMAN	Ig heavy chain V-III region VH26 OS=Homo sapiens PE=1 SV=1	1
P01776|HV315_HUMAN	Ig heavy chain V-III region WAS OS=Homo sapiens PE=1 SV=1	1
P04433|KV309_HUMAN	Ig kappa chain V-III region VG (Fragment) OS=Homo sapiens PE=1 SV=1	1
P07477|TRY1_HUMAN	Trypsin-1 OS=Homo sapiens GN=PRSS1 PE=1 SV=1	6
P02461|CO3A1_HUMAN	Collagen alpha-1(III) chain OS=Homo sapiens GN=COL3A1 PE=1 SV=4	30

P02746|C1QB_HUMAN	Complement C1q subcomponent subunit B OS=Homo sapiens GN=C1QB PE=1 SV=3	4
P00738|HPT_HUMAN	Haptoglobin OS=Homo sapiens GN=HP PE=1 SV=1	6
P01593|KV101_HUMAN	Ig kappa chain V-I region AG OS=Homo sapiens PE=1 SV=1	1
P07478|TRY2_HUMAN	Trypsin-2 OS=Homo sapiens GN=PRSS2 PE=1 SV=1	10
P01876|IGHA1_HUMAN	Ig alpha-1 chain C region OS=Homo sapiens GN=IGHA1 PE=1 SV=2	4
P01876|IGHA1_HUMAN	Ig alpha-1 chain C region OS=Homo sapiens GN=IGHA1 PE=1 SV=2	4
P01876|IGHA1_HUMAN	Ig alpha-1 chain C region OS=Homo sapiens GN=IGHA1 PE=1 SV=2	4
P01871|IGHM_HUMAN	Ig mu chain C region OS=Homo sapiens GN=IGHM PE=1 SV=3	6
P35908|K22E_HUMAN	Keratin, type II cytoskeletal 2 epidermal OS=Homo sapiens GN=KRT2 PE=1 SV=2	8
P19652|A1AG2_HUMAN	Alpha-1-acid glycoprotein 2 OS=Homo sapiens GN=ORM2 PE=1 SV=2	3
P02647|APOA1_HUMAN	Apolipoprotein A-I OS=Homo sapiens GN=APOA1 PE=1 SV=1	3
P02458|CO2A1_HUMAN	Collagen alpha-1(II) chain OS=Homo sapiens GN=COL2A1 PE=1 SV=3	23
P02461|CO3A1_HUMAN	Collagen alpha-1(III) chain OS=Homo sapiens GN=COL3A1 PE=1 SV=4	18
P02462|CO4A1_HUMAN	Collagen alpha-1(IV) chain OS=Homo sapiens GN=COL4A1 PE=1 SV=3	9
P02747|C1QC_HUMAN	Complement C1q subcomponent subunit C OS=Homo sapiens GN=C1QC PE=1 SV=3	2
P01617|KV204_HUMAN	Ig kappa chain V-II region TEW OS=Homo sapiens PE=1 SV=1	1
P02768|ALBU_HUMAN	Serum albumin OS=Homo sapiens GN=ALB PE=1 SV=2	6
P01614|KV201_HUMAN	Ig kappa chain V-II region Cum OS=Homo sapiens PE=1 SV=1	1

P01614|KV201_HUMAN	Ig kappa chain V-II region Cum OS=Homo sapiens PE=1 SV=1	1
P06309|KV205_HUMAN	Ig kappa chain V-II region GM607 (Fragment) OS=Homo sapiens PE=4 SV=1	1
P13645|K1C10_HUMAN	Keratin, type I cytoskeletal 10 OS=Homo sapiens GN=KRT10 PE=1 SV=6	4
P02458|CO2A1_HUMAN	Collagen alpha-1(II) chain OS=Homo sapiens GN=COL2A1 PE=1 SV=3	14
P05997|CO5A2_HUMAN	Collagen alpha-2(V) chain OS=Homo sapiens GN=COL5A2 PE=1 SV=3	15
P81605|DCD_HUMAN	Dermcidin OS=Homo sapiens GN=DCD PE=1 SV=2	1
P01742|HV101_HUMAN	Ig heavy chain V-I region EU OS=Homo sapiens PE=1 SV=1	1
P01742|HV101_HUMAN	Ig heavy chain V-I region EU OS=Homo sapiens PE=1 SV=1	1
P01743|HV102_HUMAN	Ig heavy chain V-I region HG3 OS=Homo sapiens PE=4 SV=1	1
P06326|HV107_HUMAN	Ig heavy chain V-I region Mot OS=Homo sapiens PE=1 SV=1	1
P01761|HV106_HUMAN	Ig heavy chain V-I region SIE OS=Homo sapiens PE=1 SV=1	1
P23083|HV103_HUMAN	Ig heavy chain V-I region V35 OS=Homo sapiens PE=1 SV=1	1
P23083|HV103_HUMAN	Ig heavy chain V-I region V35 OS=Homo sapiens PE=1 SV=1	1
P06310|KV206_HUMAN	Ig kappa chain V-II region RPMI 6410 OS=Homo sapiens PE=4 SV=1	1
P06310|KV206_HUMAN	Ig kappa chain V-II region RPMI 6410 OS=Homo sapiens PE=4 SV=1	1
P04259|K2C6B_HUMAN	Keratin, type II cytoskeletal 6B OS=Homo sapiens GN=KRT6B PE=1 SV=5	5
A6NJS3|IV1U1_HUMAN	Putative V-set and immunoglobulin domain-containing-like protein IGHV1OR21-1 OS=Homo sapiens GN=IGHV1OR21-1 PE=5 SV=1	1

O60902|SHOX2_HUMAN	Short stature homeobox protein 2 OS=Homo sapiens GN=SHOX2 PE=2 SV=4	1
P04632|CPNS1_HUMAN	Calpain small subunit 1 OS=Homo sapiens GN=CAPNS1 PE=1 SV=1	1
Q8NFW1|COMA1_HUMAN	Collagen alpha-1(XXII) chain OS=Homo sapiens GN=COL22A1 PE=1 SV=2	7
P25940|CO5A3_HUMAN	Collagen alpha-3(V) chain OS=Homo sapiens GN=COL5A3 PE=1 SV=3	7
Q5VWW1|C1QL3_HUMAN	Complement C1q-like protein 3 OS=Homo sapiens GN=C1QL3 PE=2 SV=1	1
Q5VWW1|C1QL3_HUMAN	Complement C1q-like protein 3 OS=Homo sapiens GN=C1QL3 PE=2 SV=1	1
Q5VWW1|C1QL3_HUMAN	Complement C1q-like protein 3 OS=Homo sapiens GN=C1QL3 PE=2 SV=1	1
Q7Z794|K2C1B_HUMAN	Keratin, type II cytoskeletal 1b OS=Homo sapiens GN=KRT77 PE=2 SV=3	5
P04259|K2C6B_HUMAN	Keratin, type II cytoskeletal 6B OS=Homo sapiens GN=KRT6B PE=1 SV=5	4
P01625|KV402_HUMAN	Ig kappa chain V-IV region Len OS=Homo sapiens PE=1 SV=2	1
P08727|K1C19_HUMAN	Keratin, type I cytoskeletal 19 OS=Homo sapiens GN=KRT19 PE=1 SV=4	4
Q7Z3Y8|K1C27_HUMAN	Keratin, type I cytoskeletal 27 OS=Homo sapiens GN=KRT27 PE=1 SV=2	5
P06312|KV401_HUMAN	Ig kappa chain V-IV region (Fragment) OS=Homo sapiens GN=IGKV4-1 PE=4 SV=1	1
P06313|KV403_HUMAN	Ig kappa chain V-IV region JI OS=Homo sapiens PE=4 SV=1	1
Q86Y46|K2C73_HUMAN	Keratin, type II cytoskeletal 73 OS=Homo sapiens GN=KRT73 PE=1 SV=1	4

Q86Y46|K2C73_HUMAN	Keratin, type II cytoskeletal 73 OS=Homo sapiens GN=KRT73 PE=1 SV=1	4
Q7RTS7|K2C74_HUMAN	Keratin, type II cytoskeletal 74 OS=Homo sapiens GN=KRT74 PE=1 SV=2	4
O00570|SOX1_HUMAN	Transcription factor SOX-1 OS=Homo sapiens GN=SOX1 PE=1 SV=2	1
P35030|TRY3_HUMAN	Trypsin-3 OS=Homo sapiens GN=PRSS3 PE=1 SV=2	5
Q9NY12|GAR1_HUMAN	H/ACA ribonucleoprotein complex subunit 1 OS=Homo sapiens GN=GAR1 PE=1 SV=1	1
Q7Z794|K2C1B_HUMAN	Keratin, type II cytoskeletal 1b OS=Homo sapiens GN=KRT77 PE=2 SV=3	2
Q9Y2Z2|MTO1_HUMAN	Protein MTO1 homolog, mitochondrial OS=Homo sapiens GN=MTO1 PE=1 SV=2	1
P35247|SFTPD_HUMAN	Pulmonary surfactant-associated protein D OS=Homo sapiens GN=SFTPD PE=1 SV=3	1
Q17RW2|COOA1_HUMAN	Collagen alpha-1(XXIV) chain OS=Homo sapiens GN=COL24A1 PE=2 SV=2	6
P05997|CO5A2_HUMAN	Collagen alpha-2(V) chain OS=Homo sapiens GN=COL5A2 PE=1 SV=3	12
P53420|CO4A4_HUMAN	Collagen alpha-4(IV) chain OS=Homo sapiens GN=COL4A4 PE=1 SV=3	5
P02675|FIBB_HUMAN	Fibrinogen beta chain OS=Homo sapiens GN=FGB PE=1 SV=2	3
P13647|K2C5_HUMAN	Keratin, type II cytoskeletal 5 OS=Homo sapiens GN=KRT5 PE=1 SV=3	3
Q9UEW3|MARCO_HUMAN	Macrophage receptor MARCO OS=Homo sapiens GN=MARCO PE=1 SV=1	1
P02647|APOA1_HUMAN	Apolipoprotein A-I OS=Homo sapiens GN=APOA1 PE=1 SV=1	1

P13942|COBA2_HUMAN	Collagen alpha-2(XI) chain OS=Homo sapiens GN=COL11A2 PE=1 SV=5	5
P25940|CO5A3_HUMAN	Collagen alpha-3(V) chain OS=Homo sapiens GN=COL5A3 PE=1 SV=3	5
Q8N136|DAW1_HUMAN	Dynein assembly factor with WDR repeat domains 1 OS=Homo sapiens GN=DAW1 PE=1 SV=1	1
P15814|IGLL1_HUMAN	Immunoglobulin lambda-like polypeptide 1 OS=Homo sapiens GN=IGLL1 PE=1 SV=1	1
P02787|TRFE_HUMAN	Serotransferrin OS=Homo sapiens GN=TF PE=1 SV=3	2
P02787|TRFE_HUMAN	Serotransferrin OS=Homo sapiens GN=TF PE=1 SV=3	2
Q99442|SEC62_HUMAN	Translocation protein SEC62 OS=Homo sapiens GN=SEC62 PE=1 SV=1	1
B7Z1M9|C2D4D_HUMAN	C2 calcium-dependent domain-containing protein 4D OS=Homo sapiens GN=C2CD4D PE=2 SV=2	1
B7Z1M9|C2D4D_HUMAN	C2 calcium-dependent domain-containing protein 4D OS=Homo sapiens GN=C2CD4D PE=2 SV=2	1
Q6PK04|CC137_HUMAN	Coiled-coil domain-containing protein 137 OS=Homo sapiens GN=CCDC137 PE=1 SV=1	1
Q6PK04|CC137_HUMAN	Coiled-coil domain-containing protein 137 OS=Homo sapiens GN=CCDC137 PE=1 SV=1	1
P20908|CO5A1_HUMAN	Collagen alpha-1(V) chain OS=Homo sapiens GN=COL5A1 PE=1 SV=3	4
P12107|COBA1_HUMAN	Collagen alpha-1(XI) chain OS=Homo sapiens GN=COL11A1 PE=1 SV=4	3
Q5TAT6|CODA1_HUMAN	Collagen alpha-1(XIII) chain OS=Homo sapiens GN=COL13A1 PE=1 SV=1	1
Q14055|CO9A2_HUMAN	Collagen alpha-2(IX) chain OS=Homo sapiens GN=COL9A2 PE=1 SV=2	1
P13942|COBA2_HUMAN	Collagen alpha-2(XI) chain OS=Homo sapiens GN=COL11A2 PE=1 SV=5	4

P25940|CO5A3_HUMAN	Collagen alpha-3(V) chain OS=Homo sapiens GN=COL5A3 PE=1 SV=3	4
Q9H461|FZD8_HUMAN	Frizzled-8 OS=Homo sapiens GN=FZD8 PE=1 SV=1	1
Q7Z2K8|GRIN1_HUMAN	G protein-regulated inducer of neurite outgrowth 1 OS=Homo sapiens GN=GPRIN1 PE=2 SV=2	1
O60658|PDE8A_HUMAN	High affinity cAMP-specific and IBMX-insensitive 3',5'-cyclic phosphodiesterase 8A OS=Homo sapiens GN=PDE8A PE=1 SV=2	1
Q9UH92|MLX_HUMAN	Max-like protein X OS=Homo sapiens GN=MLX PE=1 SV=	1
Q8IXF0|NPAS3_HUMAN	Neuronal PAS domain-containing protein 3 OS=Homo sapiens GN=NPAS3 PE=2 SV=1	1
Q9H340|O51B6_HUMAN	Olfactory receptor 51B6 OS=Homo sapiens GN=OR51B6 PE=2 SV=2	1
Q5T750|XP32_HUMAN	Skin-specific protein 32 OS=Homo sapiens GN=XP32 PE=1 SV=1	1
Q5T750|XP32_HUMAN	Skin-specific protein 32 OS=Homo sapiens GN=XP32 PE=1 SV=1	1
Q6UWP8|SBSN_HUMAN	Suprabasin OS=Homo sapiens GN=SBSN PE=2 SV=2	1
Q7L2R6|ZN765_HUMAN	Zinc finger protein 765 OS=Homo sapiens GN=ZNF765 PE=2 SV=2	1
P01009|A1AT_HUMAN	Alpha-1-antitrypsin OS=Homo sapiens GN=SERPINA1 PE=1 SV=3	1
P01023|A2MG_HUMAN	Alpha-2-macroglobulin OS=Homo sapiens GN=A2M PE=1 SV=3	2
A9YTQ3|AHRR_HUMAN	Aryl hydrocarbon receptor repressor OS=Homo sapiens GN=AHRR PE=2 SV=3	1
Q12791|KCMA1_HUMAN	Calcium-activated potassium channel subunit alpha-1 OS=Homo sapiens GN=KCNMA1 PE=1 SV=2	1
P12107|COBA1_HUMAN	Collagen alpha-1(XI) chain OS=Homo sapiens GN=COL11A1 PE=1 SV=4	3
P12107|COBA1_HUMAN	Collagen alpha-1(XI) chain OS=Homo sapiens GN=COL11A1 PE=1 SV=4	2

P25067|CO8A2_HUMAN	Collagen alpha-2(VIII) chain OS=Homo sapiens GN=COL8A2 PE=1 SV=2	1
P13942|COBA2_HUMAN	Collagen alpha-2(XI) chain OS=Homo sapiens GN=COL11A2 PE=1 SV=5	2
P02675|FIBB_HUMAN	Fibrinogen beta chain OS=Homo sapiens GN=FGB PE=1 SV=2	1
P78415|IRX3_HUMAN	Iroquois-class homeodomain protein IRX-3 OS=Homo sapiens GN=IRX3 PE=2 SV=3	1
Q5VZ66|JKIP3_HUMAN	Janus kinase and microtubule-interacting protein 3 OS=Homo sapiens GN=JAKMIP3 PE=2 SV=2	1
Q7Z478|DHX29_HUMAN	ATP-dependent RNA helicase DHX29 OS=Homo sapiens GN=DHX29 PE=1 SV=2	1
P20908|CO5A1_HUMAN	Collagen alpha-1(V) chain OS=Homo sapiens GN=COL5A1 PE=1 SV=3	1
P29400|CO4A5_HUMAN	Collagen alpha-5(IV) chain OS=Homo sapiens GN=COL4A5 PE=1 SV=2	1
P01024|CO3_HUMAN	Complement C3 OS=Homo sapiens GN=C3 PE=1 SV=2	1
P02671|FIBA_HUMAN	Fibrinogen alpha chain OS=Homo sapiens GN=FGA PE=1 SV=2	1
Q96PE1|GP124_HUMAN	G-protein coupled receptor 124 OS=Homo sapiens GN=GPR124 PE=1 SV=2	1
Q5T764|IFT1B_HUMAN	Interferon-induced protein with tetratricopeptide repeats 1B OS=Homo sapiens GN=IFIT1B PE=2 SV=1	1
Q5TCX8|M3KL4_HUMAN	Mitogen-activated protein kinase kinase kinase MLK4 OS=Homo sapiens GN=MLK4 PE=1 SV=1	1
O95428|PPN_HUMAN	Papilin OS=Homo sapiens GN=PAPLN PE=2 SV=4	1
Q6ZRV2|FA83H_HUMAN	Protein FAM83H OS=Homo sapiens GN=FAM83H PE=1 SV=3	1
Q02388|CO7A1_HUMAN	Collagen alpha-1(VII) chain OS=Homo sapiens GN=COL7A1 PE=1 SV=2	1

Q5D862|FILA2_HUMAN	Filaggrin-2 OS=Homo sapiens GN=FLG2 PE=1 SV=1	1
Q8WZ42|TITIN_HUMAN	Titin OS=Homo sapiens GN=TTN PE=1 SV=4	6
Q8WZ42|TITIN_HUMAN	Titin OS=Homo sapiens GN=TTN PE=1 SV=4	1
Q5THJ4|VP13D_HUMAN	Vacuolar protein sorting-associated protein 13D OS=Homo sapiens GN=VPS13D PE=1 SV=1	1

Appendix D: List of proteins identified in PCCF isolated using tandem immunoaffinity method from plasma of patients with Gleason score 8.

Accession	Description	Number of Peptides
P02768|ALBU_HUMAN	Serum albumin OS=Homo sapiens GN=ALB PE=1 SV=2	56
P02452|CO1A1_HUMAN	Collagen alpha-1(I) chain OS=Homo sapiens GN=COL1A1 PE=1 SV=5	55
P08123|CO1A2_HUMAN	Collagen alpha-2(I) chain OS=Homo sapiens GN=COL1A2 PE=1 SV=7	48
P13645|K1C10_HUMAN	Keratin, type I cytoskeletal 10 OS=Homo sapiens GN=KRT10 PE=1 SV=6	31
P02461|CO3A1_HUMAN	Collagen alpha-1(III) chain OS=Homo sapiens GN=COL3A1 PE=1 SV=4	31
P04264|K2C1_HUMAN	Keratin, type II cytoskeletal 1 OS=Homo sapiens GN=KRT1 PE=1 SV=6	25
P01857|IGHG1_HUMAN	Ig gamma-1 chain C region OS=Homo sapiens GN=IGHG1 PE=1 SV=1	18
P02458|CO2A1_HUMAN	Collagen alpha-1(II) chain OS=Homo sapiens GN=COL2A1 PE=1 SV=3	18
P01859|IGHG2_HUMAN	Ig gamma-2 chain C region OS=Homo sapiens GN=IGHG2 PE=1 SV=2	14
P08779|K1C16_HUMAN	Keratin, type I cytoskeletal 16 OS=Homo sapiens GN=KRT16 PE=1 SV=4	12
P07478|TRY2_HUMAN	Trypsin-2 OS=Homo sapiens GN=PRSS2 PE=1 SV=1	12

P35527|K1C9_HUMAN	Keratin, type I cytoskeletal 9 OS=Homo sapiens GN=KRT9 PE=1 SV=3	11
P35030|TRY3_HUMAN	Trypsin-3 OS=Homo sapiens GN=PRSS3 PE=1 SV=2	11
P01860|IGHG3_HUMAN	Ig gamma-3 chain C region OS=Homo sapiens GN=IGHG3 PE=1 SV=2	10
P02538|K2C6A_HUMAN	Keratin, type II cytoskeletal 6A OS=Homo sapiens GN=KRT6A PE=1 SV=3	10
P35908|K22E_HUMAN	Keratin, type II cytoskeletal 2 epidermal OS=Homo sapiens GN=KRT2 PE=1 SV=2	10
P04259|K2C6B_HUMAN	Keratin, type II cytoskeletal 6B OS=Homo sapiens GN=KRT6B PE=1 SV=5	9
P13647|K2C5_HUMAN	Keratin, type II cytoskeletal 5 OS=Homo sapiens GN=KRT5 PE=1 SV=3	8
P02787|TRFE_HUMAN	Serotransferrin OS=Homo sapiens GN=TF PE=1 SV=3	8
P01834|IGKC_HUMAN	Ig kappa chain C region OS=Homo sapiens GN=IGKC PE=1 SV=1	6
Q86Y46|K2C73_HUMAN	Keratin, type II cytoskeletal 73 OS=Homo sapiens GN=KRT73 PE=1 SV=1	6
Q04695|K1C17_HUMAN	Keratin, type I cytoskeletal 17 OS=Homo sapiens GN=KRT17 PE=1 SV=2	6
P0CG06|LAC3_HUMAN	Ig lambda-3 chain C regions OS=Homo sapiens GN=IGLC3 PE=1 SV=1	5
P19012|K1C15_HUMAN	Keratin, type I cytoskeletal 15 OS=Homo sapiens GN=KRT15 PE=1 SV=3	5
P13646|K1C13_HUMAN	Keratin, type I cytoskeletal 13 OS=Homo sapiens GN=KRT13 PE=1 SV=4	5
Q5XKE5|K2C79_HUMAN	Keratin, type II cytoskeletal 79 OS=Homo sapiens GN=KRT79 PE=1 SV=2	4
Q7Z3Y7|K1C28_HUMAN	Keratin, type I cytoskeletal 28 OS=Homo sapiens GN=KRT28 PE=1 SV=2	4

Q7RTS7|K2C74_HUMAN	Keratin, type II cytoskeletal 74 OS=Homo sapiens GN=KRT74 PE=1 SV=2	4
O95678|K2C75_HUMAN	Keratin, type II cytoskeletal 75 OS=Homo sapiens GN=KRT75 PE=1 SV=2	4
Q86YZ3|HORN_HUMAN	Hornerin OS=Homo sapiens GN=HRNR PE=1 SV=2	4
Q8TF68|ZN384_HUMAN	Zinc finger protein 384 OS=Homo sapiens GN=ZNF384 PE=1 SV=2	3
P08727|K1C19_HUMAN	Keratin, type I cytoskeletal 19 OS=Homo sapiens GN=KRT19 PE=1 SV=4	3
P01766|HV305_HUMAN	Ig heavy chain V-III region BRO OS=Homo sapiens PE=1 SV=1	2
Q2M2I5|K1C24_HUMAN	Keratin, type I cytoskeletal 24 OS=Homo sapiens GN=KRT24 PE=1 SV=1	2
P01777|HV316_HUMAN	Ig heavy chain V-III region TEI OS=Homo sapiens PE=1 SV=1	1
Q8N1X5|YF001_HUMAN	Uncharacterized protein FLJ37310 OS=Homo sapiens PE=2 SV=1	1
P10599|THIO_HUMAN	Thioredoxin OS=Homo sapiens GN=TXN PE=1 SV=3	1
P06309|KV205_HUMAN	Ig kappa chain V-II region GM607 (Fragment) OS=Homo sapiens PE=4 SV=1	1
P81605|DCD_HUMAN	Dermcidin OS=Homo sapiens GN=DCD PE=1 SV=2	1
P56270|MAZ_HUMAN	Myc-associated zinc finger protein OS=Homo sapiens GN=MAZ PE=1 SV=1	1
P04433|KV309_HUMAN	Ig kappa chain V-III region VG (Fragment) OS=Homo sapiens PE=1 SV=1	1
P68871|HBB_HUMAN	Hemoglobin subunit beta OS=Homo sapiens GN=HBB PE=1 SV=2	1
P02042|HBD_HUMAN	Hemoglobin subunit delta OS=Homo sapiens GN=HBD PE=1 SV=2	1
P02100|HBE_HUMAN	Hemoglobin subunit epsilon OS=Homo sapiens GN=HBE1 PE=1 SV=2	1

P69891|HBG1_HUMAN	Hemoglobin subunit gamma-1 OS=Homo sapiens GN=HBG1 PE=1 SV=2	1
P69892|HBG2_HUMAN	Hemoglobin subunit gamma-2 OS=Homo sapiens GN=HBG2 PE=1 SV=2	1
P15814|IGLL1_HUMAN	Immunoglobulin lambda-like polypeptide 1 OS=Homo sapiens GN=IGLL1 PE=1 SV=1	1
Q9Y2T7|YBOX2_HUMAN	Y-box-binding protein 2 OS=Homo sapiens GN=YBX2 PE=1 SV=2	1
Q8IYT1|FA71A_HUMAN	Protein FAM71A OS=Homo sapiens GN=FAM71A PE=2 SV=2	1
P02763|A1AG1_HUMAN	Alpha-1-acid glycoprotein 1 OS=Homo sapiens GN=ORM1 PE=1 SV=1	1
P01009|A1AT_HUMAN	Alpha-1-antitrypsin OS=Homo sapiens GN=SERPINA1 PE=1 SV=3	1
P02647|APOA1_HUMAN	Apolipoprotein A-I OS=Homo sapiens GN=APOA1 PE=1 SV=1	1
P04899|GNAI2_HUMAN	Guanine nucleotide-binding protein G(i) subunit alpha-2 OS=Homo sapiens GN=GNAI2 PE=1 SV=3	1
O43525|KCNQ3_HUMAN	Potassium voltage-gated channel subfamily KQT member 3 OS=Homo sapiens GN=KCNQ3 PE=1 SV=2	1
P02812|PRB2_HUMAN	Basic salivary proline-rich protein 2 OS=Homo sapiens GN=PRB2 PE=1 SV=3	1
Q9P0G3|KLK14_HUMAN	Kallikrein-14 OS=Homo sapiens GN=KLK14 PE=1 SV=2	1
P02533|K1C14_HUMAN	Keratin, type I cytoskeletal 14 OS=Homo sapiens GN=KRT14 PE=1 SV=4	1
Q8N145|LGI3_HUMAN	Leucine-rich repeat LGI family member 3 OS=Homo sapiens GN=LGI3 PE=2 SV=1	1
P67809|YBOX1_HUMAN	Nuclease-sensitive element-binding protein 1 OS=Homo sapiens GN=YBX1 PE=1 SV=3	1

Q10571|MN1_HUMAN	Probable tumor suppressor protein MN1 OS=Homo sapiens GN=MN1 PE=1 SV=3	1
Q16651|PRSS8_HUMAN	Prostasin OS=Homo sapiens GN=PRSS8 PE=1 SV=1	1
Q6UWP8|SBSN_HUMAN	Suprabasin OS=Homo sapiens GN=SBSN PE=2 SV=2	1
Q5TAT6|CODA1_HUMAN	Collagen alpha-1(XIII) chain OS=Homo sapiens GN=COL13A1 PE=1 SV=1	1
P02671|FIBA_HUMAN	Fibrinogen alpha chain OS=Homo sapiens GN=FGA PE=1 SV=2	1
O60763|USO1_HUMAN	General vesicular transport factor p115 OS=Homo sapiens GN=USO1 PE=1 SV=2	1
Q9UKX3|MYH13_HUMAN	Myosin-13 OS=Homo sapiens GN=MYH13 PE=1 SV=2	1
Q96Q06|PLIN4_HUMAN	Perilipin-4 OS=Homo sapiens GN=PLIN4 PE=2 SV=2	1
Q15283|RASA2_HUMAN	Ras GTPase-activating protein 2 OS=Homo sapiens GN=RASA2 PE=1 SV=3	1
P53420|CO4A4_HUMAN	Collagen alpha-4(IV) chain OS=Homo sapiens GN=COL4A4 PE=1 SV=3	1
P01024|CO3_HUMAN	Complement C3 OS=Homo sapiens GN=C3 PE=1 SV=2	1
Q9BZQ6|EDEM3_HUMAN	ER degradation-enhancing alpha-mannosidase-like protein 3 OS=Homo sapiens GN=EDEM3 PE=1 SV=2	1
Q96PE1|GP124_HUMAN	G-protein coupled receptor 124 OS=Homo sapiens GN=GPR124 PE=1 SV=2	1
Q6ZRV2|FA83H_HUMAN	Protein FAM83H OS=Homo sapiens GN=FAM83H PE=1 SV=3	1
H7BZ55|CROL3_HUMAN	Putative ciliary rootlet coiled-coil protein-like 3 protein OS=Homo sapiens PE=5 SV=2	1
Q9H2D6|TARA_HUMAN	TRIO and F-actin-binding protein OS=Homo sapiens GN=TRIOBP PE=1 SV=3	1

Q562E7|WDR81_HUMAN	WD repeat-containing protein 81 OS=Homo sapiens GN=WDR81 PE=1 SV=2	1
Q12802|AKP13_HUMAN	A-kinase anchor protein 13 OS=Homo sapiens GN=AKAP13 PE=1 SV=2	1
P08F94|PKHD1_HUMAN	Fibrocystin OS=Homo sapiens GN=PKHD1 PE=1 SV=1	1
Q03164|KMT2A_HUMAN	Histone-lysine N-methyltransferase 2A OS=Homo sapiens GN=KMT2A PE=1 SV=5	1
Q9UPA5|BSN_HUMAN	Protein bassoon OS=Homo sapiens GN=BSN PE=2 SV=4	1

Curriculum Vitae

Name:	Sabine Brett
Post-secondary Education and Degrees:	Trent University Peterborough, Ontario, Canada 2008-2012 B.Sc. The University of Western Ontario London, Ontario, Canada 2015-2016 M.Sc.
Honours and Awards:	Lawson Research Institute Studentship 2015-2016
Related Work Experience	Research Assistant, Everest Clinical Research Inc. February 2014- Septembed 2014

Publications:

Biggs CN, Siddiqui KM, Al-Zahrani AA, Pardhan S, **Brett SI**, Guo QQ, Yang J, Wolf P, Power NE, Durfee PN, MacMillan CD, Townson JL, Brinker JC, Fleshner NE, Izawa JI, Chambers AF, Chin JL, Leong HS. Prostate extracellular vesicles in patient plasma as a liquid biopsy platform for prostate cancer using nanoscale flow cytometry. Oncotarget. 2016 Feb 23;7(8):8839-49. doi: 10.18632/oncotarget.6983

Brett SI, Kim YJ, Leong HS, Biggs CN, Chin J. Extracellular Vesicles Such as Prostate Cell Fragments as a Liquid Biopsy for Prostate Cancer and Prostatic Diseases. Prostate Cancer Prostatic Dis. 2015 Sep; 18(3):213-20. Epub 2015 May 12.